Master thesis and internship[BR]- Master's Thesis : Evaluation of aerodynamic loads prediction on wind turbine blades[BR]- Stage d'insertion professionnelle

Auteur : Castelló Mora, Ignacio
Promoteur(s) : Bruls, Olivier
Faculté : Faculté des Sciences appliquées
Diplôme : Cours supplémentaires destinés aux étudiants d'échange (Erasmus, ...)
Année académique : 2019-2020
URI/URL : http://hdl.handle.net/2268.2/9149

University of Liège - Faculty of Applied Sciences

Evaluation of aerodynamic loads prediction on wind turbine blades

Graduation Studies conducted for obtaining the Master's degree in Aerospace Engineering

by
Ignacio Castelló Mora

Promotor: Olivier Brüls

Academic year 2019 - 2020

'What we do in life,
echoes in eternity.'
Marcus Aurelius.

Contents

List of Figures

List of Tables

1 Summary

In the present report it has been studied the aerodynamic loads and deformations of the NREL 5-MW and SWT 2.3-93 wind turbines obtained with two different aerodynamic methods: the Blade Element Momentum (BEM) method and a 3D panel method. The BEM method is implemented in a *SAMCEF* module called *AERO* and for the 3D panel method it has been used the open source software *Vortexje*. For the structural model it has been used the *SAMCEF* module called *MECANO* based on a flexible multibody dynamic model. And for the coupling method, *MECANO* and *AERO* are already internally coupled, while *MECANO* and Vortexje have been coupled with the *SAMCEF* module called *Supervisor*. The main purpose of the report is to compare the results obtained with both BEM and panel method in terms of efficiency and accuracy in order to see the validity and limitations of both methods. Other purpose is to study the influence of blade deformations, for which simulations have been carried out considering rigid and flexible blades. The last purpose of this report is to study the influence of gravity loads and flow asymmetries introduced by shaft tilt and yaw angles.

Firstly in order to demonstrate the validity of the *MECANO + AERO* method, the steady-state response of the NREL 5-MW and SWT 2.3-93 wind turbines has been compared with simulations run with *FAST + Aerodyn + Beamdyn*, which is based on the BEM theory as well, for several wind velocities, rotor speeds and pitch angles following the stationary control curves obtained with *FAST + Aerodyn + Beamdyn*. The simulations have been done for an axial, steady and uniform wind and without gravity loads to avoid unsteady effects. The results obtained in terms of rotor thrust and torque and blade deformations show similarity between them and show a clear influence of the blade deformations on the rotor performances.

Secondly, the dynamic response with *MECANO + AERO* and *MECANO + Vortexje* at the rated operating point has been studied because it is the most interesting point because it is where the highest aerodynamic loads occur. As in the previous case the simulations have been done for an axial, steady and uniform wind and without gravity loads. The results obtained in terms of rotor thrust and torque, blade deformations and distributions of normal force (normal to the rotor plane) and tangential force (in rotational direction) along the span, show some differences between both methods. Comparing the results with CFD results of other authors, some results seem to be better predicted by BEM method and other by the panel method. Moreover in order to demonstrate the validity of *MECANO + Vortexje*, the pressure coefficient distribution along the chord for different span sections has been compared with CFD data showing a great similarity except in the trailing edge.

After that it has been studied the influence of the tilt and yaw angle under gravitational loads at the rated operating point only with *MECANO + Vortexje* due to inability of *MECANO + AERO* to correctly predict the tilt and yaw effects. This influence has been studied for blade deformations and normal force along the span showing a clear unsteady periodic response which must be taken into account to predict fatigue loads.

Finally, it is compared the efficiency of both methods in terms of CPU time. The CPU time required by *MECANO + AERO* is much less than that required by *MECANO + Vortexje* to reach convergence of results. In order to reduce the time required by *MECANO + Vortexje* it has been done an study that shows the effect on the CPU time and rotor thrust and torque of deleting the last wake layer after different rotor revolutions.

The main conclusion is that *MECANO + AERO* method is appropriate for uniform and steady flows in terms of efficiency and accuracy making its use more convenient than *MECANO + Vortexje*. However it is inevitable that in actual operating conditions the wind direction changes, what causes that wind turbines operate at yaw angles relative to the incoming wind producing a skewed wake behind the rotor. Due to inability of *MECANO + AERO* to correctly predict these effects, in general it is more convenient to use *MECANO + Vortexje* adding some improvements, such as flow separation and rotational effects..

2 Object

There is a tendency to build wind turbines with longer blade lengths since the power obtained by the wind turbine is proportional to the rotor swept area. Furthermore, with the aim of improving the cost-effective energy efficiency, these blades are designed to have less weight. The greater size of the blades together with the reduction in weight, causes larger aeroelastic deformations. These deformations produce considerable variations in the performances of the wind turbines, so for the design of wind turbines it is required to use methods with structural and aerodynamic coupling that allow predicting reliably the loads and deformations in the rotor blades. Inaccurate predictions of loads or deformations can lead to over design the wind turbine making it inefficient.

Currently, the most used aerodynamic method for obtaining aerodynamic loads on wind turbines is the Blade Element Momentum (BEM) method due to its simplicity and its low computational cost. This method is modified with different engineering models that increase its applicability. However, as will be seen throughout the project, this has certain limitations. For this reason, Computational Fluid Dynamics (CFD) (based on the Navier-Stokes equations), capable of obtaining more accurate results for a wider range of wind conditions, are increasingly being used in the industry. On the contrary, the calculation time is much longer. This project aims to study an aerodynamic method that falls between the BEM method and the CFD: the panel method. The panel method is expected to be faster than CFD and to simulate more complex cases than the BEM method.

Thus to predict aerodynamic loads on wind turbines, Samtech offers a solution based on a flexible multibody dynamic model (with SAMCEF *MECANO* solver) of the wind turbines. In this solution, it is used an in-house module, *AERO*, to compute aerodynamic loads on both blade and tower. This module based on Blade Element Momentum (BEM) theory is computationally very efficient and enables to provide reasonable estimation of the aeroelastic behaviour of flexible blades. However, because of the fundamental assumptions of quasi-steady flows and two-dimensional aerodynamics, the method has inevitable shortcomings for simulating realistic flows, and as result, is not able to accurately predict the blade loads and ultimately leads to over-designed and inefficient wind turbines. To overcome these limitations, it has been coupled a 3D panel method, *Vortexje*, to the *MECANO* solver in order to predict more accurate aerodynamic forces in a wider range of flow conditions.

The main purpose of this project is to compare the results obtained with both *MECANO + AERO* and *MECANO + Vortexje* methods applying them to the NREL 5-MW and SWT 2.3-93 wind turbines. The comparison will be made in terms of accuracy in the prediction of aerodynamic loads and deformations, and in terms of efficiency comparing the required computation times. Moreover with the objective to demonstrate the validity of both methods, *MECANO + AERO* will be compared with *FAST + Aerodyn + Beamdyn*, which is also based on the BEM method, and *MECANO + Vortexje* will be compared with CFD results of

other authors. Other purpose is to study the influence of blade deformations on aerodynamic loads, for which simulations will be run with rigid and flexible blades. The last purpose of this project is to study with *MECANO + Vortexje* the unsteady effects induced by gravitational loads, shaft tilt and yaw angle.

3 Introduction

3.1 Thesis outline

To fulfill the aforementioned objectives, this thesis follows the following scheme:

- In Section 3, a review of the state of the art is made, in terms of different software used in the industry for the design of wind turbines and in terms of previous works. The theoretical development of the Blade Element Momentum method and the panel method are also explained, since they are the aerodynamic methods used in this project. Finally, a brief review of the main advantages and disadvantages of both methods is carried out.

- In section 4, firstly it is explained the *Bnrel* program used to obtain the wind turbine files (NREL 5-MW and SWT 2.3-93) necessary to apply the *MECANO + AERO* and *MECANO + Vortexje* methods. Next, the structural model of the studied wind turbines and the *MECANO* solver used for structural simulation are explained. Then it is developed how the aerodynamic model is performed for the use of the *AERO* method (BEM method) and the *Vortexje* method (panel method). It also indicates how to apply the panel method explained in Section 3 computationally. Finally, it briefly indicates how the coupling between *MECANO* and *Vortexje* is carried out.

- Section 5 contains the results obtained from the simulations, which are the forces and deformations of the wind turbine. To study the two wind turbines (NREL 5-MW and SWT 2.3-93) the same scheme has been carried out. First, it has been obtained the stationary control curves of rotor speed and pitch angle as a function of wind speed using *FAST + BeamDyn + AeroDyn*. Once these curves have been obtained and using them, the steady-state response has been obtained with *FAST + BeamDyn + AeroDyn* and with *MECANO + AERO* for different wind speeds and, therefore, different rotor speeds and pitch angles. Subsequently, the dynamic response of loads and deformations for the rated operating point has been obtained, firstly comparing the responses of *MECANO + AERO* and *MECANO + Vortexje* for an axial, steady and uniform wind, and secondly studying with *MECANO + Vortexje* the influence of gravitational loads, shaft tilt and yaw angle. Finally, the computational costs of both methods have been compared and an alternative is proposed to reduce the computational time of the panel method, consisting of removing the last wake layer.

- Finally, Section 6 presents the main results and conclusions obtained throughout the project. And Section 7 gives a short description of the improvements made in the *AERO* module after the completion of the project and an idea of possible future improvements that can be carried out in the panel method.

3.2 State of the art

3.2.1 Wind turbines software

Last years, advances in the design and operation of wind turbines have improved their performances, making wind energy more efficient and affordable than ever. Wind energy technology is becoming a competitive and reliable technology and forecasts reveal that progress will continue strongly. Until now, design trends have led to building longer (Figure 1) and more flexible blades, smart rotor and control, and offshore application. Despite the fact that a large part of these advances are usually attributed to the use of innovative hardware and components included in wind turbines, a large part of these advances are due to what is behind the scenes: the engineering software that led to this design. Software simulations are helping manufacturers and operators to maximize wind developments, and now researchers are also benefiting.

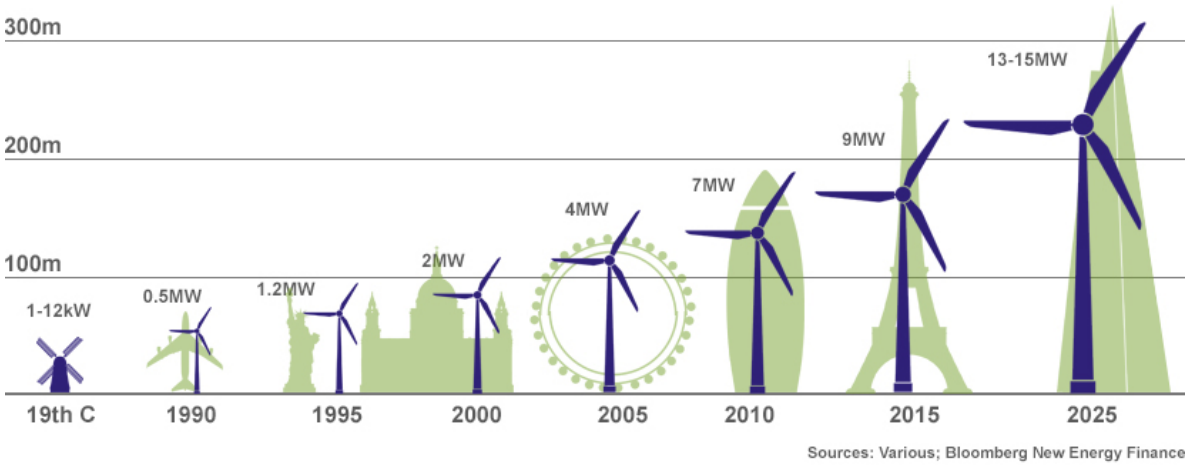

Figure 1: Evolution over the years of hub height, rotor diameter and power.

Nowadays in the industry there is a great variety of software for wind turbines simulations for different functions. Most of these programs can be classified into one of the following groups:

- Software that is used to model the air flow in a certain place, to give an approximation of the wind characteristic in those places where there are no measurements available (for example, there are places where measurements have only been taken recently and they are not yet representative).
- Feasibility analysis programs: They give information on costs, emissions, investment risk and other information that should be taken into account before setting up a wind farm.
- Wind farm modeling programs: They allow to present a proposal to make a wind farm graphically, with the final purpose of obtaining its construction permits.

- Softwares that help the design of wind turbines, using aeroelastic packages.

All of these programs are useful, but only design programs have been used in this report. This group of programs is perhaps the most extensive and important of all those previously reported. Precisely due to the importance of its function, many universities and research centers have developed software of these characteristics, but each with its own specializations and calculation methods. Some of these programs are explained below.

- *SAMCEF MECANO*: It is a software developed by Samtech for the structural model based on a flexible multibody dynamic (MBD) model. It allows to discretise the wind turbine into a number of bodies (blades, tower and drive) that will be interconnected in a single dynamic system. For the aerodynamic model it uses the module *AERO* based on the BEM theory. However it allows coupling other external aerodynamic models with the *Supervisor* module. For example, in this project, the aerodynamic model *Vortexje* will be coupled.

- *Vortexje*: It is an open source software developed by Baayen & Heinz GmbH in Berlin and implements an unsteady 3D panel method suitable for dynamic simulation of vertical and horizontal axis wind turbines. It can be easily coupled with other simulation environments.

- *FAST*: It is a computer-aided engineering (CAE) tool developed by the National Renewable Energy Laboratory and it can model the dynamic response of both two- and three-bladed, conventional, horizontal-axis wind turbines. For the aerodynamic model it uses the BEM theory and for the structural model it uses a modal approach for the discretisation method. In 1996, *NREL* has modified *FAST* to use the *AeroDyn* subroutine package developed at the University of Utah to calculate the aerodynamic forces along the blade. Furthermore, the module *BeamDyn* has been coupled with *FAST* providing new capabilities for modeling curved and twisted wind turbine blades undergoing large deformations.

- *HAWC2*: Horizontal Axis Wind turbine simulation Code of 2nd generation, as its initials indicate. It is an aeroelastic code intended for calculating wind turbine response in time domain. It was developed by Technical University of Denmark. For the aerodynamic model it uses BEM theory and for the structural model it uses multibody dynamics for the discretisation method. The aerodynamic model is modified to handle dynamic inflow, dynamic stall, skew inflow, shear effect on the induction and effects from large deflection.

- *GH Bladed*: It is an integrated software package for wind turbine performance and loading calculations developed by Garrad Hassan and Partners Ltd. For the aerodynamic model it uses BEM theory and for the structural model it uses a modal approach for the discretisation method. The late version is capable of modeling and analyzing both onshore and offshore wind turbine with variety of support specification.

- *PHATAS*: It was developed by Energy Research Centre of the Netherlands and it determines the nonlinear dynamic behaviour and the corresponding loads of a horizontal-axis wind turbine (both onshore and offshore) in time domain. For the aerodynamic model it uses BEM theory and for the structural model it uses multibody dynamics for the discretisation method.
- *FLEX5*: Since 1992 this code has been used as design and certification tool and was developed by Technical University of Denmark. For the aerodynamic model it uses BEM theory and for the structural model it uses a modal approach for the discretisation method. This code can be integrated into other softwares and work perfectly to do simulations and calculations.

3.2.2 Previous work

Below is a brief review of the main references and projects carried out by different research groups that have been use as support for carrying out this project. The Blade Element Momentum method is widely used in the industry (T.Burton et al. [8]), and several corrections have been made to the original theory as: tip losses (H. Glauert [11]), root losses, turbulent wake state (H. Glauert [12] and Buhl [7]), skewed wake (Pitt and Peters [29], and Snel and Schepers [38]), wake memory effect (Snel and Schepers [38]) or dynamic stall model, for example using models based on the Beddoes and Leishman method [5], such as the modified model developed in Dimitriadis et al. [6], or ONERA method (Mcalister et al. [25]).

Regarding the surface panel method, although it is not a widely applied method in wind turbines, it is widely used in the aeronautical industry. The open-source *Vortexje* (Baayen [3] and [4]) implements a 3D panel method based on the theory described in Katz and Plotkin [21] and Hess and Smith [16] applied to wind turbines. Previous works such as A. van Garrel [39] and Prasad and Dimitriadis [31] implement very similar panel methods for wind turbines. However Prasad and Dimitriadis [31] also includes a flow separation model, enabling more accurate results for high wind speeds. For the structural model, *Samcef/MECANO* offers a solution based on a flexible multibody dynamic model (Géradin and Cardona [13]).

In Prasad et al. [30] a study was carried out where the structural simulation of the wind turbine was done using *MECANO*, coupling it by co-simulation to the aerodynamic model. The aerodynamic models used in this study are the Blade Element Momentum and Vortex Lattice Method, demonstrating that the Vortex Lattice Method "represents adequately the dependency on motion history of unsteady aerodynamic forces which is important in order to perform aeroservoelastic simulations" (Prasad et al. [30], p.14, 2016).

The NREL 5-MW is a wind turbine defined by the National Renewable Energy Laboratory in Jonkman et al. [20]. Although no experimental data is available for the studied wind turbines NREL 5-MW and SWT 2.3-93, several previous works were carried out using higher fidelity Computational Fluid Dynamics (CFD) approaches of the NREL 5-MW wind turbine such as

Imiela et al. [19], Dose et al. [10] or Yu and Kwon [41], which will be taken as references to compare the results obtained. Other projects such as Z. Li et al. [23], Sabale and Gopal [34] and [35] or Jonkman et al. [20] have applied the Blade Element Momentum method to the NREL 5-MW. Finally a panel method has been applied to the NREL 5-MW by Schweigler [36] and Ramos et al. [33].

3.3 Aerodynamic methods

In this section a description is made of the theoretical models used in subsequent chapters to carry out the aerodynamic study of the rotor. The aerodynamic models used in this project are: the panel method, and the Blade Element Momentum (BEM) theory corrected by a blade tip loss factor and by a turbulent wake state.

3.3.1 BEM Method

The BEM method is a combination of the momentum theory and the blade element theory. On one hand, the momentum theory expresses the axial thrust and torque in terms of overall flow parameters. On the other hand, the blade element analysis provides expressions of the same quantities (thrust and torque) in terms of the lift and drag coefficients of the airfoil.

3.3.1.1 Momentum theory (MT)

The following are the hypotheses that are taken into consideration (T. Burton et al. [8], 2001, p. 41-42):

- It will be assumed that the affected air mass remains separate from the air that does not pass through the rotor disc, and therefore, does not slow down. So it can be defined a boundary surface containing the affected air mass and extending upstream and downstream forming a long stream tube of circular cross section, as it can be seen in Figure 2. As air does not flow across the boundary, the mass flow of air flowing through the stream tube will be the same for all positions along the stream tube.

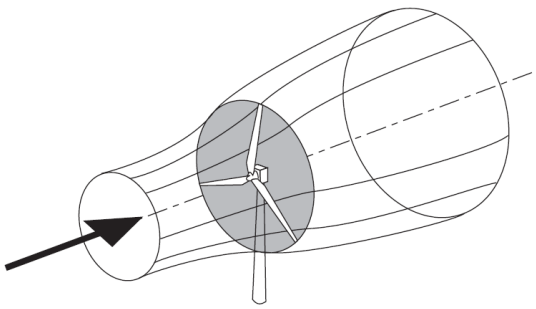

Figure 2: Stream tube of a wind turbine (T. Burton et al. [8]).

- It is considered uniform upstream wind. There is an azimuth symmetry along the stream tube, that is, the velocity and pressure profile is uniform in sections parallel to the rotor plane.
- The rotor will be considered to be isolated, without ground effects or obstacles.
- Viscous effects are considered negligible.
- Stationary movement is considered along the entire stream tube.
- There are no rotation effects in the air.

Following the development used in T. Burton et al. [8], from the linear momentum equation, the force of the fluid on the rotor, T, caused by the change of the stream speed is obtained:

$$T = 2\,\rho\,A_d\,U_\infty^2\,a\,(1-a) \tag{1}$$

where A_d is the area swept by the rotor and a is the axial flow induction factor, being the stream speed in the normal direction to the rotor plane:

$$U_{normal} = U_\infty(1-a) \tag{2}$$

where the term aU_∞ is the axial induced speed. The differential thrust experienced by the rotor corresponding to the momentum theory is:

$$dT_{MT} = 2\,\rho\,dA_d\,U_\infty^2\,a\,(1-a) \;=\; 2\,\rho\,(2\pi r dr)\,U_\infty^2\,a\,(1-a) \tag{3}$$

Then, from the angular momentum equation, the differential torque communicated to the rotor, dQ, is expressed as:

$$dQ_{MT} = 4\,\pi\,\rho\,U_\infty\,(1-a)\,\Omega\,a'\,r^3\,dr \tag{4}$$

where a' is the tangential flow induction factor. The tangential speed of the stream in the rotor plane is expressed as:

$$U_{tang} \;=\; \Omega\,r\,(1+a') \tag{5}$$

where the term $\Omega r a'$ is the tangential induced speed. In the section immediately downstream of the rotor the tangential induced speed is $2\Omega r a'$ (Figure 3).

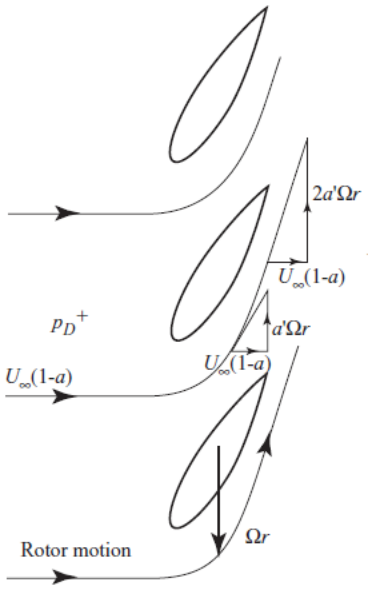

Figure 3: Tangential velocity through the rotor (T. Burton et al. [8]).

3.3.1.2 Blade element theory (BET)

In addition to the explained above, it is needed a method that takes blades into account. The Blade element theory is based on the analysis of the aerodynamic forces applied to a differential element of a blade and allows the effects of the blade geometry to be incorporated into the aerodynamic actions.

It is assumed that the blade is divided longitudinally into segments of differential length, dr, and each blade section is independent of the others. Figure 4 shows the different speeds, angles and aerodynamic forces involved in the model which are:

- $U_R \equiv$ Total relative wind speed at the considered blade section.

$$U_R = \sqrt{U_{normal}^2 + U_{tang}^2} = \sqrt{U_\infty^2(1-a)^2 + \Omega^2 r^2(1+a')^2} \tag{6}$$

- $\theta \equiv$ Blade section set angle. It depends mainly on the twist and pitch angles but also on the structural displacements of the blade section due to all flexibilities introduced in the complete model.

- $\phi \equiv$ Flow angle.

$$\phi = \arctan \frac{U_\infty(1-a)}{\Omega r(1+a')} \tag{7}$$

- $\alpha \equiv$ Angle of attack.

$$\alpha = \phi - \theta \tag{8}$$

- $dL \equiv$ Aerodynamic lift of the blade element.

$$dL = \frac{1}{2}\,\rho\, U_R^2\, c\, dr\, c_l(\alpha) \tag{9}$$

  where c is the chord of the blade section.

- $dD \equiv$ Aerodynamic drag of the blade element.

$$dD = \frac{1}{2}\,\rho\, U_R^2\, c\, dr\, c_d(\alpha) \tag{10}$$

Assuming that there is not interference of the other blades and that the aerodynamic forces on the element are due to the lift and drag of the aerodynamic section considered, and projecting these forces in the parallel and perpendicular direction to the rotor plane, it is obtained that:

- $dT \equiv$ Thrust force in the blade element.

$$dT = b\,\frac{1}{2}\,\rho\, U_R^2\, c\, dr\, (c_l(\alpha)\, \cos\phi + c_d(\alpha)\, \sin\phi) \tag{11}$$

  where b is the number of blades.

- $dF_T \equiv$ Tangential force in the blade element.

$$dF_T = b\,\frac{1}{2}\,\rho\, U_R^2\, c\, dr\, (c_l(\alpha)\, \sin\phi - c_d(\alpha)\, \cos\phi) \tag{12}$$

- $dQ \equiv$ Aerodynamic torque in the blade element. It is calculated by multiplying the tangential force by the radial position of the blade element considered.

$$dQ = r\, dF_T = b\,\frac{1}{2}\,\rho\, U_R^2\, c\, dr\, (c_l(\alpha)\, \sin\phi - c_d(\alpha)\, \cos\phi)\, r \tag{13}$$

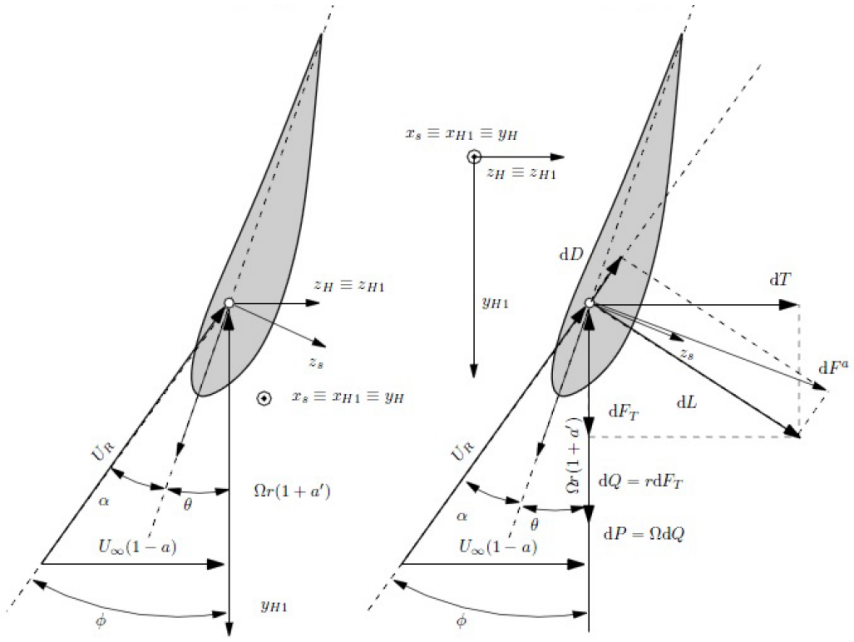

Figure 4: Velocities and forces in a blade element (Cuerva et al. [9]).

3.3.1.3 MT and BET combination (BEM)

With the Momentum and Blade element theories it has been obtained two equations for the thrust and two equations for the torque as a function of the axial and tangential flow induction factors. Equaling the expressions developed for each theory it is obtained:

$$dT_{MT} = dT_{BET} \Rightarrow 4\,\pi\,U_\infty^2\,a\,(1-a)\,r = b\,\frac{1}{2}\,U_R^2\,c\,(c_l(\alpha)\,\cos\phi + c_d(\alpha)\,\sin\phi) \tag{14}$$

$$dQ_{MT} = dQ_{BET} \Rightarrow 4\,\pi\,U_\infty\,(1-a)\,\Omega\,a'\,r^3 = b\,\frac{1}{2}\,U_R^2\,c\,(c_l(\alpha)\,\sin\phi - c_d(\alpha)\,\cos\phi)\,r \tag{15}$$

For a given wind speed, rotation speed of the rotor, aerodynamic profiles, flow angle and a number of blades, the previous expressions become a system of two equations for the unknowns a and a', which will depend of the radial position.

3.3.1.4 Tip Loss Correction

The model considered does not take into account that the circulation in the blade tip is null. Taking into account the Kutta boundary condition, the blade tip thrust must be zero. To solve this problem, the Blade Element Momentum theory is corrected by a correction factor

for circulation losses, F. The model used in this project to represent this loss factor is the called the Prandtl model (Glauert [11]), whose proposed form is:

$$F = \frac{2}{\pi} \arccos\left(\exp\left(-\frac{b}{2}\frac{R-r}{r}\frac{1}{\sin\phi}\right)\right) \tag{16}$$

where R is rotor radius. This loss factor is used to modify the thrust and torque equations (3 and 4) obtained by the momentum theory:

$$dT_{MT} = 4\,\pi\,r\,\rho\,U_\infty^2\,a\,(1-a)\;F\,dr \tag{17}$$

$$dQ_{MT} = 4\,\pi\,r^3\,\rho\,U_\infty\,(1-a)\,\Omega\,a'\,F\,dr \tag{18}$$

3.3.1.5 Glauert correction

For high values of the axial flow induction factor, a, or high values of the thrust coefficient $C_T = \frac{T}{\frac{1}{2}\rho U_\infty^2 A_d} = 4a(1-a)$, the wake becomes turbulent and draws air from outside the wake using a mixing process that energize the slow air that has passed through the rotor. Experimental studies have shown that equation 1 of the momentum theory is only valid for an axial flow induction factor less than about $0.3 - 0.4$. To take into account this effect, a correction developed by Glauert [12] will be applied to the rotor thrust coefficient. This Glauert correction features an automatic coupling with the loss factor, F, that ensures continuity between the two parts regardless of the value of the loss factor. According to Moriarty and Hansen [26], the linear momentum theory does not fit the experimental results from the value of $a \simeq 0.4$ and the Glauert correction does, as shown in Figure 5. The modification of the Glauert empirical relation that include the tip loss correction was derived by Buhl [7] as follows:

$$C_T = \frac{T}{\frac{1}{2}\rho U_\infty^2 A_d} = \frac{8}{9} + \left(4F - \frac{40}{9}\right) a + \left(\frac{50}{9} - 4F\right) a^2 \tag{19}$$

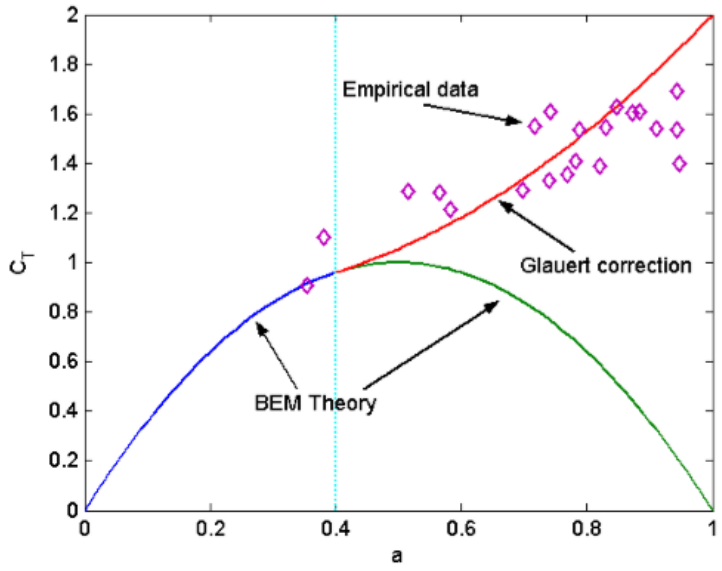

Figure 5: Comparison between linear momentum theory and Glauert correction and experimental values (Moriarty and Hansen [26], 2005, p.7).

3.3.2 Panel Method

In order to obtain the pressure distribution on the wind turbine a panel method will be implemented. In this section it has been explained what the panel method implemented consists in.

The fluid field around the body can be divided into two regions. A near-surface region where it should be considered viscous effects and rotational flow, and an external region where viscous effects are negligible and flow is irrotational. It will be considered that the fluid is incompressible, $\nabla \cdot \overline{v} = 0$, where $\overline{v}$ is the velocity vector field.

Although it is left for future developments the near-surface region can be taken into account introducing the 'blowing' velocity, that will be implemented as a boundary condition. This velocity is perpendicular to the surface and is used to simulate the boundary layer in this region. To calculate the 'blowing' velocity it is necessary to know the boundary layer displacement thickness, so boundary layer equations must be solved.

Considering that ϕ is the velocity potential, for the case of non-viscous, incompressible and irrotational fluid, the following equations and boundary conditions must be fulfilled:

- The equations in terms of velocity field are expressed:

$$\nabla \cdot \overline{v} = 0 \tag{20}$$

$$\nabla \times \overline{v} = 0 \tag{21}$$

It can also be expressed in terms of the potential, where the equation of Laplace governs our problem:

$$\nabla^2 \phi = 0 \tag{22}$$

where $\overline{v} = \nabla\phi$ since the velocity field is conservative.

- The boundary conditions require that the disturbance induced by the blade will decay far from the blade:

$$\overline{x} \to \infty, \quad \overline{v} \to \overline{v}_\infty \tag{23}$$

which is automatically fulfilled by the singular solutions (source and doublet).

- The normal component of velocity on the solid boundaries of the blade must be:

$$\nabla\phi_b \cdot \overline{n} = \overline{u}_S \cdot \overline{n} + v_n \tag{24}$$

where $\overline{n}$ is an outward normal to the surface. The local surface velocity $\overline{u}_S$ can represent the rotation, translation or deformation velocity of the surface. And the normal velocity v_n can represent the 'blowing' velocity to simulate the boundary layer effects.

The panel method arrives at a solution of the Laplace Equation 22 by summing up certain elementary solutions located on the body boundary. In this case, following the solution implemented by Katz and Plotkin [21] and A. van Garrel [39], it will be used the elementary solutions known as the source singularity distribution, $\sigma(\overline{y}, t)$, and the doublet singularity distribution, $\mu(\overline{y}, t)$, where $\overline{y}$ belongs to the boundaries. Thus the velocity potential distribution on a point $\overline{x}$ belonging to the fluid volume, can be defined as the contribution of freestream velocity potential, $\phi_\infty(\overline{x}, t)$, and perturbation velocity potential distributions, $\varphi_\sigma(\overline{x}, t)$ and $\varphi_\mu(\overline{x}, t)$, due to sources and doublets respectively:

$$\phi = \phi_\infty + \varphi_\sigma + \varphi_\mu \tag{25}$$

where

$$\varphi_\sigma(\overline{x}, t) = \frac{-1}{4\pi} \iint_S \sigma(\overline{y}, t) \frac{1}{r} dS \tag{26}$$

$$\varphi_\mu(\overline{x}, t) = \frac{-1}{4\pi} \iint_S \mu(\overline{y}, t) \frac{\overline{n} \cdot \overline{r}}{r^3} dS \tag{27}$$

The vector $\overline{n}$ is the unit normal vector to the surface and $\overline{r}$ is the distance between the evaluation point $\overline{x}$ belonging to the fluid volume and the point $\overline{y}$ belonging to the surface,

$$\overline{r} = \overline{x} - \overline{y} \tag{28}$$

Moreover, the source and doublet distribution must satisfy Equation 24. The source strength $\sigma(\overline{y},t)$ and the doublet strength $\mu(\overline{y},t)$ can be defined as function of the freestream velocity potential ϕ_∞ and the velocity potential on the surface ϕ_b as follow:

$$\sigma(\overline{y},t) \;=\; \nabla(\phi_b \;-\; \phi_\infty)\cdot\overline{n} \tag{29}$$

$$\mu(\overline{y},t) \;=\; \phi_\infty \;-\; \phi_b \tag{30}$$

Combining Equation 29 with the Equation 24, the source strength can be expressed in terms of known quantities:

$$\sigma(\overline{y},t) \;=\; (\overline{u}_S \;-\; \overline{u}_\infty)\cdot\overline{n} \;+\; v_n \tag{31}$$

Thus, it will result in a set of equations with the doublet strengths as the unknowns. Applying the surface gradient to the Equation 30, the tangential component of the velocity potential on the surface can be obtained:

$$\nabla_S\mu \;=\; \nabla_S\phi_\infty \;-\; \nabla_S\phi_b \;\rightarrow\; \nabla_S\phi_b \;=\; \nabla_S\phi_\infty - \nabla_S\mu \tag{32}$$

From the normal and tangential components of the velocity potential (Equations 24 and 32), an equation for the velocity potential on the surface is obtained:

$$\nabla\phi_b(\overline{x},t) \;=\; (\nabla\phi_b \;\cdot\; \overline{n})\,\overline{n} \;+\; \nabla_S\phi_b \;=\; (\overline{u}_S\cdot\overline{n} \;+\; v_n)\overline{n} \;+\; \nabla_S\phi_\infty - \nabla_S\mu \tag{33}$$

Finally, another expression for the velocity potential on the surface can be obtained by substituting 31 in 33:

$$\nabla\phi_b(\overline{x},t) \;=\; \overline{u}_\infty \;+\; \sigma\,\overline{n} \;-\; \nabla_S\mu \tag{34}$$

To take into account the influence of the wake on the panel method, the wake surfaces will be introduced at the trailing edge of the lifting surface. As shown in Figure 6, to impose the Kutta condition, according to Morino's Kutta condition (introduced by Morino and Kuo [27]), it will be considered that the doublet strength at the first point of the wake will be equal to the difference of doublet strength across the trailing edge.

$$\mu_{w_t} \;=\; \Delta\mu_t \tag{35}$$

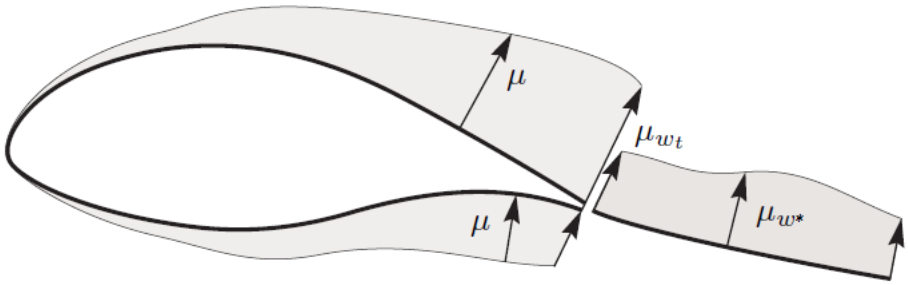

Figure 6: Trailing edge Morino's Kutta condition (A. van Garrel [39], 2016, p.23).

As stated in A. van Garrel [39] following the theorems of Helmholtz and Kelvin for vorticity dynamics, the equations for the evolution of wake panel position $\overline{x}_w$ and wake panel doublet strength μ_w are:

$$\frac{d\overline{x}_w}{dt} = \overline{u}, \qquad \overline{x}_w(t_0) = \overline{x}_{te}(t_0), \tag{36}$$

$$\frac{D\mu_w}{Dt} = 0, \qquad \mu_w(t_0) = \mu_{wt}(t_0), \tag{37}$$

Once the doublet strength distribution is found, the velocity $\overline{v}$ and velocity potential ϕ at each point in the field are known and the corresponding pressure p will be calculated by the Bernouilli equation for unsteady potential flow:

$$\frac{p_\infty - p}{\rho} = \frac{(\nabla\phi)^2}{2} + \frac{\partial\phi}{\partial t} \tag{38}$$

The pressure coefficient is by definition:

$$C_p = \frac{p - p_\infty}{\frac{1}{2}\rho\, v_{ref}^2} \tag{39}$$

where

$$\overline{v}_{ref} = \overline{u}_\infty - \overline{u}_S \tag{40}$$

Finally, the total force and moment vector can be calculated using the following equations:

$$\overline{F}(t) = -\iint_S p\,\overline{n}\,dS \tag{41}$$

$$\overline{M}(t) = \iint_S p\,\overline{n} \times \overline{r}\,dS \tag{42}$$

where $\overline{r}$ is the vector that points from the moment reference point to the surface.

3.4 BEM method vs Panel method

The BEM method is one of the most widely used methods to calculate the induced velocities in the wind turbine blades due to its simplicity and high calculation speed. However the original BEM method has some limitations. For example, it considers that the axial induced velocity in the actuator disk is half of the axial induced velocity in the far wake, which is not entirely accurate. Furthermore, the BEM method leads to errors when large out-of-plane blade deflections occur since the theory assumes that the moment is balanced in a plane parallel to the rotor. Another limitation is that it does not take into account the presence of radial flow since it assumes that the forces acting on the blades are two-dimensional. It also does not account for losses at the blade tip and root. However, its main drawback is its inability to predict unsteady effects, due to unsteady flows or non-axial flows. For example, it assumes that the flow around the profile is always in equilibrium and that the flow is accelerated instantaneously to adjust to the changes in the vorticity in the wake due to new operating conditions of the wind turbine or the air flow, when actually it takes a while to adjust to a changing wake. Furthermore, the original theory does not take into account the skewed inflow. However, due to its wide use, different engineering models have been developed with the aim of reducing the limitations of the original theory. Therefore, the BEM method is considered a reliable method. The corrections introduced in the BEM theory used by *AERO* are the tip losses, a correction for large induced velocities or turbulent wake state and a correction for rotational stall delay.

The panel method is not as widely used in the industry because it is more complex and requires longer computing times. However, it does not make as many simplifications as the original BEM method and some of the corrections made in the BEM method such as blade tip losses and turbulent wake state are already intrinsic to the panel method. In addition, it does not require the use of experimental data on the coefficients of lift, drag and moments of the different profiles, which can be an advantage if such data is not available. However the main reason for using the panel method is its intrinsic ability to account for unsteady effects, modeling the dynamic wake effect and skewed wake aerodynamics.

4 Wind turbine model

The first wind turbine model which is going to be studied is a 5-MW reference horizontal-axis wind turbine defined by *NREL* in Jonkman et al. [20]. This wind turbine has three blades, a rotor radius of 63 m and a hub height of 90 m. And it has been adopted by many researchers as a reference for evaluating the capabilities of their aeroelastic and aerodynamic models.

In Figure 7, the geometry of the full wind turbine configuration is presented. The rotor is installed with a shaft tilt angle of 5.0° and rotates clockwise as viewed from upwind. To increase the tower clearance, the blade is set at a precone angle of 2.5°.

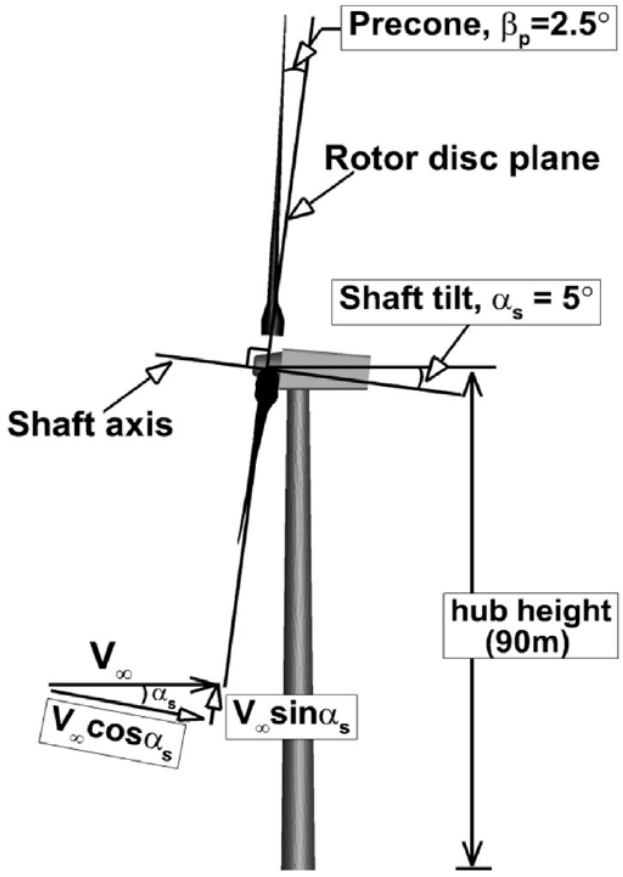

Figure 7: Modeling of the NREL 5-MW reference wind turbine (Yu and Kwon [41], 2014, p. 186).

Table 1: General data of the NREL 5-MW wind turbine.

NREL 5-MW	
Rated power	5 MW
Rotor diameter	126 m
Number of blades	3
Power control	Variable speed, collective pitch
Minimum rotor speed	6.9 rpm
Maximum rotor speed	12.1 rpm
Cut-in, Rated, Cut-Out Wind Speed	3 m/s, 11.4 m/s, 25 m/s
Hub height	90 m
Shaft tilt	5°
Precone	2.5°

After the study of the NREL 5MW, the study of a commercial Siemens wind turbine will be carried out, specifically the SWT - 2.3 - 93. This wind turbine has three blades, a rotor radius of 46.5 m and a hub height between 80 and 101 m (in this study it will be considered to be 90 m). The rated power of this wind turbine is 2.3 MW.

Figure 8: Siemens SWT-2.3-93 wind turbine.

Table 2: General data of the SWT-2.3-93 wind turbine.

SWT 2.3-93	
Rated power	2.3 MW
Rotor diameter	93 m
Number of blades	3
Power control	Variable speed, collective pitch
Minimum rotor speed	6.5 rpm
Maximum rotor speed	16 rpm
Cut-in, Rated, Cut-Out Wind Speed	3 m/s, 12 m/s, 25 m/s
Hub height	90 m
Shaft tilt	5°
Precone	2.5°

4.1 BNREL program: wind turbine models from .txt files

In order to obtain the wind turbine model in the correct format, the program *BNREL* will be used. *BNREL* is a fortran program of Samtech created by the coworker Frédéric Cugnon. This program creates the wind turbine models necessary to apply both *MECANO + AERO* method (based on the BEM theory) and *MECANO + Vortexje* method (based on the panel method), from *.txt* files with NREL format. The Figure 9 shows what the inputs and the outputs are, in addition to the routines and functions of the program.

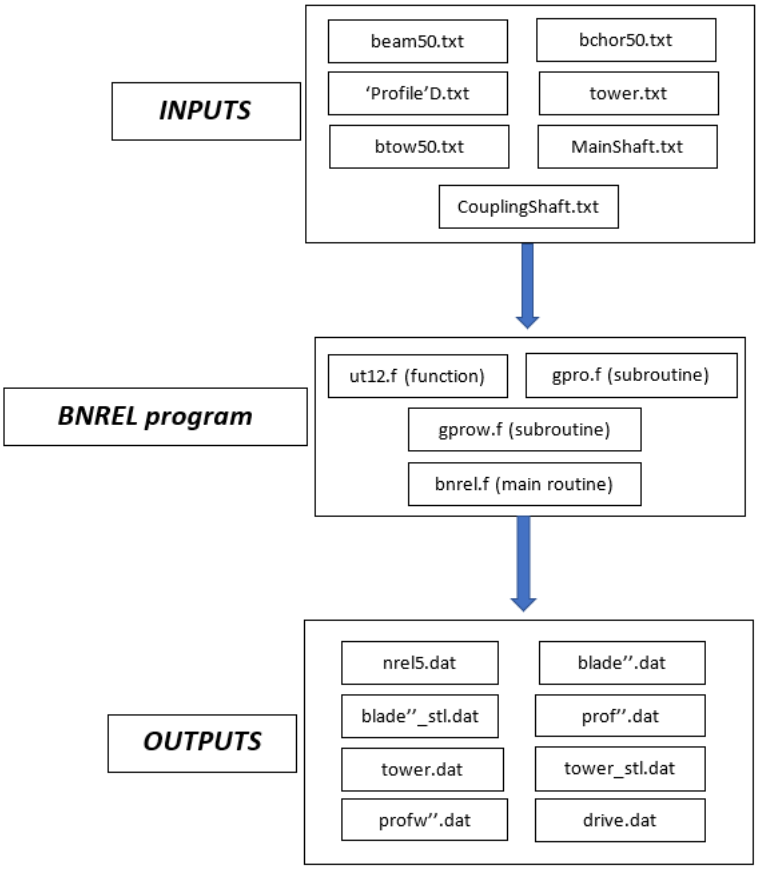

Figure 9: Diagram of BNREL program for the 5 MW NREL wind turbine.

The files that need to be read to run the program are explained below. It should be noted that the entries defined below have been extracted from Jonkman et al. [20] and some data will not be used because these files are prepared by NREL to be run with other programs. The data shown below is for the NREL 5-MW wind turbine. The data for the SWT 2.3-93 can be found in the Appendix A.

- *beam50.txt*: This file contains the information of the distributed blade structural properties. The Table 3 shows the data that the file must contain. The entries are:

  1. 'Radius': Spanwise locations along the blade-pitch axis relative to the rotor center (apex).
  2. 'BlFract': Fractional distance along the blade-pitch axis from the root (0.0) to the tip (1.0). The relation between 'Radius' and 'BlFract' is shown in the next equation:

$$Radius = RR + (DL - RR) * BlFract \tag{43}$$

where RR is the radius of the blade root and DL is the blade length.

3. 'AeroCent': By definition, the quantity (AeroCent - 0.25) is the fractional distance to the aerodynamic center from the blade-pitch axis along the chordline, positive toward the trailing edge.
4. 'StrcTwst': Structural-twist angle.
5. 'BMassDen': Distributed blade section mass per unit length.
6. 'FlpStff': Flapwise section stiffness given about the principal structural axes of each cross section as oriented by the structural-twist angle.
7. 'EdgStff': Edgewise section stiffness given about the principal structural axes of each cross section as oriented by the structural-twist angle.
8. 'GJStff': Blade torsion stiffness.
9. 'EAStff': Blade extensional stiffness.
10. 'FlpIner': Flapwise section inertia given about the principal structural axes of each cross section as oriented by the structural-twist angle.
11. 'EdgIner': Edgewise section inertia given about the principal structural axes of each cross section as oriented by the structural-twist angle.

Table 3: Distributed Blade Structural Properties of NREL 5MW (Jonkman et al. [20]).

Radius (m)	BlFract (-)	AeroCent (-)	StrcTwst (°)	BMassDen (kg/m)	FlpStff (N·m^2)	EdgStff (N·m^2)	GJStff (N·m^2)	EAStff (N)	Alpha (-)	FlpIner (kg·m)	EdgIner (kg·m)
1.50	0	0.25	13.308	678.935	1.81E+10	1.81E+10	5.56E+09	9.73E+09	0	972.86	973.04
1.70	0.00325	0.25	13.308	678.935	1.81E+10	1.81E+10	5.56E+09	9.73E+09	0	972.86	973.04
2.70	0.01951	0.24951	13.308	773.363	1.94E+10	1.96E+10	5.43E+09	1.08E+10	0	1091.52	1066.38
3.70	0.03577	0.2451	13.308	740.55	1.75E+10	1.95E+10	4.99E+09	1.01E+10	0	966.09	1047.36
4.70	0.05203	0.23284	13.308	740.042	1.53E+10	1.98E+10	4.67E+09	9.87E+09	0	873.81	1099.75
5.70	0.06829	0.22059	13.308	592.496	1.08E+10	1.49E+10	3.47E+09	7.61E+09	0	648.55	873.02
6.70	0.08455	0.20833	13.308	450.275	7.23E+09	1.02E+10	2.32E+09	5.49E+09	0	456.76	641.49
7.70	0.10081	0.19608	13.308	424.054	6.31E+09	9.14E+09	1.91E+09	4.97E+09	0	400.53	593.73
8.70	0.11707	0.18382	13.308	400.638	5.53E+09	8.06E+09	1.57E+09	4.49E+09	0	351.61	547.18
9.70	0.13335	0.17156	13.308	382.062	4.98E+09	6.88E+09	1.16E+09	4.03E+09	0	316.12	490.84
10.70	0.14959	0.15931	13.308	399.655	4.94E+09	7.01E+09	1.00E+09	4.04E+09	0	303.6	503.86
11.70	0.16585	0.14706	13.308	426.321	4.69E+09	7.17E+09	8.56E+08	4.17E+09	0	289.24	544.7
12.70	0.18211	0.13481	13.181	416.82	3.95E+09	7.27E+09	6.72E+08	4.08E+09	0	246.57	569.9
13.70	0.19837	0.125	12.848	406.186	3.39E+09	7.08E+09	5.47E+08	4.09E+09	0	215.91	601.28
14.70	0.21465	0.125	12.192	381.42	2.93E+09	6.24E+09	4.49E+08	3.67E+09	0	187.11	546.56
15.70	0.23089	0.125	11.561	352.822	2.57E+09	5.05E+09	3.36E+08	3.15E+09	0	160.84	468.71
16.70	0.24715	0.125	11.072	349.477	2.39E+09	4.95E+09	3.11E+08	3.01E+09	0	148.56	453.76
17.70	0.26341	0.125	10.792	346.538	2.27E+09	4.81E+09	2.92E+08	2.88E+09	0	140.3	436.22
19.70	0.29595	0.125	10.232	339.333	2.05E+09	4.50E+09	2.61E+08	2.61E+09	0	124.61	398.18
21.70	0.32846	0.125	9.672	330.004	1.83E+09	4.24E+09	2.29E+08	2.36E+09	0	109.42	362.08
23.70	0.36098	0.125	9.11	321.99	1.59E+09	4.00E+09	2.01E+08	2.15E+09	0	94.36	335.01
25.70	0.3935	0.125	8.534	313.82	1.36E+09	3.75E+09	1.74E+08	1.94E+09	0	80.24	308.57
27.70	0.42602	0.125	7.932	294.734	1.10E+09	3.45E+09	1.44E+08	1.63E+09	0	62.67	263.87
29.70	0.45855	0.125	7.321	287.12	8.76E+08	3.14E+09	1.20E+08	1.43E+09	0	49.42	237.06
31.70	0.49106	0.125	6.711	263.343	6.81E+08	2.73E+09	8.12E+07	1.17E+09	0	37.34	196.41
33.70	0.52358	0.125	6.122	253.207	5.35E+08	2.55E+09	6.91E+07	1.05E+09	0	29.14	180.34
35.70	0.5561	0.125	5.546	241.666	4.09E+08	2.33E+09	5.75E+07	9.23E+08	0	22.16	162.43
37.70	0.58862	0.125	4.971	220.638	3.15E+08	1.83E+09	4.59E+07	7.61E+08	0	17.33	134.83
39.70	0.62115	0.125	4.401	200.293	2.39E+08	1.58E+09	3.60E+07	6.48E+08	0	13.3	116.3
41.70	0.65366	0.125	3.834	179.404	1.76E+08	1.32E+09	2.74E+07	5.40E+08	0	9.96	97.98
43.70	0.68618	0.125	3.332	165.094	1.26E+08	1.18E+09	2.09E+07	5.31E+08	0	7.3	98.93
45.70	0.7187	0.125	2.89	154.411	1.07E+08	1.02E+09	1.85E+07	4.60E+08	0	6.22	85.78
47.70	0.75122	0.125	2.503	138.935	9.09E+07	7.98E+08	1.63E+07	3.76E+08	0	5.19	69.96
49.70	0.78376	0.125	2.116	129.555	7.63E+07	7.10E+08	1.45E+07	3.29E+08	0	4.36	61.41
51.70	0.81626	0.125	1.73	107.264	6.11E+07	5.18E+08	9.07E+06	2.44E+08	0	3.36	45.44
53.70	0.84878	0.125	1.342	98.776	4.95E+07	4.55E+08	8.06E+06	2.12E+08	0	2.75	39.57
55.70	0.8813	0.125	0.954	90.248	3.94E+07	3.95E+08	7.08E+06	1.82E+08	0	2.21	34.09
56.70	0.89756	0.125	0.76	83.001	3.47E+07	3.54E+08	6.09E+06	1.60E+08	0	1.93	30.12
57.70	0.91382	0.125	0.574	72.906	3.04E+07	3.05E+08	5.75E+06	1.09E+08	0	1.69	20.15
58.70	0.93008	0.125	0.404	68.772	2.65E+07	2.81E+08	5.33E+06	1.00E+08	0	1.49	18.53
59.20	0.93821	0.125	0.319	66.264	2.38E+07	2.62E+08	4.94E+06	9.22E+07	0	1.34	17.11
59.70	0.94636	0.125	0.253	59.34	1.96E+07	1.59E+08	4.24E+06	6.32E+07	0	1.1	11.55
60.20	0.95447	0.125	0.216	55.914	1.60E+07	1.38E+08	3.66E+06	5.33E+07	0	0.89	9.77
60.70	0.9626	0.125	0.178	52.484	1.28E+07	1.19E+08	3.13E+06	4.45E+07	0	0.71	8.19
61.20	0.97073	0.125	0.14	49.114	1.01E+07	1.02E+08	2.64E+06	3.69E+07	0	0.56	6.82
61.70	0.97886	0.125	0.101	45.818	7.55E+06	8.51E+07	2.17E+06	2.99E+07	0	0.42	5.57
62.20	0.98699	0.125	0.062	41.669	4.60E+06	6.43E+07	1.58E+06	2.13E+07	0	0.25	4.01
62.70	0.99512	0.125	0.023	11.453	2.50E+05	6.61E+06	2.50E+05	4.85E+06	0	0.04	0.94
63.00	1	0.125	0	10.319	1.70E+05	5.01E+06	1.90E+05	3.53E+06	0	0.02	0.68

- *bchor50.txt*: This file contains the information of the distributed blade aerodynamic properties. The Table 4 shows the data that the file must contain. The entries are:

  1. 'RNodes': Spanwise locations along the blade-pitch axis relative to the rotor center (apex). If the locations here are different from the *beam50.txt*, the data will be interpolated.
  2. 'AeroTwst': Aerodynamic-twist angle. The values of the structural twist are as-

sumed to be identical to the aerodynamic twist. This column will not be used by *BNREL* program.

3. 'DRNodes': This data is not used by *BNREL* program.
4. 'Chord': Chord of the section. The chord in other locations will be calculated interpolating between these values.
5. 'Nfoil': Number of profile.
6. 'PrnElm': Name of the file which contains the normalized coordinates of the profile.

Table 4: Distributed Blade Aerodynamic Properties of NREL 5MW (Jonkman et al. [20]).

RNodes (m)	AeroTwst (°)	DRNodes (m)	Chord (m)	NFoil	PrnElm
2.8667	13.308	2.7333	3.542	1	CYLD.txt
5.6	13.308	2.7333	3.854	1	CYLD.txt
8.3333	13.308	2.7333	4.167	2	CYLD.txt
11.75	13.308	4.1	4.557	3	DU40_A17D.txt
15.85	11.48	4.1	4.652	4	DU35_A17D.txt
19.95	10.162	4.1	4.458	4	DU35_A17D.txt
24.05	9.011	4.1	4.249	5	DU30_A17D.txt
28.15	7.795	4.1	4.007	6	DU25_A17D.txt
32.25	6.544	4.1	3.748	6	DU25_A17D.txt
36.35	5.361	4.1	3.502	7	DU21_A17D.txt
40.45	4.188	4.1	3.256	7	DU21_A17D.txt
44.55	3.125	4.1	3.01	8	NACA64_A17D.txt
48.65	2.319	4.1	2.764	8	NACA64_A17D.txt
52.75	1.526	4.1	2.518	8	NACA64_A17D.txt
56.1667	0.863	2.7333	2.313	8	NACA64_A17D.txt
58.9	0.37	2.7333	2.086	8	NACA64_A17D.txt
61.6333	0.106	2.7333	1.419	8	NACA64_A17D.txt
63	0.106	0	1	8	NACA64_A17D.txt

- *'profile'D.txt*: There are as many files of this type as there are profiles on the wind turbine blade. These files contain the normalized coordinates of the profile.
- *tower.txt*: This file contains the information of the distributed tower structural properties. This file is similar to *beam50.txt*. The entries are:

1. 'Elevation': Vertical locations along the tower relative to the tower base.
2. 'HtFract': Fractional height along the tower centerline from the tower base (0.0) to the tower top (1.0).
3. 'TMassDen': Distributed tower section mass per unit length.

4. 'TwFAStif': Fore-aft direction stiffness.
5. 'TwSSStff':Side-side direction stiffness.
6. 'TwGJStif': Tower torsion stiffness.
7. 'TwEAStif': Tower extensional stiffness.
8. 'TwFAIner': Fore-aft direction inertia.
9. 'TwSSIner': Side-side direction inertia.

Table 5: Distributed Tower Structural Properties of NREL 5MW (Jonkman et al. [20]).

Elevation (m)	HtFract (-)	TMassDen (kg/m)	TwFAStif ($N \cdot m^2$)	TwSSStif ($N \cdot m^2$)	TwGJStif ($N \cdot m^2$)	TwEAStif (N)	TwFAIner (kg•m)	TwSSIner (kg•m)	TwFAcgOf (m)	TwSScgOf (m)
0.00	0.0	5590.87	614.34E+9	614.34E+9	472.75E+9	138.13E+9	24866.3	24866.3	0.0	0.0
8.76	0.1	5232.43	534.82E+9	534.82E+9	411.56E+9	129.27E+9	21647.5	21647.5	0.0	0.0
17.52	0.2	4885.76	463.27E+9	463.27E+9	356.50E+9	120.71E+9	18751.3	18751.3	0.0	0.0
26.28	0.3	4550.87	399.13E+9	399.13E+9	307.14E+9	112.43E+9	16155.3	16155.3	0.0	0.0
35.04	0.4	4227.75	341.88E+9	341.88E+9	263.09E+9	104.45E+9	13838.1	13838.1	0.0	0.0
43.80	0.5	3916.41	291.01E+9	291.01E+9	223.94E+9	96.76E+9	11779.0	11779.0	0.0	0.0
52.56	0.6	3616.83	246.03E+9	246.03E+9	189.32E+9	89.36E+9	9958.2	9958.2	0.0	0.0
61.32	0.7	3329.03	206.46E+9	206.46E+9	158.87E+9	82.25E+9	8356.6	8356.6	0.0	0.0
70.08	0.8	3053.01	171.85E+9	171.85E+9	132.24E+9	75.43E+9	6955.9	6955.9	0.0	0.0
78.84	0.9	2788.75	141.78E+9	141.78E+9	109.10E+9	68.90E+9	5738.6	5738.6	0.0	0.0
87.60	1.0	2536.27	115.82E+9	115.82E+9	89.13E+9	62.66E+9	4688.0	4688.0	0.0	0.0

- *btow50.txt*: This file contains the information of the distributed tower aerodynamic properties. The entries of this file are the same as in *bchor50.txt*.

Table 6: Distributed Tower Aerodynamic Properties of NREL 5MW.

Rnodes (m)	AeroTwst (°)	DRNodes (m)	Chord (m)	Nfoil	Pname
0	0	555	3.87	1	CYLD.txt
80	0	555	6	1	CYLD.txt
180	0	555	6	1	CYLD.txt

- *MainShaft.txt*: This file contains the information of the distributed main shaft properties. The entries are:

1. 'ShFract': Fractional distance along the rotor axis.
2. 'ExtRad': External radius.
3. 'IntRad': Internal radius.
4. 'YT': Young module.

5. 'NT': Poisson coefficient.
6. 'M': Mass density.

Table 7: Distributed Main shaft Properties of NREL 5MW.

ShFract	ExtRad (m)	IntRad (m)	YT (Pa)	NT	M
0	0.5	0.025	2E+11	0.3	7800
0.2	0.5	0.025	2E+11	0.3	7800
0.4	0.5	0.025	2E+11	0.3	7800
0.6	0.5	0.025	2E+11	0.3	7800
0.8	0.5	0.025	2E+11	0.3	7800
1	0.5	0.025	2E+11	0.3	7800

- *CouplingShaft.txt*: This file contains the information of the distributed coupling shaft properties.The entries of this file are the same as in *MainShaft.txt*.

Table 8: Distributed Coupling shaft Properties of NREL 5MW.

ShFract	ExtRad (m)	IntRad (m)	YT (Pa)	NT	M
0	0.12	0.0025	2E+11	0.3	7800
0.5	0.12	0.0025	2E+11	0.3	7800
1	0.12	0.0025	2E+11	0.3	7800

The files which contains the routines and functions that make up the program are:

- *bnrel.f*: This file is the main routine of the program. It provides the turbine model files necessary to apply the *MECANO + AERO* method and the turbine model files necessary to apply the *MECANO + Vortexje* coupling method.
- *gpro.f*: This file is a subroutine. It creates the profiles files (*.dat*) along the blade with dimensional values from the files *'profile'D.txt*, which as mentioned above, contain the normalized coordinates of the profile.
- *gprow.f*: This file is another subroutine and it has the same aim as *gpro.f* but for the tower.
- *ut12.f*: This file is a function to know the actual length of a chain of characters.

4.2 Structural model: *MECANO* solver

For the structural model of the wind turbine *MECANO* solver offers a solution based on a flexible multibody dynamic (MBD) model (Géradin and Cardona [13]). In the MBD method, the wind turbine is discretised into a number of bodies that will be interconnected: three blades, the tower and the drive. Depending on the objective of the simulation these bodies can be flexible or rigid. The dynamics of the structure can be then evaluated using equations of motion, which are usually derived from Lagrange's equations or Newton-Euler equations. The MBD method benefits from high modelling flexibility due to its capability to generate and couple together an arbitrary number of separate bodies in a single dynamic system. To obtain the discretised equations governing the wind turbine motion, a finite-element method has been adopted.

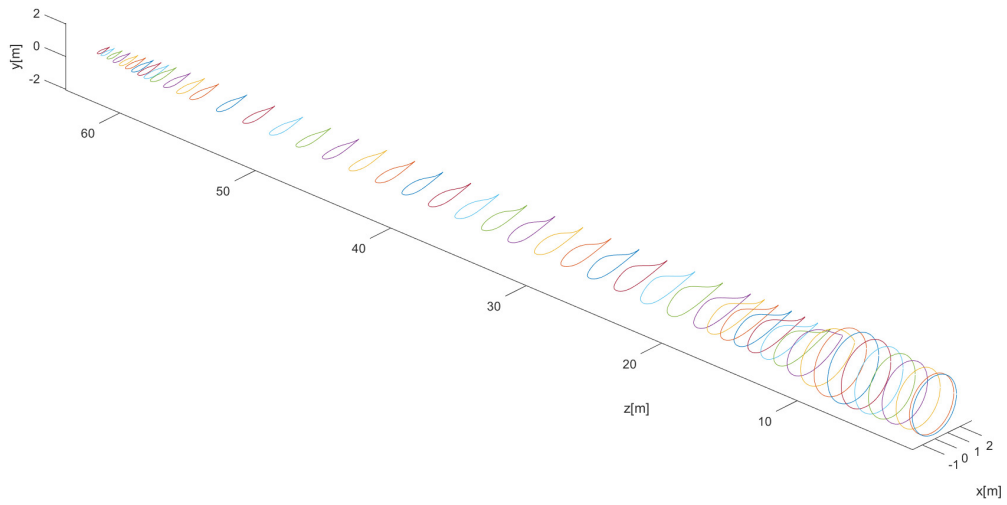

Figure 10: Spatial distribution of profiles, chord and thickness of the blade along the span for NREL 5-MW.

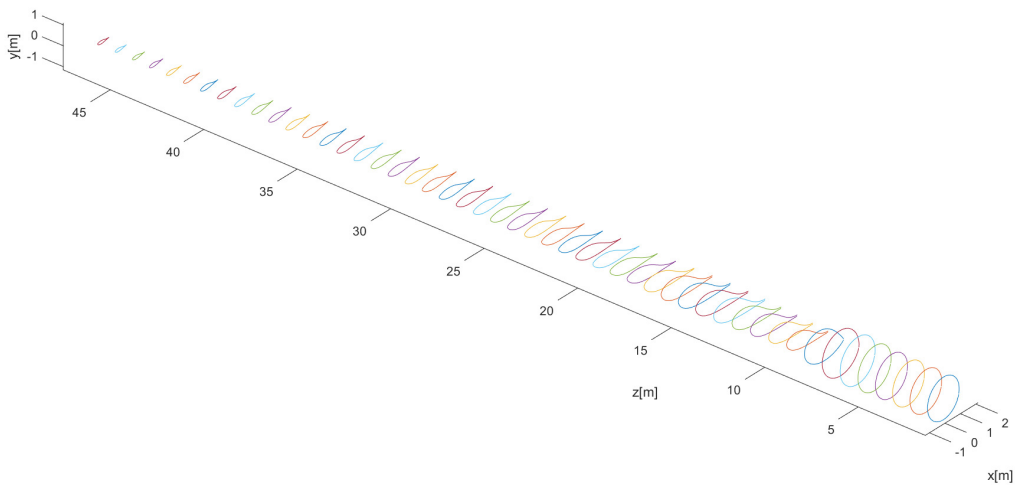

Figure 11: Spatial distribution of profiles, chord and thickness of the blade along the span for SWT 2.3-93.

Firstly, the blade is divided into a number of beam elements. It is discretised by different profiles in different positions (Figures 10 and 11) taking into account the following considerations:

- In the inner sections, thick profiles will be used, that is, with a high relative thickness, and therefore the aerodynamic characteristics will be low. The high thickness will allow a greater capacity to accommodate a large amount of structural material, with the aim of being able to withstand high structural efforts to which the blade will be subjected in that area.
- In the outer sections, thin profiles with good aerodynamic properties and high efficiencies will be used, since their structural responsibility is less and their main task is to extract power from the fluid stream.

Apart from the cylindrical profiles used in the inner sections, the profiles used in both NREL 5-MW and SWT-2.3-93 wind trurbines are:

- NREL 5MW:
  - DU40
  - DU35
  - DU30
  - DU25
  - DU21

  - NACA64

- SWT-2.3-93:
  - FFA W3 301
  - FFA W3 211

In each position it is created a node on the pitch axis. Then around this node, other nodes are introduced to represent the profile. In order to introduce rigid links between the nodes, these nodes are linked with the pitch axis node through *rigid body elements*. Then the pitch axis nodes are linked between them through *beams* with the structural properties defined previously.

Once the beam models have been defined, it is necessary to develop a model based on *quadrilateral cells* due to the nature of the forces applied when *Vortexje* is used, this is, pressure forces (Figures 12 and 13).

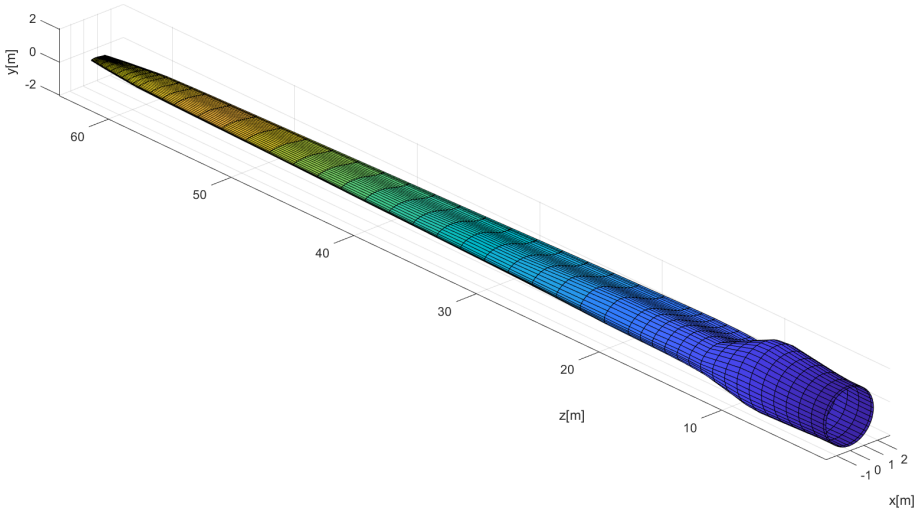

Figure 12: Model of the blade for NREL 5 MW.

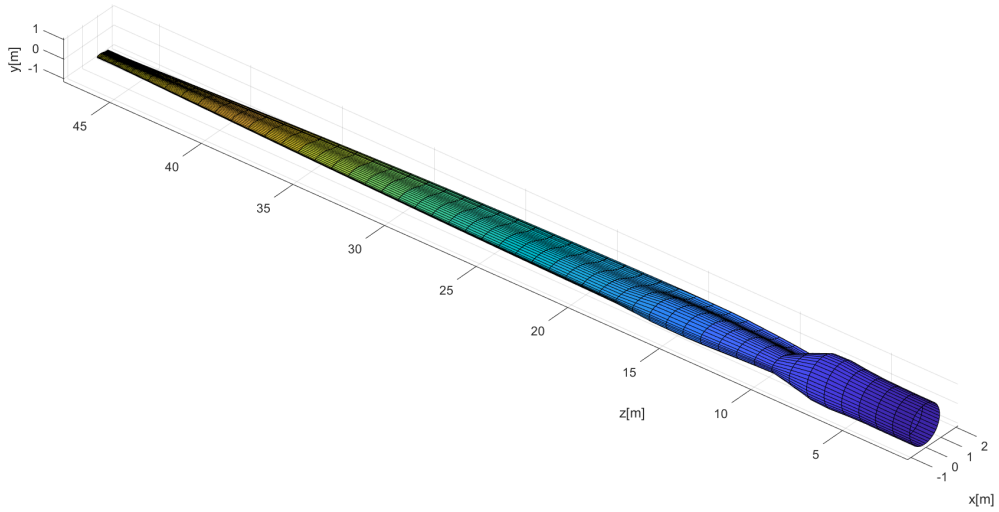

Figure 13: Model of the blade for SWT 2.3-93.

The tower is modeled in the same way as the blades (Figure 14). And finally, the shaft is modeled by *beams* with hollow and closed circle profiles.

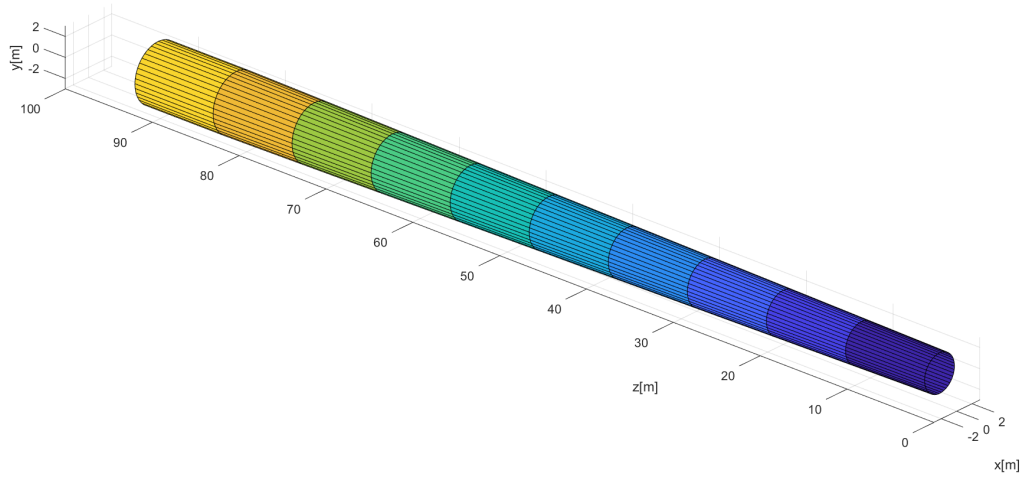

Figure 14: Model of the tower for NREL 5-MW and SWT 2.3-93.

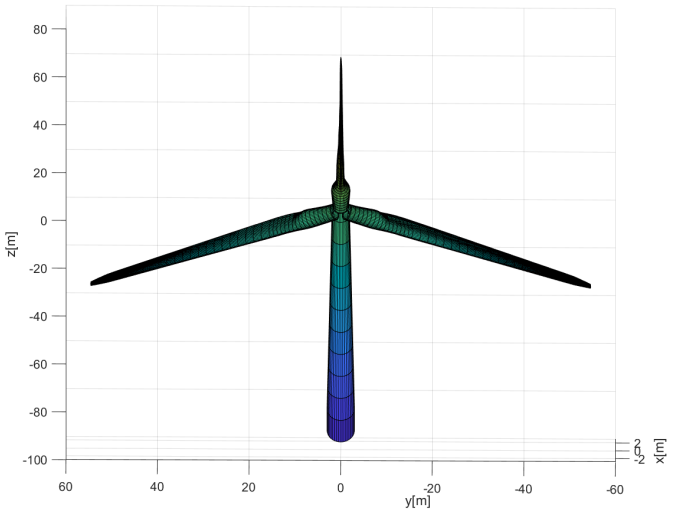

Figure 15: Model of the tower and blades for NREL 5-MW.

The rotational movement of the blades around the blade-pitch axis, the rotational movement of the rotor around the rotor axis and the rotational movement of the rotor around the axis of the tower (yaw) are modeled by *hinge joints*.

The equations of motion of the articulated structure discretised by finite elements take the general form:

$$[M]\{\ddot{q}\} + \{g^{int}\} = \{g^{ext}\} \tag{44}$$

where the notation is simplified by including in the internal forces g^{int} the contribution of the kinematic constraints and that of elastic, plastic, damping, friction, ..., forces.

Three type of analysis can be performed:

- static analysis
- kinematic or quasi-static analysis
- dynamic analysis.

At each time step, a set of non-linear equations has to be solved. These equations express the equilibrium of the system at a given time. In a static analysis, these equations take stiffness effects (linear or not) into account. In a kinematic analysis, the effects due to kinematic velocities are added to the effects taken into account by the static analysis. Finally, the dynamic analysis takes all the effects of the kinematic analysis into account including also inertia effects, which are absent in the static and the kinematic analysis.

A Newton-Raphson strategy (true or modified) is used in order to solve this non-linear problem. The modified strategy consists in suppressing the updating of the structural iteration matrix to reduce the CPU consumption. This suppression is decided automatically by the program if the convergence rate is good enough.

The assembled mass matrix $[M]$ is singular, what leads to having to adopt an implicit method of solution for time integration of equations of motion. *MECANO* allows to choose the follow methods:

- Newmark implicit predictor-corrector scheme (Newmark [28])
- Hilber-Hughes-Taylor implicit predictor-corrector scheme (Hughes et al. [17])
- Generalized midpoint method
- Chung Hulbert scheme (Hulbert and Chung [18])
- Generalized-α scheme (Arnold and Brüls [2])

In this project, the Generalized-α scheme developed in Arnold and Brüls [2] has been used. In order to explain it, firstly the one-step method of Newmark will be outlined.

4.2.0.1 Newmark method

It consists in calculating the displacements, velocities, and accelerations at time t_{n+1} in terms of the same quantities at time t_n from a Taylor series expansion limited to 2nd order:

$$\{q_{n+1}\} = \{q_n\} + \Delta t\,\{\dot{q}_n\} + \left(\frac{1}{2} - \beta\right)\Delta t^2\{\ddot{q}_n\} + \beta\Delta t^2\{\ddot{q}_{n+1}\} \tag{45}$$

$$\{\dot{q}_{n+1}\} = \{\dot{q}_n\} + (1-\gamma)\,\Delta t\{\ddot{q}_n\} + \gamma\Delta t\{\ddot{q}_{n+1}\} \tag{46}$$

where β and γ are two free parameters of the method. The usual values given to these parameters to obtain an implicit scheme are:

- $\beta = \frac{1}{4}$ and $\gamma = \frac{1}{2}$ corresponds to the assumption of average constant acceleration over the time step. This set of values provides the Newmark unconditional scheme with maximum accuracy.
- $\beta = \frac{1}{6}$ and $\gamma = \frac{1}{2}$ corresponds to the assumption of linear acceleration over the time step.

The implicit method implies solving the system of equations of motion expressed at time t_{n+1}. To this purpose, the Newmark formula is used to express the acceleration $\{\ddot{q}_{n+1}\}$ in terms of $\{q_n\}$, $\{\dot{q}_n\}$, $\{\ddot{q}_n\}$ and $\{q_{n+1}\}$.

$$\frac{[M]}{\beta\,\Delta t^2}\{q_{n+1}\} + \{g^{int}_{n+1}\} = \{g^{ext}_{n+1}\} + \frac{[M]}{\beta\,\Delta t^2}\left[\{q_n\} + \Delta t\{\dot{q}_n\} + \left(\frac{1}{2} - \beta\right)\Delta t^2\{\ddot{q}_n\}\right] \tag{47}$$

This equation, with known right-hand side, is non-linear in $\{q_{n+1}\}$ through the term of internal forces. It is thus solved iteratively using the Newton-Raphson method, which consists in calculating an improved approximation from an initial approximation:

$$\{^{i+1}q_{n+1}\} = \{^{i}q_{n+1}\} + \{^{i}\Delta q\} \tag{48}$$

and also,

$$\{^{i+1}g^{int}_{n+1}\} = \{^{i}g^{int}_{n+1}\} + \{^{i}\Delta g\} = \{^{i}g^{int}_{n+1}\} + \left[\frac{\partial\{^{i}g^{int}_{n+1}\}}{\partial\{^{i}q_{n+1}\}} + \frac{\partial\{^{i}g^{int}_{n+1}\}}{\partial\{^{i}\dot{q}_{n+1}\}}\frac{\partial\{^{i}\dot{q}_{n+1}\}}{\partial\{^{i}q_{n+1}\}}\right]\{^{i}\Delta q\} \tag{49}$$

with the tangent stiffness and damping matrices

$$[K_T] = \frac{\partial\{g^{int}\}}{\partial\{q\}} \tag{50}$$

$$[C] = \frac{\partial\{g^{int}\}}{\partial\{\dot{q}\}} \tag{51}$$

by solving the linear system:

$$\left[\frac{[M]}{\beta\,\Delta t^2} + \frac{[C]\gamma}{\beta\,\Delta t} + [K_T]\right]\{^{i}\Delta q\} = \{^{i}R_{n+1}\} \tag{52}$$

and the residual vector:

$$\{^{i}R_{n+1}\} = \{g^{ext}_{n+1}\} + \frac{[M]}{\beta\,\Delta t^2}\left[\{q_n\} + \Delta t\{\dot{q}_n\} + \left(\frac{1}{2} - \beta\right)\Delta t^2\{\ddot{q}_n\}\right] - \{^{i}g^{int}_{n+1}\} - \frac{[M]}{\beta\,\Delta t^2}\{^{i}q_{n+1}\} \tag{53}$$

This iteration is continued until the dynamic equilibrium is satisfied in d'Alembert's sense.

4.2.0.2 Generalized-α method

The Generalized-α scheme (Arnold and Brüls [2]) is obtained using a vector $\{a\}$ of acceleration-like variables in the Newmark integration formula.

$$\{q_{n+1}\} = \{q_n\} + \Delta t\,\{\dot{q}_n\} + \left(\frac{1}{2} - \beta\right)\Delta t^2\{a_n\} + \beta\Delta t^2\{a_{n+1}\} \tag{54}$$

$$\{\dot{q}_{n+1}\} = \{\dot{q}_n\} + (1-\gamma)\,\Delta t\{a_n\} + \gamma\Delta t\{a_{n+1}\} \tag{55}$$

Those additional variables are related to the accelerations by the following equation:

$$(1 - \alpha_m)\{a_{n+1}\} + \alpha_m\{a_n\} = (1 - \alpha_f)\{\ddot{q}_{n+1}\} + \alpha_f\{\ddot{q}_n\} \tag{56}$$

where optimal algorithmic parameters for second-order ODEs are:

$$\alpha_m = \frac{2\rho_\infty - 1}{\rho_\infty + 1} \tag{57}$$

$$\alpha_f = \frac{\rho_\infty}{\rho_\infty + 1} \tag{58}$$

$$\gamma = 0.5 + \alpha_f - \alpha_m \tag{59}$$

$$\beta = 0.25\,(\gamma + 0.5) \tag{60}$$

This procedure allows to introduce some numerical damping in the high frequency spectrum of the system under consideration. This numerical damping has a stabilizing effect on the time integration procedure while guaranteeing very good accuracy of integration of the low frequency range (including rigid body motion in particular). Compare to Hilber-Hughes-Taylor [17] and Chung-Hulbert [18], this scheme enforce exactly equilibrium at every time step, which guaranty second-order accuracy also for the accelerations and less sensitivity to variable time steps.

Damping is controlled by the spectral radius at infinity ρ_∞: an undamped scheme is characterized by $\rho_\infty = 1$, while $\rho_\infty = 0$ provides asymptotic annihilation of the high frequency response.

4.3 Aerodynamic model

4.3.1 *AERO* method

To compute aerodynamic loads on both blade and tower of the wind turbine, *Samtech* offers an in-house module based on BEM theory. It does this by dividing the blade into a number of

AERO elements along the span of the blade. It calculates the forces for each segment, which are used by the structural program to calculate the wind turbine deflections and vice versa, making the interaction fully aeroelastic.

The files that make up the wind turbine model (structure + aerodynamic model) and that are necessary to run the simulation with *MECANO* are shown in the diagram of the Figure 16.

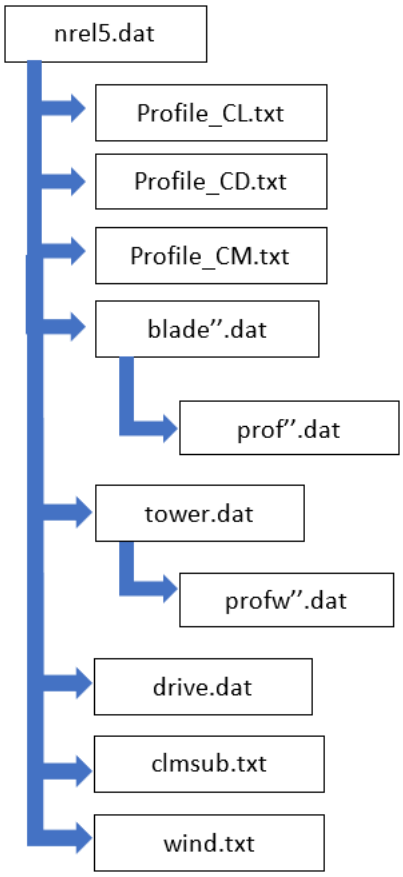

Figure 16: Diagram of the files of the wind turbine model for *AERO* method.

- *prof''.dat*: It creates the nodes of the profiles of the blade and the *rigid body elements* between these nodes and the pitch axis nodes.
- *profw''.dat*: It creates the nodes of the profiles of the tower and the *rigid body elements* between these nodes and the pitch axis nodes.
- *blade.dat*: There is one file for each blade and it creates the beams, the cells and the *AERO* elements for the blades.
- *tower.dat*: It creates the beams, the cells and the *AERO* elements for the tower.

- *drive.dat*: It creates the beams to model the shaft.
- *Profile_CL.txt*: These files contain the lift coefficient of the profile based on angle of attack.
- *Profile_CD.txt*: These files contain the drag coefficient of the profile based on angle of attack.
- *Profile_CM.txt*: These files contain the moment coefficient of the profile based on angle of attack.
- *wind.dat*:It contains the wind function.
- *clmsub.dat*: It assigns the mechanical boundary conditions to the existing mesh.
- *nrel5.dat*: This is the main file and it joins the wind turbine elements by hinge joints.

Due to the introduction of the *AERO* elements, it is necessary to incorporate files that contain the aerodynamic coefficients of the profiles. Usually the available experimental information on the aerodynamic coefficients of the profiles is limited to a number of angles of attack. For this reason, this information must be extrapolated to the whole range of angles of attack. Firstly, according to Kooijman [22] the experimental data were extended to -180^{o} and 180^{o} using results from the ECN tool StC (Stall Coefficients) for an aspect ratio of 17 (Lindenburg [24]). Then, according to Jonkman et al. [20] these coefficients have been corrected by making corrections for three-dimensional behaviour. "The lift and drag coefficients have been corrected for rotational stall delay using Selig and Eggars method for 0^{o} to 90^{o} angles of attack, and then the drag coefficients have been corrected using Viterna method for 0^{o} to 90^{o} angles of attack" (Jonkman et al. [20], 2009, p. 8).

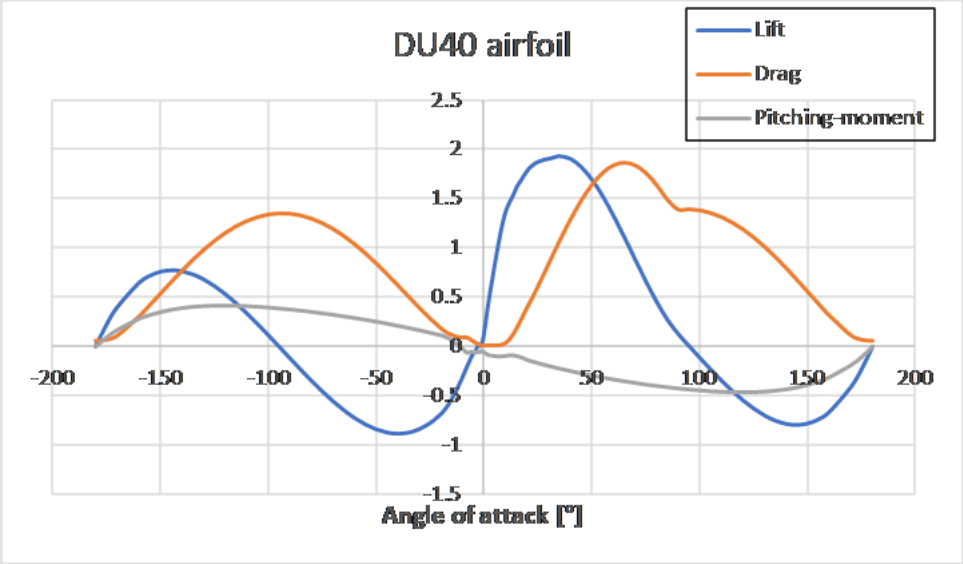

Figure 17: Corrected coefficients of the DU40 airfoil.

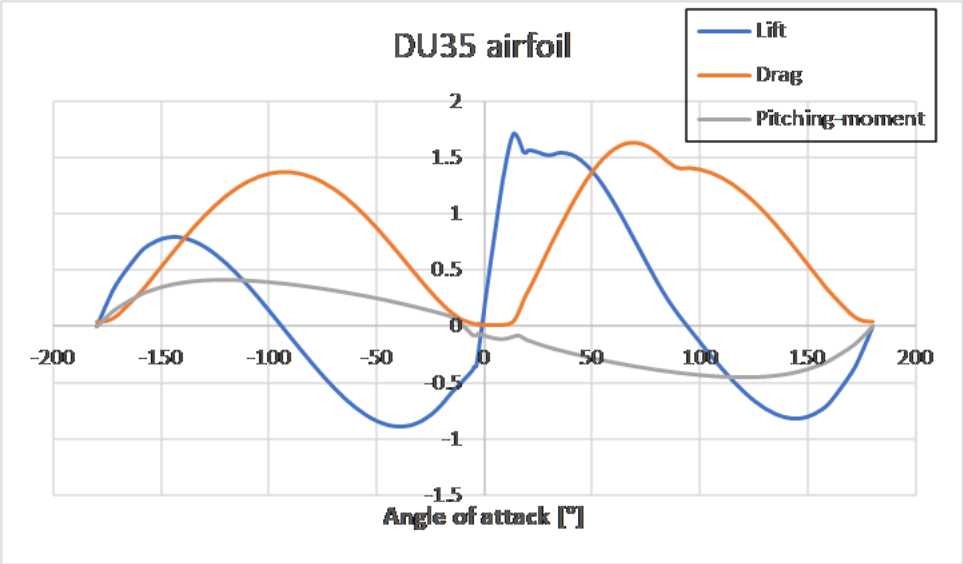

Figure 18: Corrected coefficients of the DU35 airfoil.

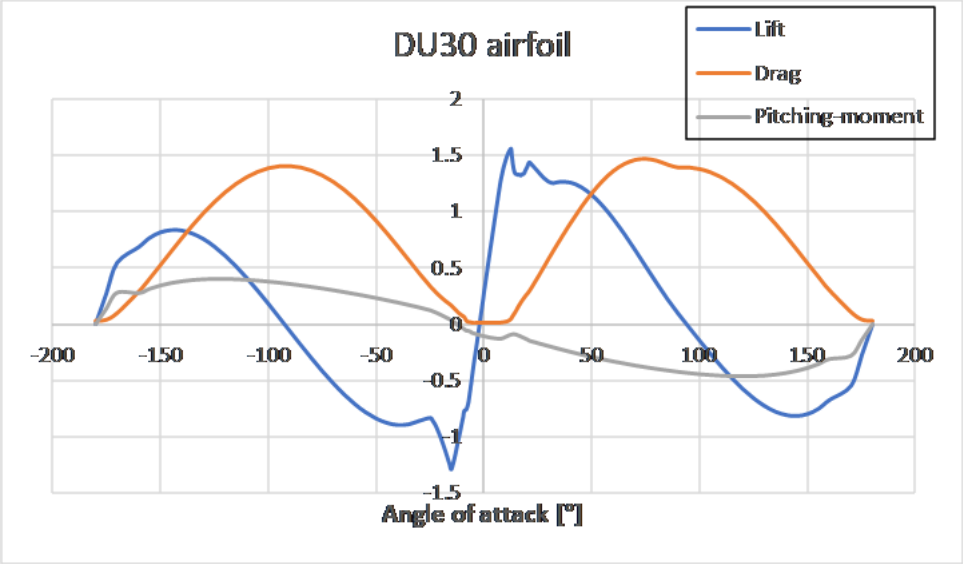

Figure 19: Corrected coefficients of the DU30 airfoil.

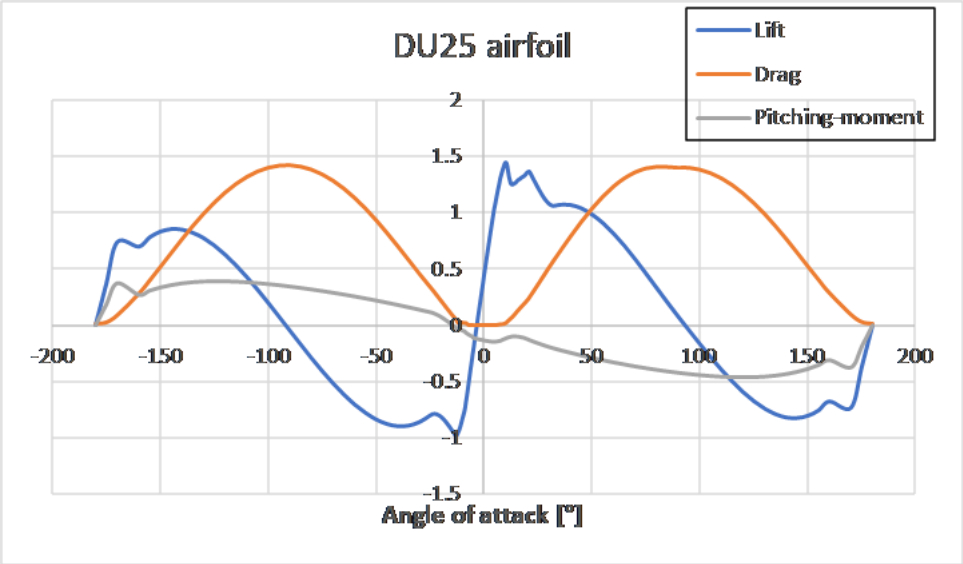

Figure 20: Corrected coefficients of the DU25 airfoil.

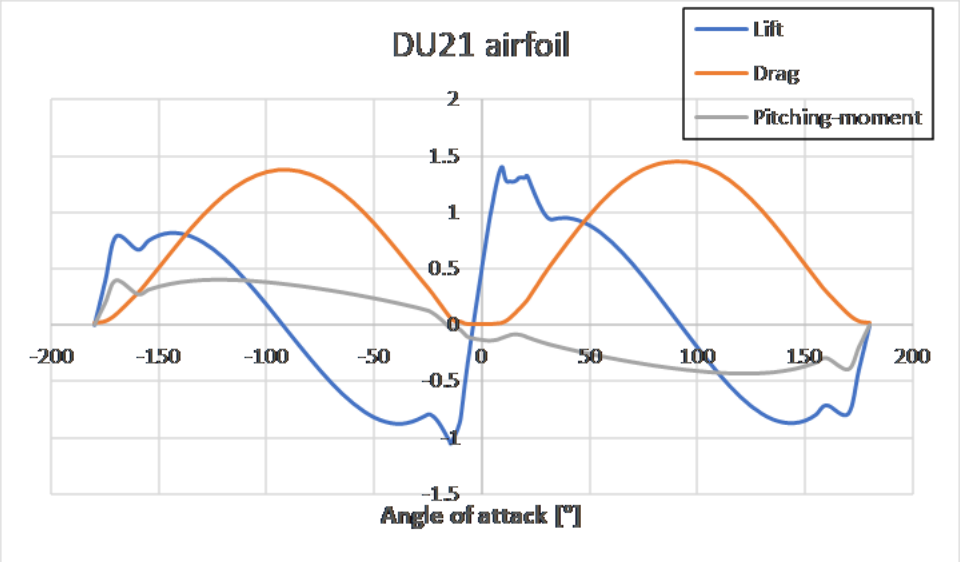

Figure 21: Corrected coefficients of the DU21 airfoil.

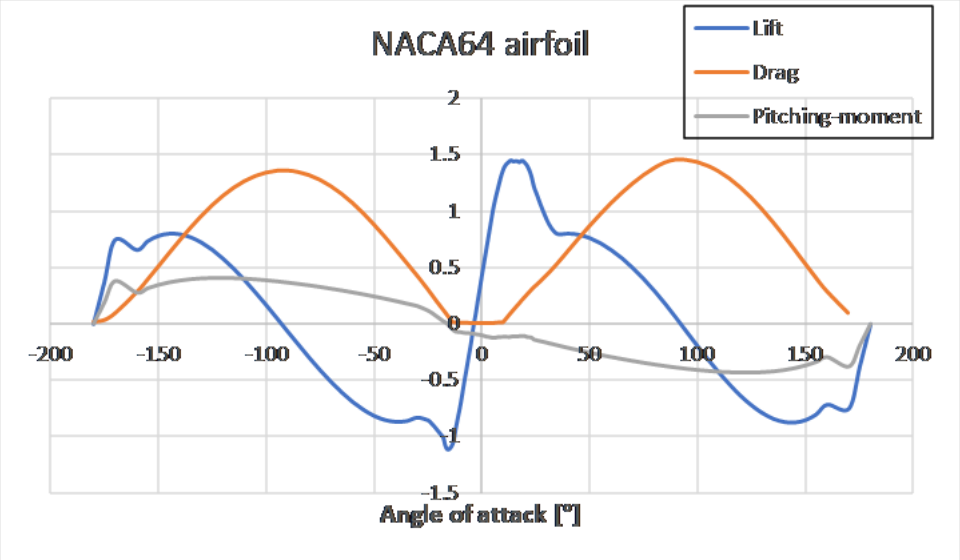

Figure 22: Corrected coefficients of the NACA64 airfoil.

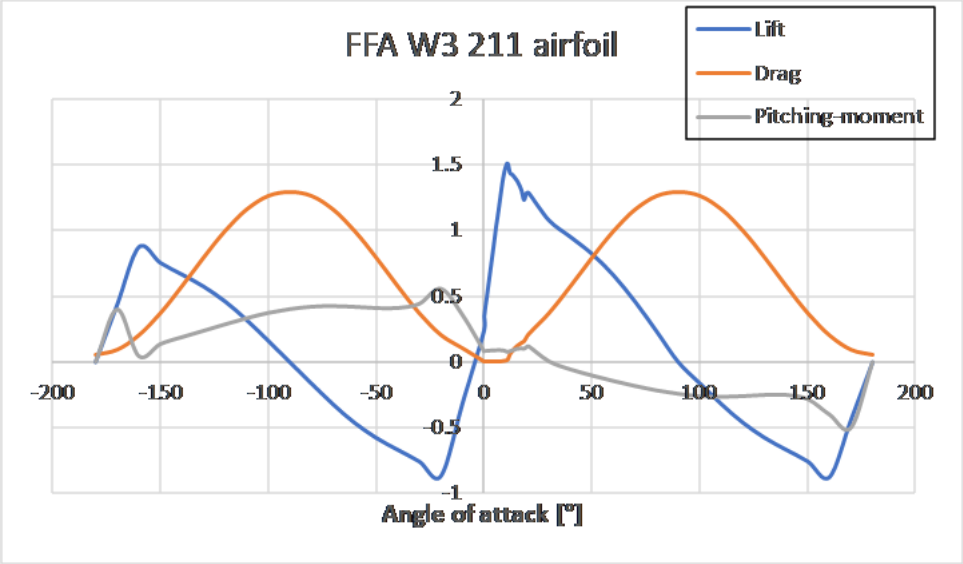

Figure 23: Corrected coefficients of the FFA W3 211 airfoil.

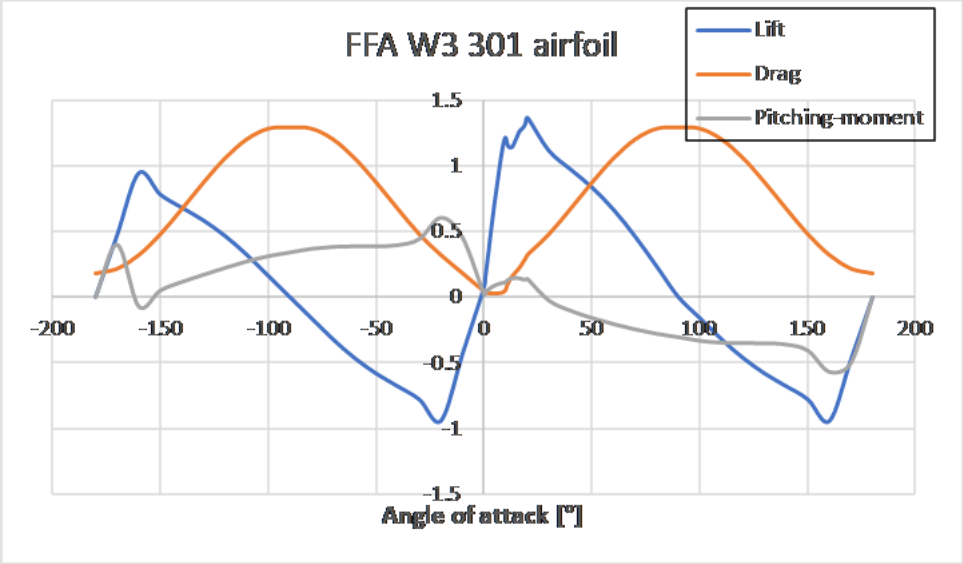

Figure 24: Corrected coefficients of the FFA W3 301 airfoil.

4.3.2 Panel method: *Vortexje*

To predict aerodynamic forces in a wider range of flow conditions it has been used *Vortexje* (Baayen [3]). *Vortexje* is an open source that allows the application of the 3D panel method based on sources and doublets for the simulation of aerodynamic loads on a dynamic system. The calculation of aerodynamic forces and moments is given by the orientation of the blades

in the flow, the shape of the blades and their interaction with the wake.

The main advantage that the panel method has over CFD is the computational cost. The solution of the panel method equations only requires meshing the 2D surface (wake and bodies immersed in the flow), while the numerical solution of the Navier-Stokes equations requires 3D meshing of the entire region of the flow, increasing considerably the computational cost.

On the other hand, as previously indicated in the Section 3.3.2, the method considers non-viscous, incompressible and irrotational fluid, which limits its applicability to subsonic cases at angles of attack in which there is no flow separation. Furthermore, the implemented method does not allow to calculate the viscous forces, although there are ways to incorporate these viscous effects.

The basic ideas of the panel method have been outlined in the Section 3.3.2. In order to apply the panel method in a computer, the blade and its wake are discretised into a number of panels, and then, it is assigned to each panel both a source and a doublet strength, σ and μ, respectively. For the present project, each blade has been discretized with 1920 quadrilateral panels (40 panels along the chord and 48 panels along the span). To store the information, the numbering used is that shown in Figure 25. In addition to the blades, the wake is also discretized, whose number of panels increase over time. In the following, the index 'b' will be used to refer to the panels that make up the blade, while the index 'w' will be used for the panels of the wake. Moreover, a collocation point is defined in each panel at the center of the panel.

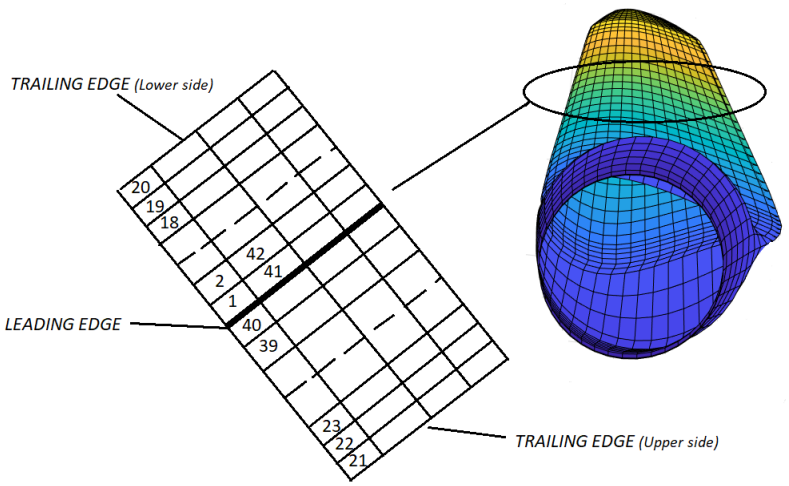

Figure 25: Numbering of the panels.

In order to solve the potential flow equations described in the Section 3.3.2, those equations will be discretized to be solved numerically. The method implemented in *Vortexje* is based on

Katz and Plotkin [21], which has been use in other previous works such as A. van Garrel [39] and Prasad and Dimitriadis [31]. From the Dirichlet boundary condition on a thick body it is obtained that the perturbation potential is zero (Katz and Plotkin [21]):

$$\varphi_\sigma + \varphi_\mu = 0 \tag{61}$$

In *Vortexje* it is assumed that source and doublet strengths are constant in each panel. So taking into account Equations 26 and 27, the follow equation is obtained which will be evaluated for each collocation point:

$$\sum_{b=1}^{N_b} A_{i,b}\,\mu_b + \sum_{wt=1}^{N_{wt}} A_{i,wt}\,\mu_{wt} + \sum_{b=1}^{N_b} B_{i,b}\,\sigma_b = 0 \tag{62}$$

$$[A]_{(N_b,N_b)}\,\{\mu_b\}_{N_b} + [A_{wt}]_{(N_b,N_{wt})}\,\{\mu_{wt}\}_{N_{wt}} + [B]_{(N_b,N_b)}\,\{\sigma_b\}_{N_b} = 0 \tag{63}$$

where $A_{i,b}$ are the doublet influence coefficients of the blade, $A_{i,wt}$ are the doublet influence coefficients of the panels of the wake that are attached to the trailing edge and $B_{i,b}$ are the source influence coefficients, at the collocation point of panel 'i' due to panel 'b' or 'wt' :

$$A_{i,b} = \frac{-1}{4\pi} \iint_{S_b} \frac{\overline{n}\cdot\overline{r}}{r^3} dS \tag{64}$$

$$A_{i,wt} = \frac{-1}{4\pi} \iint_{S_{wt}} \frac{\overline{n}\cdot\overline{r}}{r^3} dS \tag{65}$$

$$B_{i,b} = \frac{-1}{4\pi} \iint_{S_b} \frac{1}{r} dS \tag{66}$$

in which

$$\overline{r} = \overline{x_i} - \overline{y}, \qquad \text{and} \qquad \overline{y} \in S \tag{67}$$

The integrals of Equations 64, 65 and 66 can be solved analytically following the development of Hess and Smith [16] knowing the four panel corner points of the panel 'b' or 'w', designated as $(x_1, y_1, 0)$, $(x_2, y_2, 0)$, $(x_3, y_3, 0)$ and $(x_4, y_4, 0)$, and the collocation point of the panel 'i' (x, y, z).

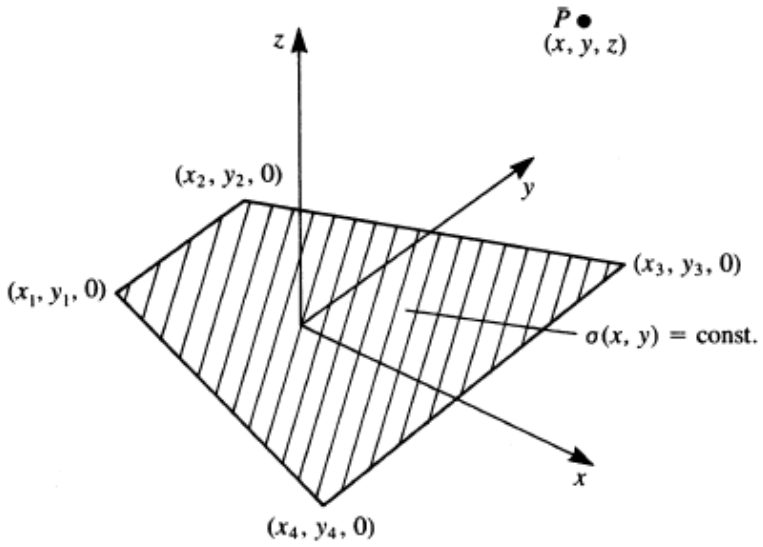

Figure 26: Quadrilateral panel with constant-strength source and doublet (Katz and Plotkin [21], 2001, p.245).

Using their results, the influence coefficients can be written as:

$$\begin{aligned} k &= 1, 2, 3, 4 \\ l &= 2, 3, 4, 1 \end{aligned}$$

$$A_{i,(b,wt)} = \frac{1}{4\pi} \sum_{k,l} \left[\tan^{-1} \left(\frac{m_{k,l} e_k - h_k}{z r_k} \right) - \tan^{-1} \left(\frac{m_{k,l} e_l - h_l}{z r_l} \right) \right] \tag{68}$$

$$\begin{aligned} B_{i,b} = \frac{-1}{4\pi} \Bigg\{ & \sum_{k,l} \left[\frac{(x - x_k)(y_l - y_k) - (y - y_k)(x_l - x_k)}{d_{k,l}} \ln \frac{r_k + r_l + d_{k,l}}{r_k + r_l - d_{k,l}} \right] \\ & - |z| \sum_{k,l} \left[\tan^{-1} \left(\frac{m_{k,l} e_k - h_k}{z r_k} \right) - \tan^{-1} \left(\frac{m_{k,l} e_l - h_l}{z r_l} \right) \right] \Bigg\} \end{aligned} \tag{69}$$

where

$$d_{k,l} = \sqrt{(x_l - x_k)^2 + (y_l - y_k)^2} \tag{70}$$

$$m_{k,l} = \frac{y_l - y_k}{x_l - x_k} \tag{71}$$

$$r_m = \sqrt{(x - x_m)^2 + (y - y_m)^2 + z^2}, \quad m = 1, 2, 3, 4 \tag{72}$$

$$e_m = (x - x_m)^2 + z^2, \quad m = 1, 2, 3, 4 \tag{73}$$

$$h_m = (x - x_m)(y - y_m), \quad m = 1, 2, 3, 4 \tag{74}$$

With these equations, the source and doublet influence coefficients are determined knowing only the geometry of the panels.

At the moment it has been only taken into account the influence of the wake panels that are attached to the trailing edge. In order to distinguish between the panels of the wake that are attached to the trailing edge and those that are not, the latter will be identified with the index w^*. According to the Equation 37, each wake panel keeps its doublet strength throughout the simulation, so the doublet strength μ_{w^*} is known from previous steps. Thus the influence of the old wake panels will be taken into account to calculate the source strength of the blade panels σ_b. Therefore, the source strength is determined through Equation 31 by adding the induced velocity by the wake panels that are not attached to the trailing edge.

$$\sigma_b = (\overline{u}_S - \overline{u}_\infty - \overline{C}_{i,w^*}\,\mu_{w^*}) \cdot \overline{n} + v_n \tag{75}$$

where $\overline{C}_{i,w^*}$ are the aerodynamic influence coefficients for the velocity induced by non-attached wake panels and they are calculated using the doublet panel - vortex ring equivalence (refs. [21] and [39]).

$$\overline{C}_{i,w^*} = \frac{-1}{4\,\pi} \int\limits_{\partial S_{w^*}} \frac{\overline{r}}{r^3} \times d\bar{l} \tag{76}$$

Knowing the four panel corner points of the panel 'wt', designated as $\overline{p}_1$, $\overline{p}_2$, $\overline{p}_3$ and $\overline{p}_4$, and the collocation point of the panel 'i' $\overline{p}_C$, Equation 76 can be written as:

$$\begin{aligned} k &= 1,\ 2,\ 3,\ 4 \\ l &= 2,\ 3,\ 4,\ 1 \end{aligned}$$

$$\overline{C}_{i,w^*} = \frac{1}{4\,\pi} \sum_{k,l} \left[\frac{\overline{r}_k \times \overline{r}_l}{|\overline{r}_k \times \overline{r}_l|^2}\, \overline{r}_0 \cdot \left(\frac{\overline{r}_k}{r_k} - \frac{\overline{r}_l}{r_l} \right) \right] \tag{77}$$

where

$$\overline{r}_k = \overline{p}_k - \overline{p}_C \tag{78}$$

$$\overline{r}_l = \overline{p}_l - \overline{p}_C \tag{79}$$

$$\overline{r}_0 = \overline{r}_l - \overline{r}_k \tag{80}$$

Once the source strength is calculated, the doublet strengths of the trailing edge wake panels can be determined according to the Morino's Kutta condition 35 by the doublet strength of the upper and lower side of the trailing edge panels μ_{bu} and μ_{bl} :

$$\mu_{wt} = \mu_{bu} - \mu_{bl} \tag{81}$$

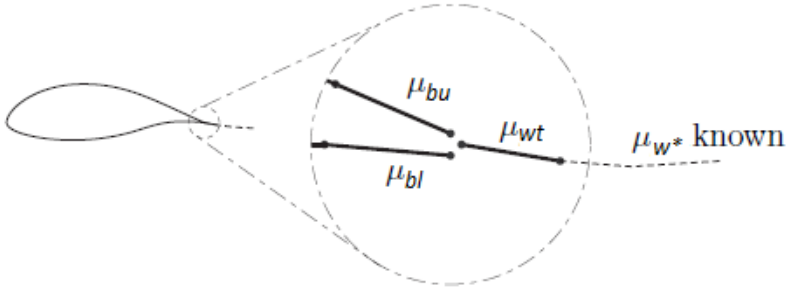

Figure 27: Numerical Kutta condition (A. van Garrel [39], 2016, p. 32

Therefore, as the doublet strengths of the trailing edge wake panels are a function of the trailing edge panels, the Equation 63 can be reordered by adding or subtracting the doublet influence coefficients of the trailing edge wake panels $A_{i,wt}$ to the the doublet influence coefficients of the trailing edge panels. Thus, using the Morino's Kutta condition, the equation that must be solve is a system of linear equations, where the unknowns are μ_b:

$$[A^*]_{(N_b,N_b)} \{\mu_b\}_{N_b} = - [B]_{(N_b,N_b)} \{\sigma_b\}_{N_b} \tag{82}$$

4.4 Coupling methodology: *MECANO- Vortexje*

In *SAMCEF*, it is possible to solve a multi-physics problem by co-simulation two single physics solvers. For the coupling of *MECANO* module and *Vortexje*, the *SAMCEF Supervisor* module will be used. The purpose of the supervisor module is to facilitate the exchange of physical data between *MECANO* and *Vortexje* modules, and the synchronization of these modules.

In order to explain how the solution schemes are implemented in the supervisor, it is assumed that the aerodynamic problem is represented by the equation $f(x, y; t) = 0$ and the structural problem is defined by $g(x, y; t) = 0$, where $x(t)$ and $y(t)$ are the solutions of the problem, that

is to say, $x(t)$ represents the panel surface pressures and $y(t)$ represents the nodal positions of the structure. The complete set of equations can be defined as:

$$F(x, y, t) = \begin{pmatrix} f(x, y; t) \\ g(x, y; t) \end{pmatrix} = \begin{pmatrix} 0 \\ 0 \end{pmatrix} \tag{83}$$

Using a time discretisation method where the time varies between 0 and t_n it will be looked for the solution $x(t)$ and $y(t)$:

$$\left\{ \begin{pmatrix} x_0 \\ y_0 \end{pmatrix}, ..., \begin{pmatrix} x_i \\ y_i \end{pmatrix}, ..., \begin{pmatrix} x_n \\ y_n \end{pmatrix} \right\} \tag{84}$$

starting with the initial conditions x_0 and y_0.

In this project, it will be used the so-called staggered solution scheme, where both fields are solved separately and data is only exchanged at the time step level. Because one of the goals of the supervisor is to couple existing programs (without direct access to the source code), it is allowed an approach where only information is exchanged at given time instances. For the staggered solution scheme, both solutions (x, y) are advanced in time using their own time integration scheme and solver, and only vector data is exchanged at defined time instances.

$$F(x, y, t) = \begin{pmatrix} f(x; y, t) \\ g(y; x, t) \end{pmatrix} = \begin{pmatrix} 0 \\ 0 \end{pmatrix} \tag{85}$$

In the above equation $f(x, y; t) = 0$ is solved for the unknown x, for a given (and fixed) value of y and t. The same is done for the equation $g(x, y; t) = 0$ for fixed values of x and t. Because at a given time the value of x or y is held constant, while the other value is solved, the solution process becomes sequential. This means at a given time instant first one unknown is solved, and then the other one.

In the Supervisor module for the present project it has been implemented a Prediction and Substitution algorithm. Taking into account that x and y are the panel surface pressures and the nodal positions respectively, Figure 28 shows the algorithm used.

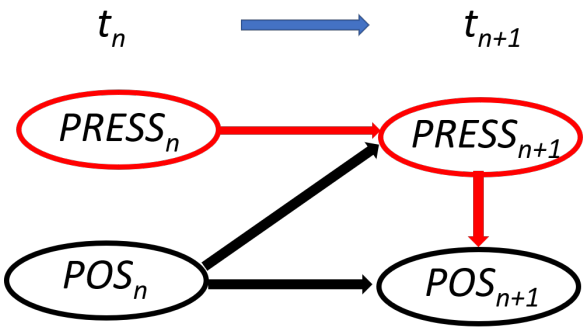

Figure 28: Implemented exchange mechanisms.

At time t_n the solution for both $PRESS$ and POS is known. The solution of POS at time t_{n+1} is predicted, but a prediction does not necessary mean a change in values, so the prediction of POS at time t_{n+1} will be POS_n. Therefore, $PRESS_{n+1}$ is solved keeping constant the value of POS. After convergence of solution $PRESS_{n+1}$, it is substituted in the second equation and POS_{n+1} is solved. Having now found the solution at t_{n+1}, the next time step can be solved.

5 Computation of aerodynamic loads and deformations

In this section it has been calculated the aerodynamic loads and deformations of NREL 5-MW and SWT 2.3-93 wind turbines.

5.1 NREL 5-MW wind turbine

5.1.1 Stationary control curves

The control system of a wind turbine is designed in order to:

- Find the maximum operating efficiency that maximizes the power coefficient.
- Ensure safe operation under all wind conditions.

For the wind turbine under study, it has been chosen a conventional configuration of variable rotor speed and variable blade pitch. This kind of wind turbines uses two basic control systems: a generator torque controller and a blade pitch controller. The blade pitch controller will operate at wind speeds greater than rated speed, while the generator torque controller will operate at wind speeds below rated.

The aim of the generator torque controller is to maximize the power capture at wind speeds below the rated wind speed $U_{in} < U_\infty < U_{N0}$, where U_{in} is the cut-in speed and U_{N0} is the rated velocity. To achieve it, it is necessary to vary the rotor speed, $\Omega(U_\infty)$, when the wind speed varies. This speed is achieved balancing the aerodynamic torque of the rotor Q_A with the appropriate resistant torque of the generator Q_G (which is the magnitude that is actually controlled).

On the other hand, the objective of the blade pitch controller is to regulate the generator speed above the rated wind speed, $U_{N0} < U_\infty < U_{out}$, where U_{out} is the stop speed. For wind speeds higher than the rated U_{N0}, the power and the rotor speed Ω will be kept constant in order to limit aerodynamic loads and preserve the structural integrity of wind turbine. Since the rotor speed is constant, the only way to keep the power constant when wind speed varies is by changing the pitch angle $\theta(U_\infty)$. Therefore, it is important to accurately predict the aerodynamic blade loads, because inaccuracies lead to over-designed and inefficient wind turbines.

The control curves that will be use in this study have been calculated using *FAST* with *AeroDyn* and using the subroutine for the *Control System DLL* (Appendix C of Jonkman et al. [20]). Moreover, in order to model blade structural dynamics, *BeamDyn* has been coupled with *FAST*. The results obtained for the blade pitch angle and rotational speed of the rotor are shown in Table 9.

Table 9: Blade pitch angle and rotational speed of the rotor for the control of NREL 5-MW.

Wind speed (m/s)	Pitch angle (°)	Rotor speed (rpm)
3	0	6.97
4	0	7.27
5	0	7.51
6	0	7.88
7	0	8.47
8	0	9.30
9	0	10.29
10	0	11.25
11	0	11.94
11.4	0	12.1
12	3.20	12.1
13	5.85	12.1
14	7.97	12.1
15	9.74	12.1
16	11.28	12.1
17	12.69	12.1
18	14.00	12.1
19	15.27	12.1
20	16.48	12.1
21	17.65	12.1
22	18.77	12.1
23	19.84	12.1
24	20.87	12.1
25	21.89	12.1

In the Figure 29 it is shown the curve of the rotational speed of the rotor $\Omega(U_\infty)$, where the rotational speed increases with wind speed until reaching Ω_{N0} (given by structural limitations) at a wind speed U_{N0}. From this point the rotational speed remains constant.

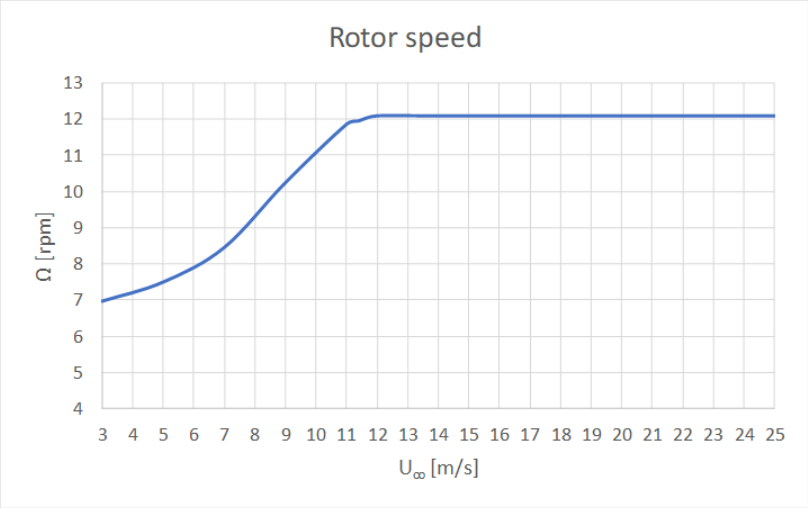

Figure 29: Rotation speed variation as a function of wind speed of NREL 5-MW.

The Figure 30 shows the variation of the pitch angle $\theta(U_\infty)$. It is observed that the pitch angle is $\theta = 0°$ up to wind speed U_{N0} and then the pitch angle increases in order to decrease the angle of attack of the profiles, which leads to a reduction in aerodynamic loads on the blades of the wind turbine, because it decreases drag and especially lift forces.

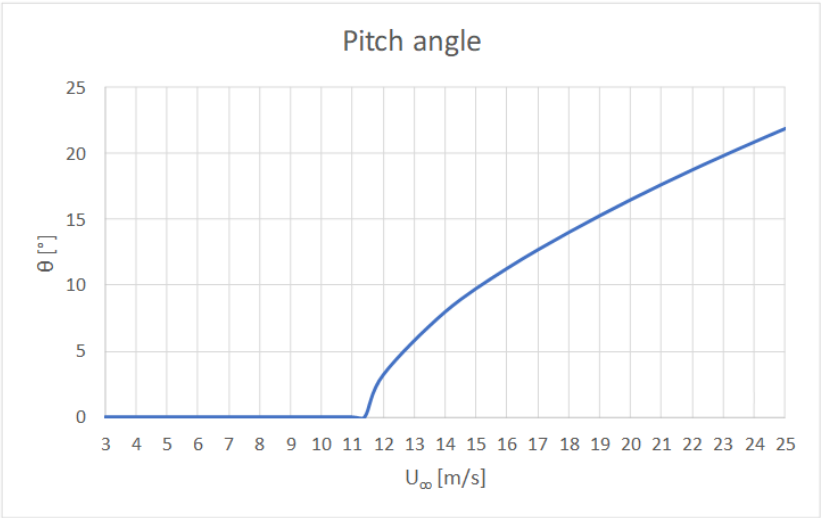

Figure 30: Pitch angle variation as a function of wind speed of NREL 5-MW.

5.1.2 Steady-state response

The steady-state response of the wind turbine has been obtained as a function of wind speed. The wind has been considered axial, steady and uniform, so the tilt angle of the rotor shaft has not been taken into account in order to avoid the flow asymmetry produced by the component of the wind parallel to the plane of the rotor. For the same reason, the yaw angle will remain at 0°. Furthermore, with the same objective of avoiding variations along the azimuth in the variables to be measured, neither the wind shear effect nor gravitational loads will be taken into account. The steady-state response has been obtained through simulations with a duration enough for the transient response die out, and then an average of the last 20 seconds has been made.

In order to prove the accuracy of *MECANO + AERO* method, the steady-state response is going to be compared with the results obtained with *FAST + BeamDyn + Aerodyn* using the same conditions, taking into account the control curves of the Figures 29 and 30. The simulation with *FAST + BeamDyn + Aerodyn* is based on the Blade Element Momentum (BEM) method, and as stated previously, *MECANO + AERO* is also based on BEM method. Moreover, in order to show the influence of the deformation, a simulation was performed considering rigid blades and tower. In this section the tower has been included in the simulations, although the tower shadow effect and the wind shear effect have not been taken into account. Therefore, the only effect considered is its deformation due to aerodynamic forces.

Firstly, the Figures 31 and 32 show the rotor power and the rotor torque respectively. They both increase until reach a peak corresponding to the rated wind speed, and then, according to *FAST* simulation, are held constant due to the control carried on the wind turbine. However, it is observed that with *MECANO + AERO* with flexible and rigid elements, they are not totally constant; this is because the control curves (Figures 29 and 30) have been obtained using *FAST*. In the simulation carried out using *FAST*, a power value of 5.3 MW is obtained, which after taking into account that the efficiency of the generator is 94.4 %, a rated power of 5 MW is obtained.

The rotor thrust (Figure 33) increases until reach a peak and then decreases again. This is because when the wind speed and the rotation speed of the rotor increases, maintaining the pitch angle to zero, aerodynamic forces on the blades increase. However, when the pitch angle begins to increase from the nominal wind speed, the angle of attack of the profiles begins to decrease and, therefore, the aerodynamic forces on the blades decrease.

The main cause of the differences in results between the simulations with flexible and rigid elements is due to the torsion produced in the blades, since this causes variations in the angle of attack and, therefore, the aerodynamic forces will vary. From these figures it is concluded that the effect of the aeroelastic deformation of the blades in large wind turbines is not negligible and has a clear influence on the aerodynamic rotor performance, and therefore, it must be taken into account when designing the wind turbine.

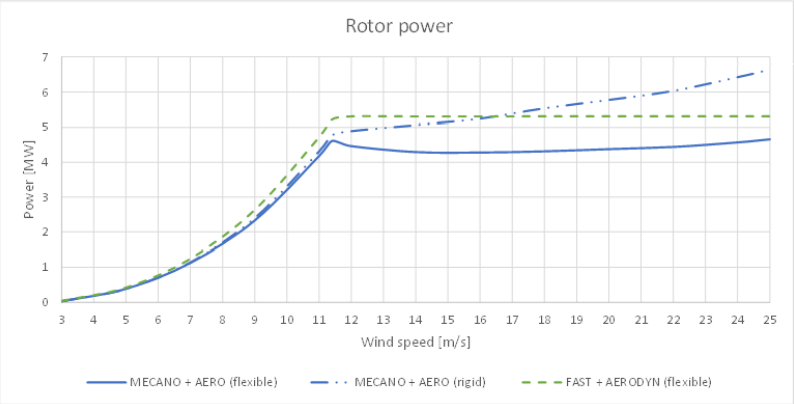

Figure 31: Steady-state response of the rotor power as a function of wind speed.

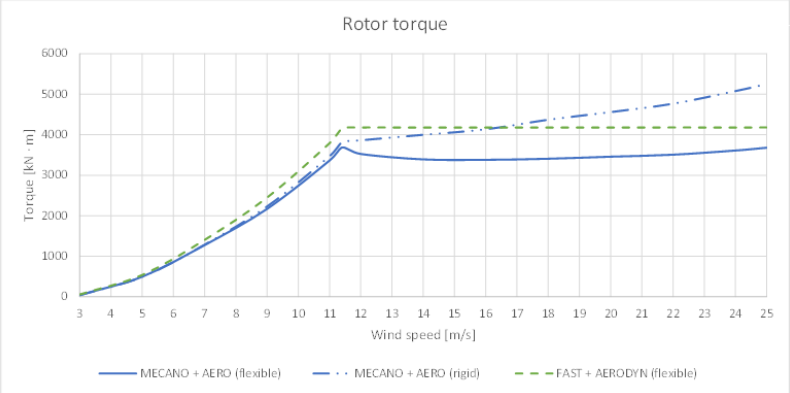

Figure 32: Steady-state response of the rotor torque as a function of wind speed.

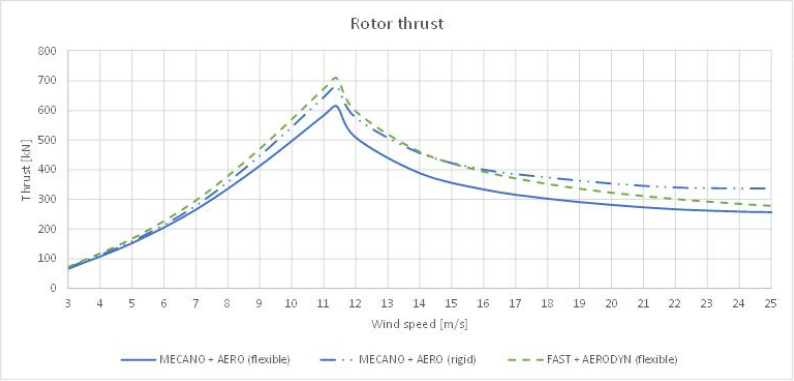

Figure 33: Steady-state response of the rotor thrust as a function of wind speed.

In the Figure 34 the deflection of the blade tip relative to the undeflected blade-pitch axis and the deflections of tower top relative to the centerline of the undeflected tower are represented for the simulations with *MECANO + AERO* and *FAST + BeamDyn + Aerodyn*. The peaks clearly observed in the out-of-plane deflection of the tip blade and the fore-aft deflection of the tower top are due to the peak observed previously in the rotor thrust.

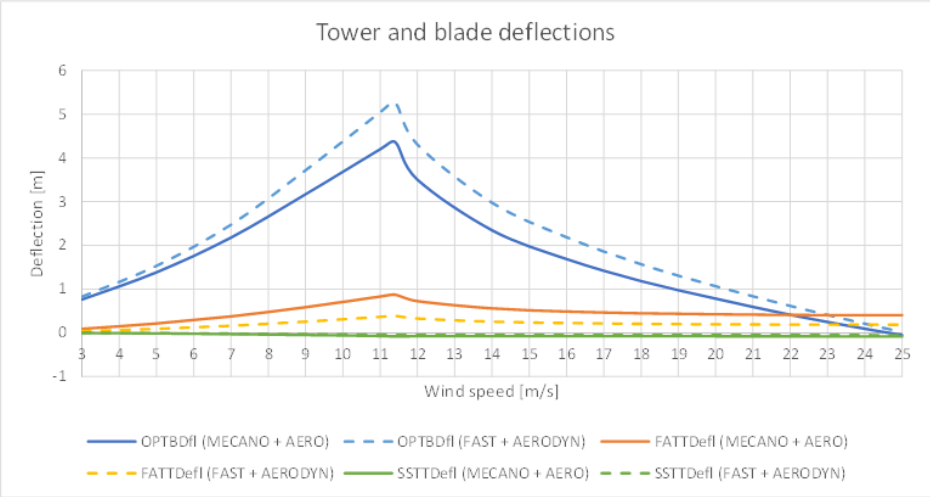

Figure 34: Steady-state response of the tower and blade deflections as a function of wind speed. (*OPTBDfl*: Out-of-plane tip blade deflection. *FATTDfl*: Fore-aft tower top deflection. *SSTTDfl*: Side-to-side tower top deflection.)

As can be seen in the previous figures, the results obtained with *MECANO + AERO* are consistent and similar to those obtained with *FAST + AeroDyn*. However there are some differences despite using both the BEM theory and using beams in the structural model. They can be explained through Figure 35, which shows the blade tip torsion, where a large difference can be seen. The higher nose-down torsion predicted by *MECANO + AERO* decreases the aerodynamic forces and therefore the deflections. After investigating the causes, it has been concluded that this difference is due to a mismatch in the position of the pitch axis. While in the simulations carried out with *MECANO + AERO* it has been considered that the pitch axis and the aerodynamic center coincide, in *FAST + Aerodyn* it has been considered that in most of the blade the distance between them is 12.5% of the profile chord (as indicated in Jonkman et al. [20]). This causes the pitch moments to be different and therefore the torsion. With the aim of verifying that this is true, a simulation has been carried out with *FAST + Aerodyn* for a wind of $11.4\,m/s$, a rotation speed of $12.1\,rpm$ and a pitch angle of 0°, considering that the aerodynamic center and the pitch axis coincide. Indeed, the result obtained is closer to that obtained with *MECANO + AERO*, obtaining a nose-down tip torsion of 2.8°. Therefore, knowing the cause of the difference, *MECANO + AERO* method can be considered validated.

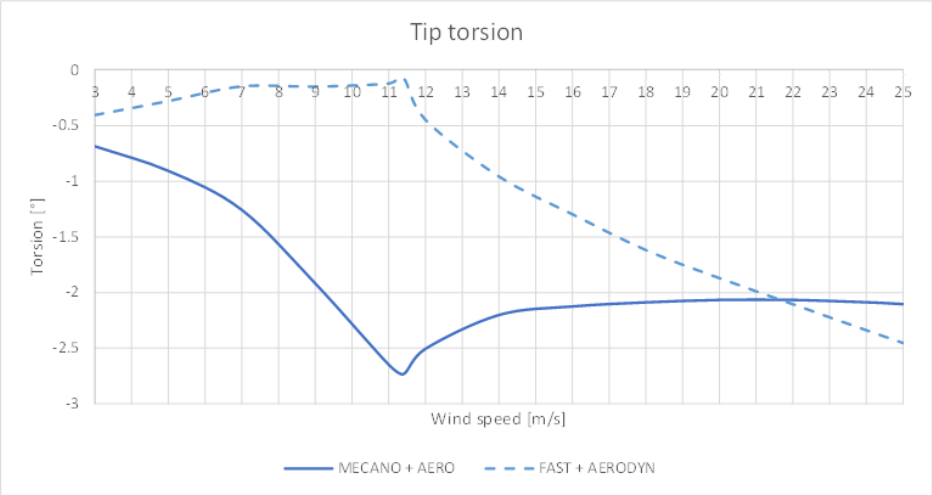

Figure 35: Steady-state response of the blade tip torsion as a function of wind speed.

5.1.3 Dynamic response

As seen previously, maximum aerodynamic loads occur at rated wind speed, making this the operating point of greatest interest. For this reason, this section will consider the next operating point: $U_\infty = 11.4$ m/s, $\Omega = 12.1$ rpm and $\theta = 0°$.

In this section it will be studied the dynamic response by introducing a uniform flow and an asymmetric flow by introducing some corrections on the unperturbed wind field in order to take into account the effects of rotor tilt, yaw angle and the gravitational forces, which cause an unsteady periodic response. In these simulations only the rotor has been modeled and a material damping has been introduced.

5.1.3.1 Uniform flow

In this section it is compared the response of the wind turbine using *MECANO + AERO* and *MECANO + Vortexje* with rigid and flexible elements for a uniform flow. Due to the absence of periodical variations caused by the effects of rotor tilt, gravitational forces or yaw angle, the responses converge to quasi-steady states.

Firstly, in order to demonstrate the validity of the *MECANO + Vortexje* method, Appendix B shows the comparison of the pressure coefficient along the chord for different blade sections between experimental data and *MECANO + Vortexje* results for the NREL Phase VI wind turbine. As there are no experimental data from NREL 5 MW, the results of the pressure coefficient distribution obtained by *MECANO + Vortexje* with rigid and flexible elements have been compared in Figure 36 with those obtained using a coupled CFD-CSD method (Yu and

Kwon [41]). It is observed that the results obtained with the simulation are quite consistent with the CFD results. However, at the trailing edge of the profile the pressure difference is not 0 as stated by the pressure Kutta condition. This is because as stated previously, the *Vortexje* program implements the Morino's Kutta condition (Morino and Kuo [27]) which always results in a nonphysical pressure mismatch at the trailing edge. Nevertheless the results are very similar considering that the panel method does not take into account complex physical phenomena such as boundary layer, recirculation bubble, laminar/turbulent velocity fields, etc. Furthermore, as indicated in Section 5.1.4, the simulation time required by the CFD-CSD method is considerably longer.

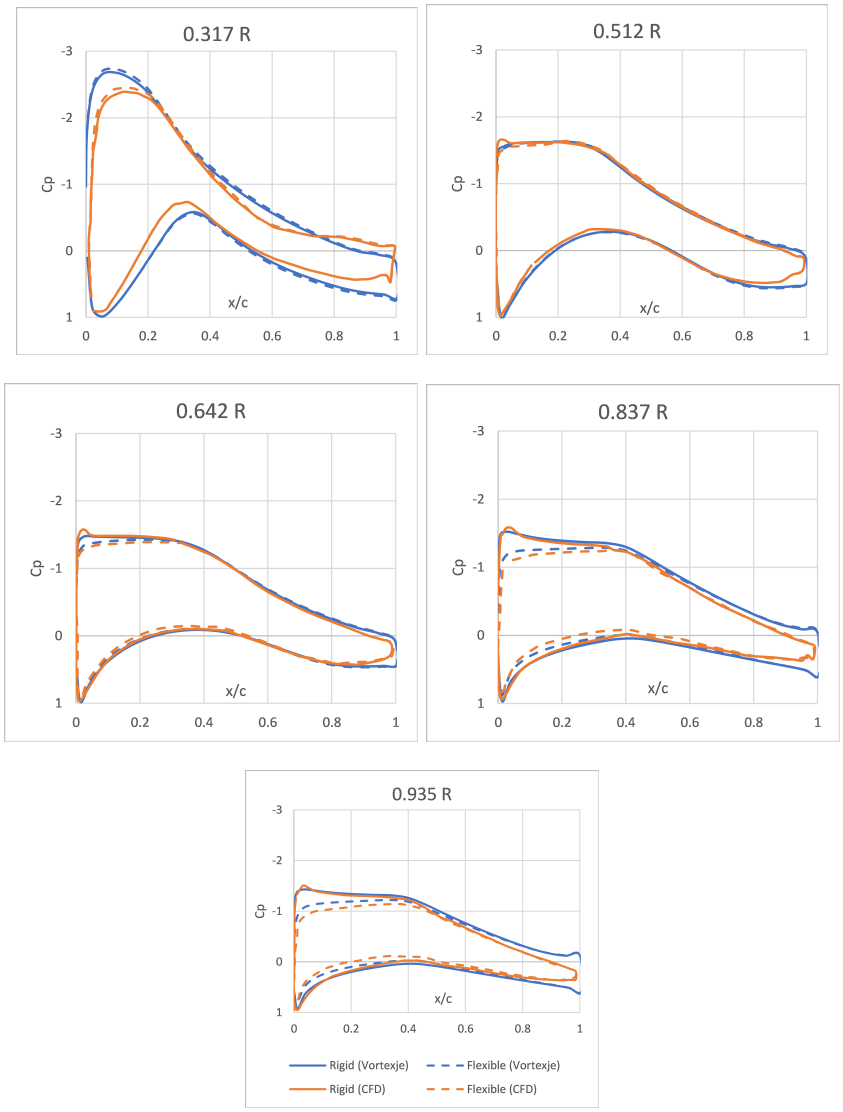

Figure 36: Pressure coefficient along the chord in different blade span sections.

Then, the comparison between *MECANO + AERO* and *MECANO + Vortexje* is carried out. Figures 37 and 38 show the aerodynamic rotor torque and thrust, respectively, so these values do not include centrifugal and inertial loads. And Figure 39 shows the blade deformations of the flexible cases, specifically: the out-of-plane deflection, in-plane deflection and torsion of the blade tip. Moreover the distribution of normal force (normal to the rotor plane), tangential force (in rotational direction) and out-of-plane blade deflection along the span are represented in Figures 40, 41 and 42. The final numerical values reached are collected in the Table 10.

Table 10: Final values of aerodynamic rotor thrust, aerodynamic rotor torque, out-of-plane tip deflection, in plane tip deflection and tip torsion.

	Rotor thrust (kN)	Rotor torque (kN·m)	Out-of-plane tip deflection (m)	In-plane tip deflection (m)	Tip torsion (°)
MECANO + AERO (rigid)	695.0	4480.6	-	-	-
MECANO + Vortexje (rigid)	853.7	5248.1	-	-	-
MECANO + AERO (flexible)	622.9	4356.2	4.41	0.080	-2.78
MECANO + Vortexje (flexible)	809.5	5201.5	6.05	0.187	-2.03

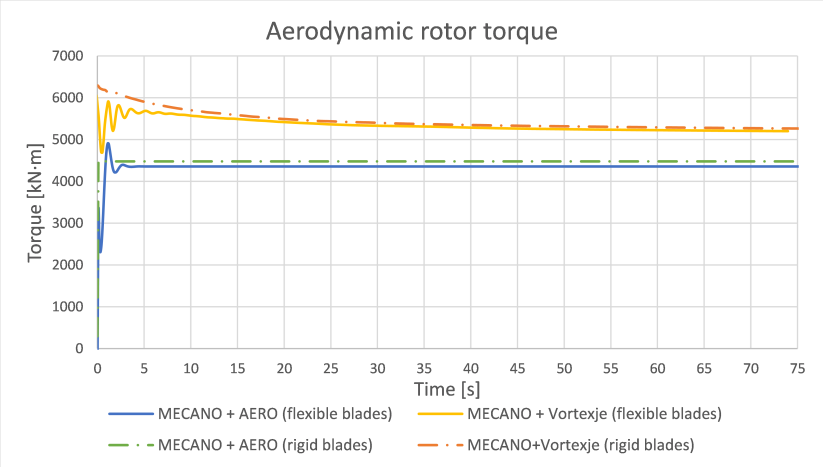

Figure 37: Dynamic response of the aerodynamic rotor torque.

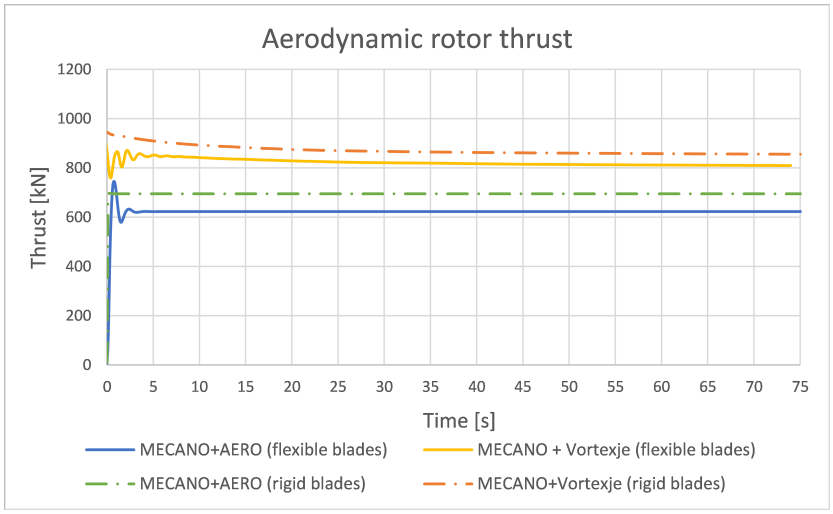

Figure 38: Dynamic response of the aerodynamic rotor thrust.

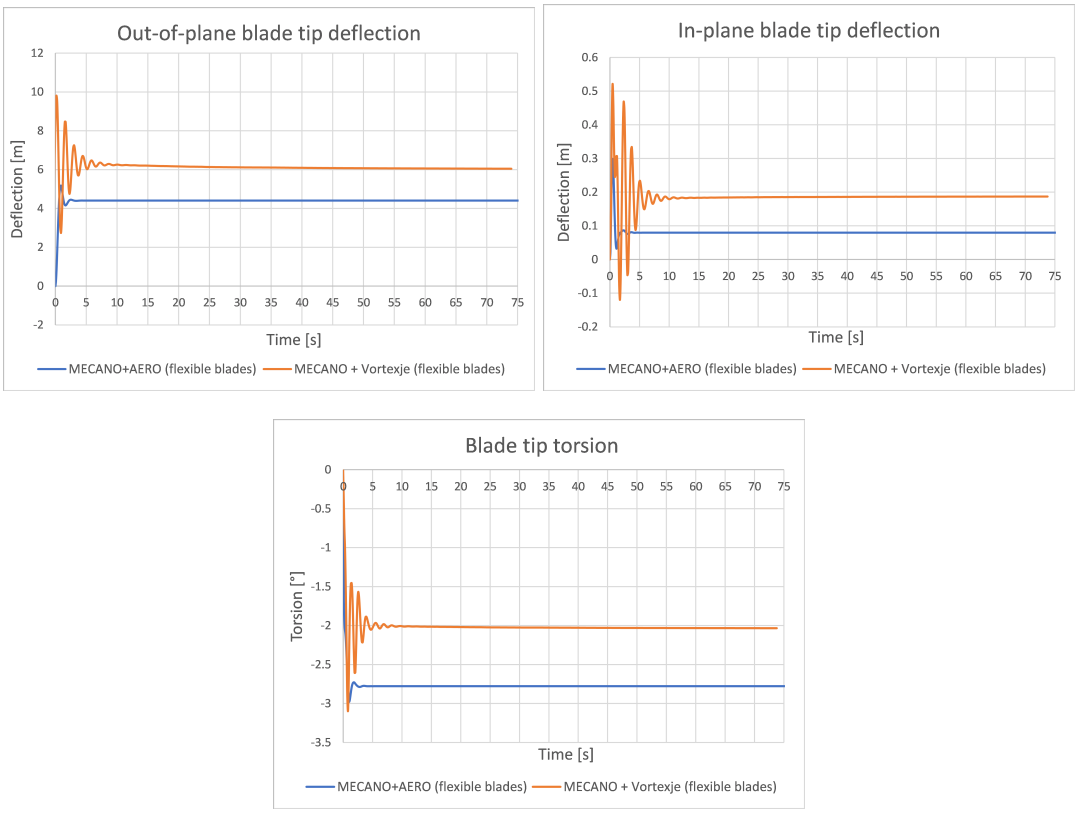

Figure 39: Dynamic response of the out-of-plane and in-plane blade tip deflection and blade tip torsion.

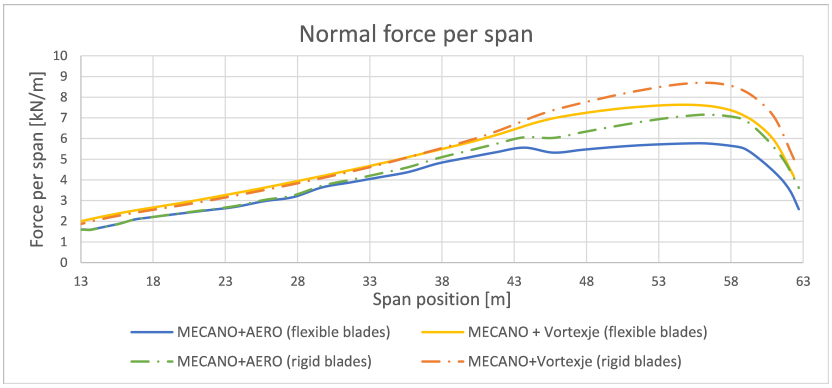

Figure 40: Distribution of normal force per span.

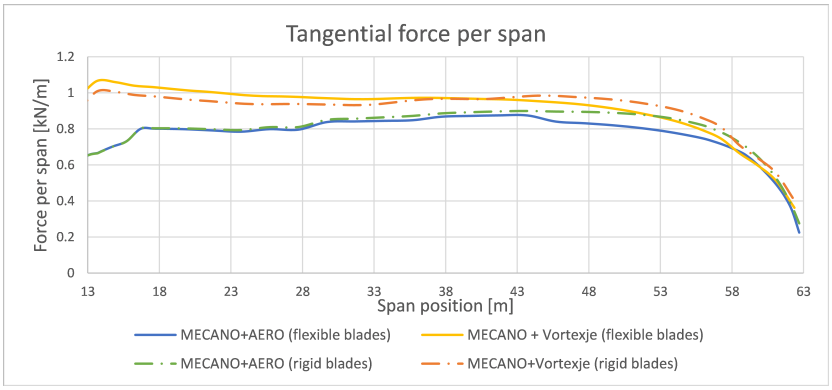

Figure 41: Distribution of tangential force per span.

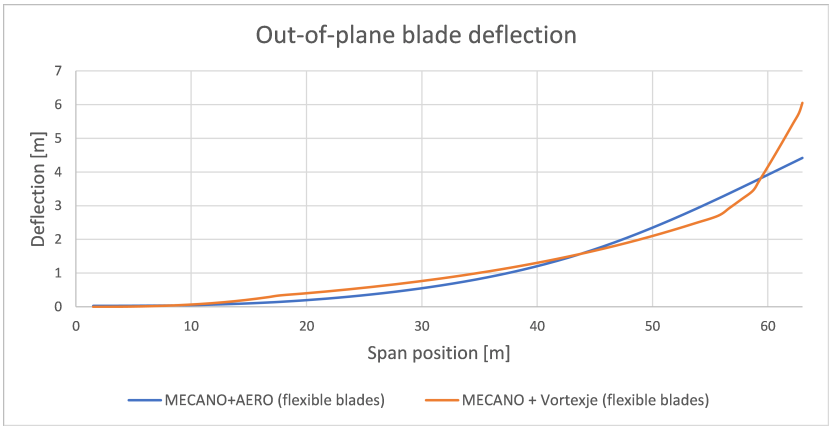

Figure 42: Out-of-plane blade deflection along the span.

Comparing the flexible and rigid cases, the aerodynamic loads for the rigid cases are higher

than for the flexible cases. In respect of the deformations, they are quite significant since with *Vortexje* it has been obtained an out-of plane blade tip deflection of approximately 6 meters and a blade tip torsion of 2° (nose-down) and with *AERO* 4 meters and 2.8° respectively. The distance along shaft from hub center to yaw axis is 5 m, and taking into account the shaft tilt of 5° and the precone of 2.5°, the clearance between the blade tip and the tower would be 13.2° without deformation and 7.22° taking into account the out-of-plane blade deflection obtained with *Vortexje*. The main difference between rigid and flexible cases is due to the nose-down torsion which reduces the effective angle of attack and causes a reduction in the aerodynamic loads. The distribution of normal and tangential forces show that the results are very similar in the inner sections but in the outer sections there are certain deviations because the deformations increase with the radial position.

Comparing the results of *MECANO* + *Vortexje* and *MECANO* + *AERO*, *MECANO* + *Vortexje* predicts higher aerodynamic loads, higher tip deflections and a lower tip torsion than *MECANO* + *AERO*. Due to the lack of experimental data, the results obtained by CFD in Yu and Kwon [41], Dose et al. [10] and Imiela et al. [19] will be considered since the most accurate results are obtained by CFD. According to Dose et al.[10] and Imiela et al. [19] the rotor thrust is 771 kN and 808 kN respectively, so it can be observed that *MECANO* + *Vortexje*, whose result is 809.5 kN, predicts a better result than *MECANO* + *AERO*, 622.9 kN. Since the out-of-plane tip deflection is directly related to the rotor thrust, this is also better predicted by *Vortexje*: Dose et al. [10] and Imiela et al. [19] provide values of 5.57 and 6 meters respectively. However, the rotor torque seems to be better predicted by *AERO* (4356.2 kN·m) than *Vortexje* (5201.5 kN·m) since according to Yu and Kwon [41], Dose et al. [10] and Imiela et al. [19] it is 4200 kN·m, 4333 kN·m and 4467 kN·m, respectively. In order to explain the main reasons that can lead to errors in the results, Table 11 indicates the aerodynamic effects that the BEM and panel methods of *AERO* and *Vortexje* take into account or not intrinsically or by means of engineering models.

Table 11: Aerodynamic effects that *AERO* and *Vortexje* take into account or not. I = Intrinsec, EM = Engineering model.

Aerodynamic effect	**BEM method (*AERO*)**	**Panel method (*Vortexje*)**
Axial/Tangential induction	I	I
Radial induction	-	I
Tip loss	EM	I
Root loss	-	I
Turbulent wake state	EM	I
Rotational stall delay	EM	-
Dynamic stall	-	-
Flow separation	EM	-

As it has been seen in previous sections the original BEM method has some limitations. However, due to its wide use in industry, several engineering models have been developed to reduce these limitations. As indicated in the section 4.3.1, corrections have been made in *AERO* module for the tip loss and turbulent wake state. It must be noted that the rotational stall delay and flow separation are taken into account by *AERO* method through corrections in the aerodynamic coefficients data of the profiles, as shown in Section 4.3.1. BEM method uses experimental profile data (lift, drag and moment coefficients), which can be an advantage or a disadvantage. It would be a disadvantage when such information is not available or it can be an advantage since the use of experimental data can lead to more reliable results. For the NREL 5-MW wind turbine, the experimental data used is reliable and comes from reliable sources. On the other hand, the panel method already intrinsically includes some of the aerodynamic effects and do not use experimental data. However, as previously observed in the Figure 36, it can lead to non-physically correct results such as the existence of a pressure difference at the trailing edge which, taking into account the long blade length of the NREL 5MW wind turbine, can lead to errors in overall results such as rotor torque. But its biggest drawback is that it considers attached flow, which is not true when the angle of attack is high, which causes a separation of the flow. To take into account this flow separation it would be necessary to attach a viscous boundary layer solution to the inviscid panel method as it has been done in the works of Prasad and Dimitriadis [31] and Ramos et al. [33]. Apart from taking into account the viscous effects using a strong coupling between the viscous and inviscid parts, Ramos et al. [33] takes into account the rotational effects produced from Coriolis and centrifugal forces (Ramos et al. [32]). Ramos et al. [33] shows that adding the viscous effects and rotational effects on the NREL 5-MW wind turbine would cause a decrease in the tangential and normal forces along the blade, making the results obtained in Figures 40 and 41 by *MECANO + AERO* and *MECANO + Vortexje* much more similar. Consequently the rotor thrust and torque and blade deformations would also be more similar.

5.1.3.2 Influence of gravity loads, tilt angle and yaw angle

The main advantage of the application of the panel method over the blade element momentum method is its capability to predict the effects of asymmetries in the flow, like those produced by the shaft tilt and yaw angles. It is inevitable that in actual operating conditions the wind direction changes, what causes that wind turbines operate at yaw angles relative to the incoming wind producing a skewed wake behind the rotor. A similar effect is produced by the shaft tilt.

Although it is not included in the BEM model of *AERO* module, other BEM models are corrected to take into account this skewed wake effect. For example, *AeroDyn* uses a formulation based on an equation developed by Glauert (Moriarty and Hansen [26]), but as it is stated in the same reference, this correction has limitations. This correction is only valid for lightly loaded rotors since it assumes a cylindrical wake and in some cases the correction is too large. Therefore, the unreliability of the skewed wake corrections applied to the BEM method and

the implication that this has in predicting fatigue loads, make the use of the panel method more appropriate in some applications.

In this section it will be studied the effects of the shaft tilt and yaw angle with *MECANO + Vortexje*. Moreover, gravity loads will be introduced and their effects will be studied as well. Although gravity loads can be applied in both methods since it is introduced in the structural model, only *MECANO + Vortexje* will be used. Three different cases have been simulated: in the first case only the gravity loads have been taken into account, in the second one gravity loads and shaft tilt have been introduced, and in the third case the impact of the yaw angle under gravity loads is evaluated. The simulations have been done with flexible blades.

Table 12 shows the mean values of the aerodynamic rotor thrust, torque and deformations calculated during the last rotation when gravity loads and shaft tilt are taken into account. Comparing these values with those obtained previously in Table 10, it can be deduced that the changes of the mean values are practically negligible. On the other hand, Figure 43 shows the azimuth variation of out-of-plane and in-plane tip deflection and tip torsion during the last rotation. It can be seen the unsteady periodic response due to the rotor shaft tilt and gravity loads. Azimuth 0° corresponds to the blade pointing vertically upwards. From Figure 43 it can be deduced that the main cause of variations in deformations is the gravity. In some cases the shaft tilt decreases the amplitude of the variation as in out-of-plane tip deflection, in other cases increases the amplitude as in tip torsion, and in other cases it hardly has any influence as in the in-plane tip deflection. Furthermore, it can be seen that the shaft tilt produces a phase shift in the out-of-plane tip deflection.

Table 12: Mean values of aerodynamic rotor thrust, aerodynamic rotor torque, out-of-plane tip deflection, in plane tip deflection and tip torsion under gravity loads and a shaft tilt of 5° with *MECANO + Vortexje*.

	Rotor thrust (kN)	Rotor torque (kN·m)	Out-of-plane tip deflection (m)	In-plane tip deflection (m)	Tip torsion (°)
Gravity - no tilt - no yaw	812.1	5226.8	6.07	0.190	-2.02
Gravity - tilt - no yaw	809.5	5199.0	6.05	0.188	-2.03

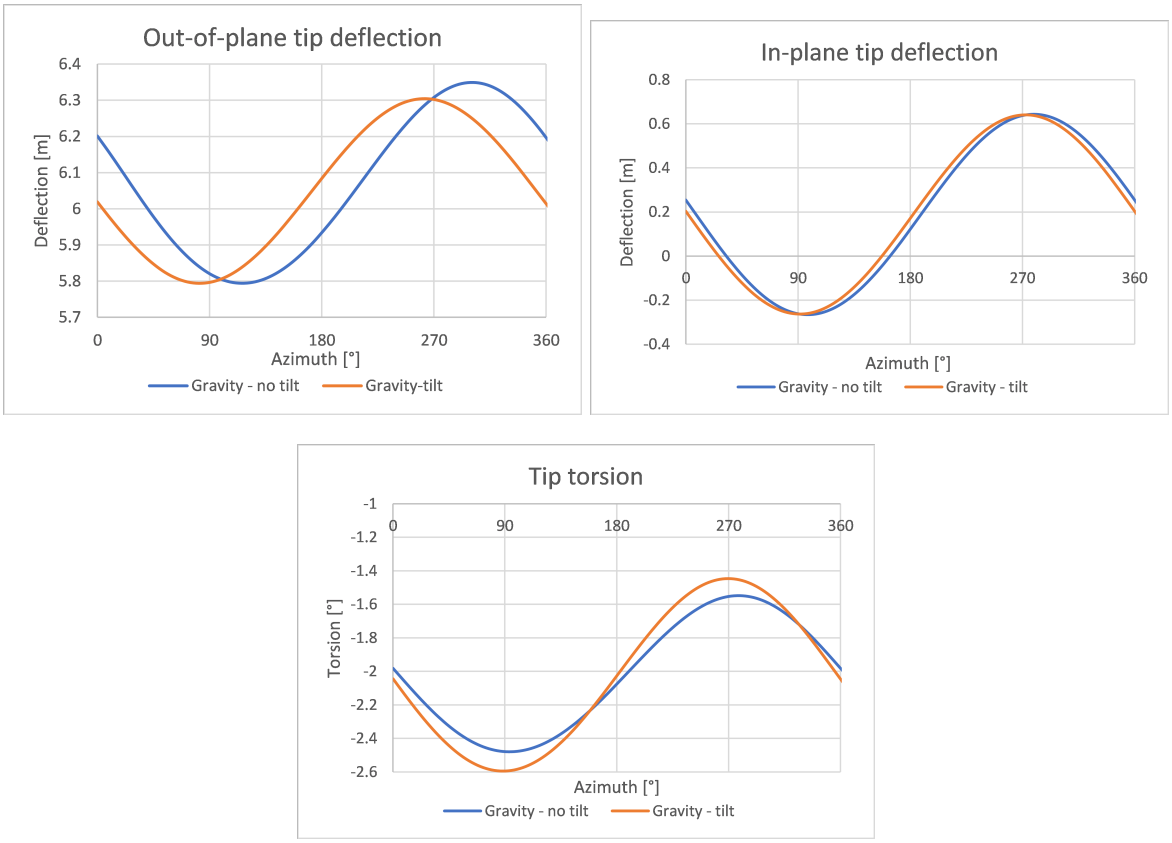

Figure 43: Out-of-plane and in-plane tip deflections and tip torsion under gravity loads and a shaft tilt of 5° with *MECANO + Vortexje*.

In the out-of-plane blade deflection it is observed that the gravity load produces a peak-to-peak variation close to 9% of the mean value which is reduced to approximately 8% if the shaft tilt is included. This variation must be taken into account when designing the wind turbine in order to avoid collisions between the blade tip and tower. When only the gravity loads are taken into account, the lowest value of the deflection is found in the lower half because the gravity tends to bring the blade tip closer to the undeflected rotor plane reducing the blade deflection, and the highest value is found in the upper half because the gravity tends to move the blade tip away from the undeflected rotor plane increasing the blade deflection. The phase shift observed between the tilted and non-tilted rotors can be explained through Figure 44, which represents the azimuth variation of the normal force per span for different span positions. As it can be observed, there is a similar phase shift between the tilted and non-tilted rotors. For the tilted case, the normal forces decrease between $270 - 90°$ and they increase between $90 - 270°$ with respect to the non-tilted case. This is caused by an effect similar to the skewed wake effect produced by the yaw angle that will be explained later. The tilt angle causes that the position of the blade relative to the wake to vary over one rotation, so that when the blade is in the upper half it finds a denser wake than in the bottom half and,

therefore, the induced velocities in the upper half will be larger causing the forces to be smaller.

In the in-plane blade deflection it is observed a peak-to-peak variation close to 0.9 m for both tilted and non-tilted cases. The highest and lowest values occur at 270° and 90° respectively where gravity force is aligned with edgewise direction.

Finally, a peak-to-peak variation close to 46% of the mean value is observed in the tip torsion for non-tilted rotor. This variation is magnified by the tilt effect increasing the variation close to 57% of the mean value. The minus sign indicates that the torsion is nose-down, so the lowest and highest values of nose-down tip torsion are found at 270° and 90° respectively. This may be one reason why the Figure 44 shows that the maximum and minimum are close to 270° and 90° respectively in the mid and outer span positions. A higher nose-down torsion decreases the angle of attack causing a decrease in aerodynamic forces, while a lower nose-down torsion causes the opposite effect.

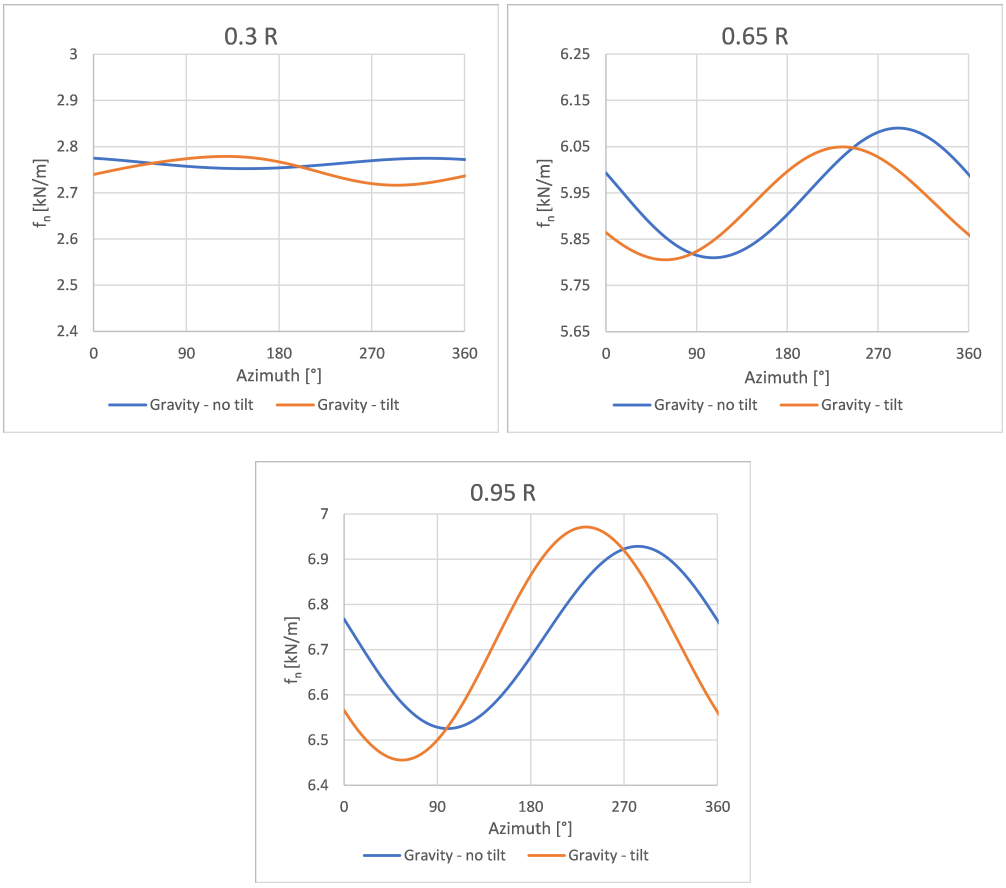

Figure 44: Normal force per span in different blade sections under gravity loads and a shaft tilt of 5° with *MECANO + Vortexje*.

After studying the shaft tilt influence, the yaw angle influence is studied. The yaw angle produces a reduction in axial velocity and a skewed wake behind the rotor that leads to variations in the induced velocities throughout a rotation. Table 13 shows the mean values obtained when the wind turbine operates at a yaw angle of 30° and gravity loads are included. It is observed that the mean values of aerodynamic rotor thrust and torque are lower than previous cases (Tables 10 and 12) due to the reduction of axial velocity.

Table 13: Mean values of aerodynamic rotor thrust, aerodynamic rotor torque, out-of-plane tip deflection, in plane tip deflection and tip torsion under gravity loads and a yaw angle of 30° with *MECANO + Vortexje*.

	Rotor thrust (kN)	Rotor torque (kN·m)	Out-of-plane tip deflection (m)	In-plane tip deflection (m)	Tip torsion (°)
Gravity - no tilt - yaw	712.4	4102.6	5.51	0.199	-2.17

In order to see the influence of the skewed wake, Figure 45 show the azimuth variation of the out-of-plane and in-plane tip deflections and tip torsion during the last rotation. It has a high influence in the out-of-plane tip deflection: it is observed a peak-to-peak variation close to 34% of the mean value while, as seen previously, if only gravity is taken into account this variation is close to 9%. Moreover the maximum value is approximately 0.3 m higher. This higher peak-to-peak variation can be explained through Figure 46, which represents the azimuth variation of the normal force per span for different span positions. In the outer span position it is observed that the maximum and minimum values of normal force are higher and lower than values obtained with axial wind, respectively (Figure 44). This is because when the blade is at an azimuth of 90° it is deepest into the wake, so the induced velocities will be higher, the forces lower and the out-of-plane deformation lower, occurring the opposite when the blade is at 270°. Therefore, it is important to take this effect into account when designing the wind turbine.

The in-plane tip deflection is hardly affected by the yaw angle. A considerable effect is also observed in the tip torsion, since the peak-to-peak variation is approximately 74% while with axial wind it was 46%.

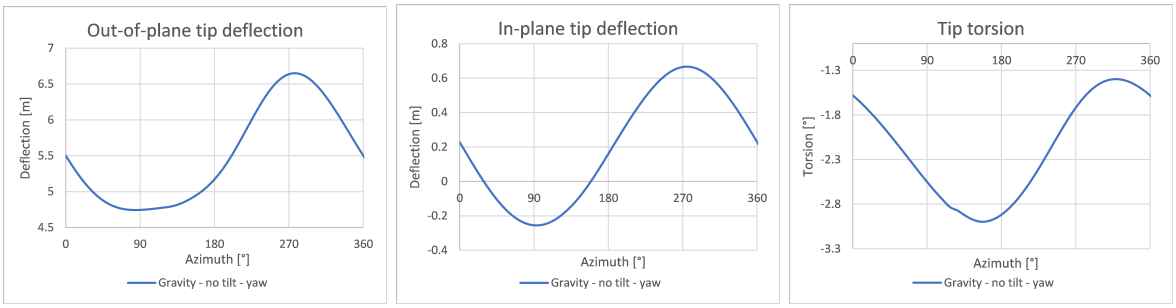

Figure 45: Out-of-plane and in-plane tip deflections and tip torsion under gravity loads and a yaw angle of 30° with *MECANO + Vortexje*.

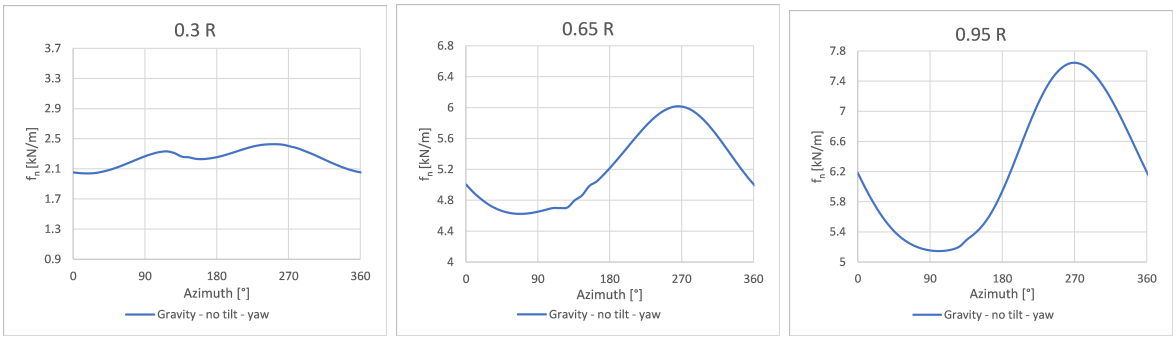

Figure 46: Normal force per span in different blade sections under gravity loads and a yaw angle of 30° with *MECANO + Vortexje*.

5.1.4 Efficiency

The simulations have been carried out on a computer with *Intel(R) Xeon(R) Gold 6248 CPU* processors with a clock frequency of 2.5 GHz. It consists of 2 sockets or physical processors with 20 cores per socket and 1 thread per core, that is to say, 40 virtual processors.

The time step used in the simulations with *MECANO + AERO* is $\Delta t = 0.1\,s$. The results converge very quickly, after approximately one revolution, that is to say, after 50 iterations. The CPU time required until convergence is $\sim 9\,s$, requiring an average value of CPU time of $0.18\,s$ per time step. However, due to its high efficiency, in this project the simulations have been carried out for more revolutions.

For *MECANO + Vortexje* simulations, a time step of $\Delta t = 0.125\,s$ has been used. The results converge after approximately 16 revolutions, where the first revolution has been simulated without coupling with *MECANO*. The time steps and CPU time required until convergence are 600 and 75016 s (21 hours approximately) respectively. However, in order to obtain higher

efficiency in the simulations, a function can be implemented in *Vortexje* that removes the last wake layer when it reaches a certain distance. Figure 47 shows the values of aerodynamic rotor thrust and torque when the last wake layer is removed after 2.5, 4 and 7 revolutions and when the last wake layer is not deleted, for an axial wind of $11.4\,m/s$ and a speed rotor of $12.1\,rpm$. And Figure 48 shows the required CPU time for each new time step for the different cases. It is observed that if the last wake layer is not removed, the evolution is quadratic, and when the last wake layer is deleted, the evolution becomes linear from 2.5, 4 and 7 revolutions. Focusing on the results obtained by removing the last wake layer after 7 revolutions and comparing them with the no wake deletion case, the errors are 0.64% for the aerodynamic rotor thrust and 1.15% for the aerodynamic rotor torque. On the other hand, the CPU time required to complete the same revolutions (16 revolutions) is $56136\,s$, which means a reduction of 25.2%. Therefore, if time is the priority over the accuracy of the results, the removal of the last layer after 7 revolutions turns out to be a good solution. However in this project, the option of not removing the last wake layer was chosen.

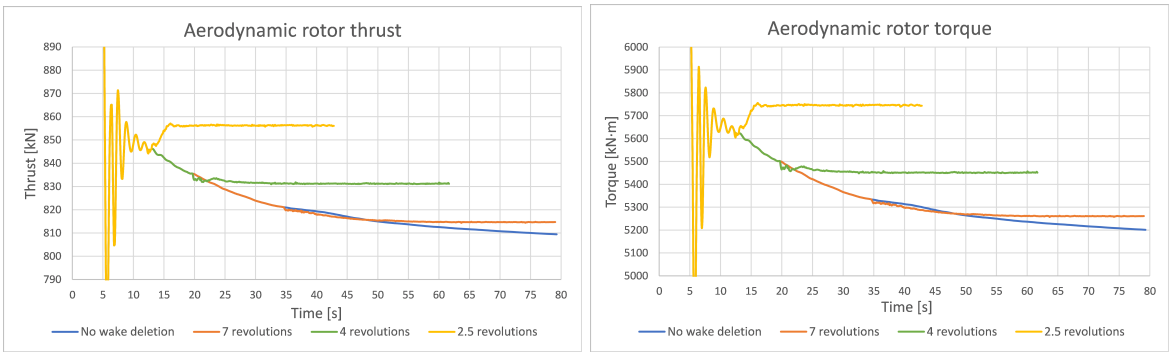

Figure 47: Aerodynamic rotor thrust and torque when the last wake layer is removed after 2.5, 4 and 7 revolutions. $V_{wind} = 11.4\,m/s$, $\Omega = 12.1\,rpm$.

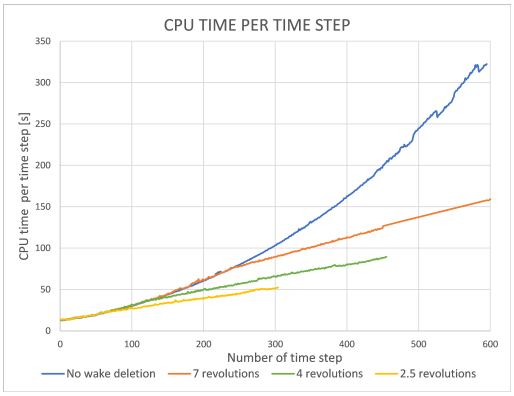

Figure 48: Required CPU time for each new time step when the last wake layer is removed after 2.5, 4 and 7 revolutions.

Table 14 shows the simulation time needed to simulate the revolutions number 6, 9, 12 and 15 by *MECANO + AERO* and *MECANO + Vortexje* without last wake removal and removing it after 7 revolutions.

Table 14: Simulation time needed to simulate the revolution number 6, 9, 12 and 15.

Revolution number	*MECANO + AERO*	*MECANO + Vortexje* (removal after 7 revolutions)	*MECANO + Vortexje* (without removal)
6th	9 s	0 h 45 min 3 s	0 h 45 min 1 s
9th	9 s	1 h 5 min 18 s	1 h 22 min 12 s
12th	9 s	1 h 38 min 2 s	2 h 15 min 38 s
15th	9 s	2 h 6 min 57 s	3 h 26 min 36 s

In order to compare the computational costs of the BEM method and the panel method with CFD calculations, it has been taken as CFD reference the computational costs described in Yu and Kwon [41] and that led to the CFD results shown previously in the Figure 36. To reach those results the CPU time was approximately 654240 s (7.5 days approximately) using 180 processors with 2.93 GHz CPUs. Other CFD reference is Dose et al. [10], where simulations were computed on 360 Intel Xeon CPU E5-2650 cores with a clock frequency of 2.2 GHz. In this reference the simulations were run for 25 rotor revolutions requiring a CPU time of 403200 s (4.7 days approximately) per simulation. Although it is difficult to compare the CPU times due to the use of different number and types of processors, different duration of the simulations and different time steps, it can be deduced that simulations with CFD require much more simulation time.

5.2 SIEMENS 2.3 MW wind turbine

5.2.1 Stationary control curves

Following the structure used in Section 5.1, firstly, the control curves for the SWT 2.3-93 wind turbine were obtained using *FAST + Aerodyn + BeamDyn* using flexible elements and considering a conventional configuration of variable rotor speed and variable collective blade pitch. For this, it was necessary to modify the subroutine for the Control System DLL (Appendix C of Jonkman et al.[20]) including the parameters of the new wind turbine. Taking into account that the gearbox ratio is 91 : 1 and considering that the generator efficiency is 94.4%, the main required parameters are the following:

Table 15: Parameters for wind turbine control.

Desired (reference) HSS speed for pitch controller (rpm)	$16 \times 91 = 1456$
Maximum generator torque (HSS side) (N·m)	$1.1 \times \frac{2.3\times10^6}{0.944} \times \frac{1}{1456} \times \frac{60}{2\pi} = 17577.56$
Generator torque constant (N·m/rpm^2)	0.0060319
Rated generator speed (HSS side) (rpm)	$0.99 \times 1456 = 1441.44$
Rated generator power (W)	$\frac{2.3\times10^6}{0.944} = 2436441$

The maximum generator torque has been chosen to be 10% above the rated generator torque, and the rated generator speed has been chosen to be 99% of desired HSS speed for pitch controller. In the region where $U_{in} < U_\infty < U_{N0}$, the generator torque is proportional to the square of the generator speed $Q_{gen} = K\,\Omega_{gen}^2$, where K is the generator torque constant defined in Table 15 calculated by taking into account the optimum power coefficient $C_{p_{opt}}$ of the turbine. In order to calculate $C_{p_{opt}}$, a number of simulations have been run for a wind speed of 8 m/s and different values of rotor speeds and pitch angles. The higher value of C_p found has been $C_p = 0.4364$ for a rotor speed of $\Omega = 12.5$ rpm and a pitch angle of $\theta = 0°$. Therefore, taking into account that the gearbox ratio is 91 : 1, the generator torque constant K is:

$$P_{gen} = \Omega_{gen}\, Q_{gen} = \frac{1}{2}\,\rho\,\pi\,R^2\,U_\infty^3\,C_{p_{opt}} \quad \rightarrow \quad Q_{gen} = 7804.7\,\text{N·m} \tag{86}$$

$$K = \frac{Q_{gen}}{\Omega_{gen}^2} = 0.0060319\,\text{N·m/rpm}^2 \tag{87}$$

The results obtained for the blade pitch angle and rotational speed of the rotor are shown in Table 16 and Figures 49 and 50.

Table 16: Blade pitch angle and rotational speed of the rotor for the control of SWT 2.3-93.

Wind speed (m/s)	Pitch angle (°)	Rotor speed (rpm)
3	0	6.59
4	0	7.26
5	0	8.26
6	0	9.58
7	0	11.14
8	0	12.80
9	0	14.34
10	0	15.48
10.5	0	15.78
10.9	0	16
11.5	3.09	16
12	4.96	16
13	8.03	16
14	10.38	16
15	12.22	16
16	13.70	16
17	14.95	16
18	16.09	16
19	17.17	16
20	18.25	16
21	19.33	16
22	20.41	16
23	21.43	16
24	22.31	16
25	22.96	16

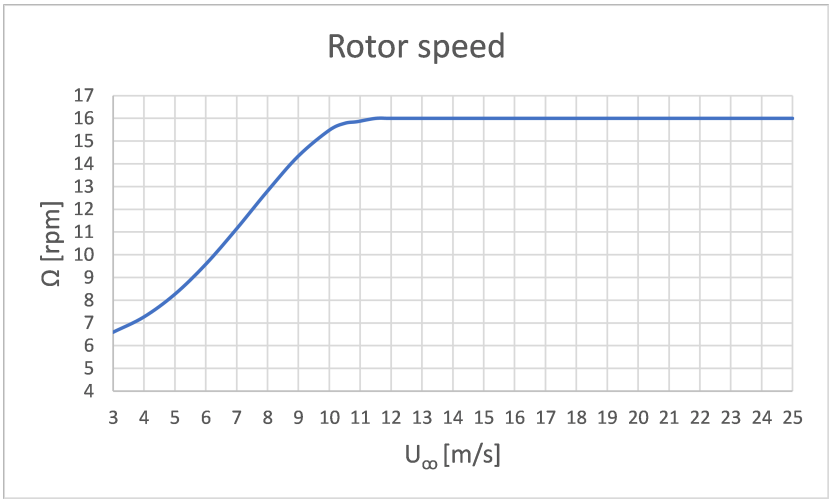

Figure 49: Rotation speed variation as a function of wind speed of SWT 2.3-93.

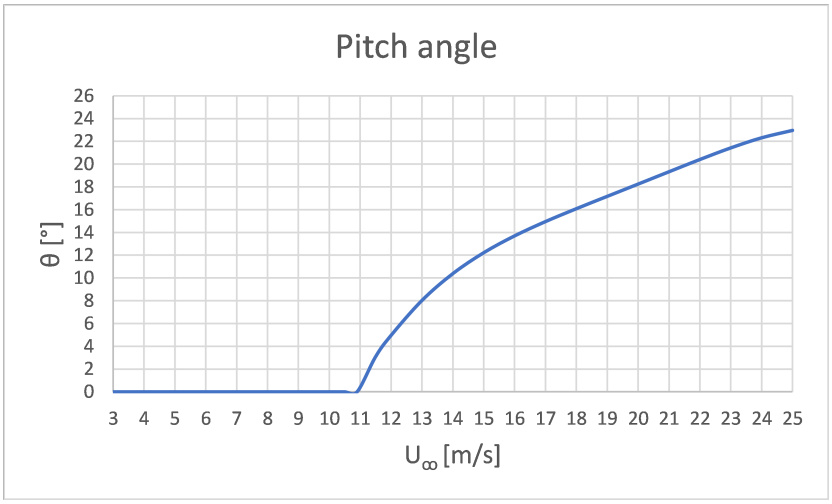

Figure 50: Pitch angle variation as a function of wind speed of SWT 2.3-93.

5.2.2 Steady-state response

Using the control law obtained in the previous section, the steady-state response for different wind speed values has been obtained by *FAST + Beamdyn + Aerodyn* and *MECANO + AERO* considering the same assumptions as for NREL 5-MW wind turbine (Section 5.1.2). The simulations carried out with *MECANO + AERO* have been done with rigid and flexible elements, while those carried out with *FAST + Beamdyn + Aerodyn* have only been done with flexible elements. Figures 51, 52 and 53 show the power, torque and thrust of the rotor respectively, and Figures 54 and 55 show the tip deflections of the tower and blade, and the

blade tip torsion, respectively. The rated wind speed obtained with *FAST* is 10.9 m/s, obtaining a power of 2.44 MW, which considering a generator efficiency of 94.4% a rated power of 2.3 MW is obtained.

Between the rigid and flexible cases, a smaller difference is observed than in the NREL 5-MW due to the smaller blade span of the SWT 2.3-93 wind turbine. This highlights the influence of blade span and the need to use more accurate programs as larger blades are built. Furthermore, it is observed that the loads are higher for the flexible case, contrary to what happened with the NREL 5-MW wind turbine. This is mainly due to the fact that, as Figure 55 shows, the torsion is nose-up whereas in NREL 5-MW it was nose-down.

The results obtained using *MECANO + AERO* and *FAST* are almost identical except from wind speeds above 18 m/s where the results start to diverge. This is possibly due to the fact that small differences in pitch and torsion angles produce deviations in the prediction of aerodynamic loads that are magnified when the wind speed is higher because the aerodynamic loads are proportional to the square of the wind speed.

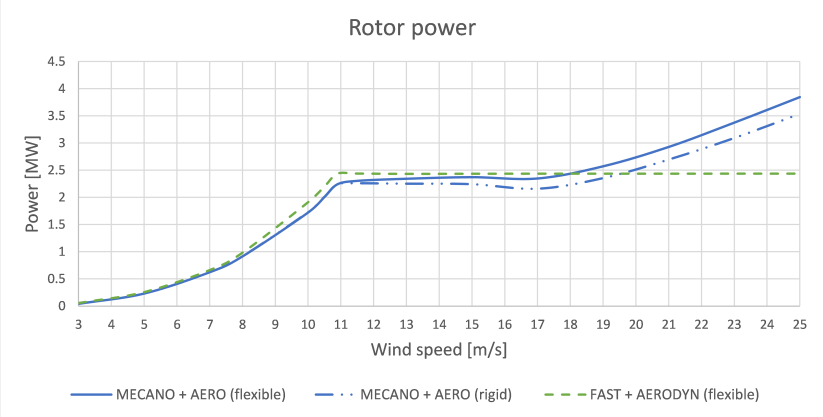

Figure 51: Steady-state response of the rotor power as a function of wind speed.

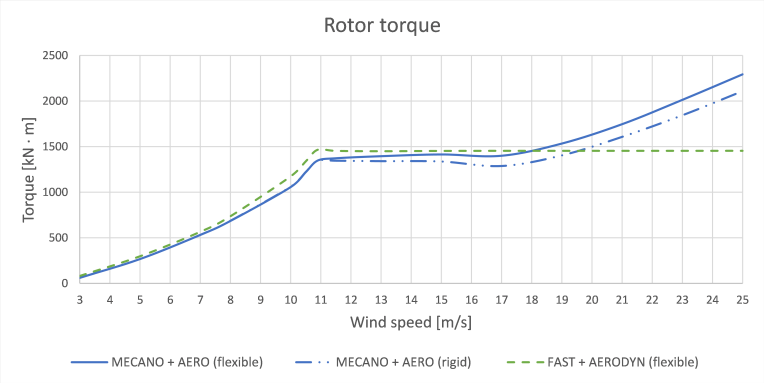

Figure 52: Steady-state response of the rotor torque as a function of wind speed.

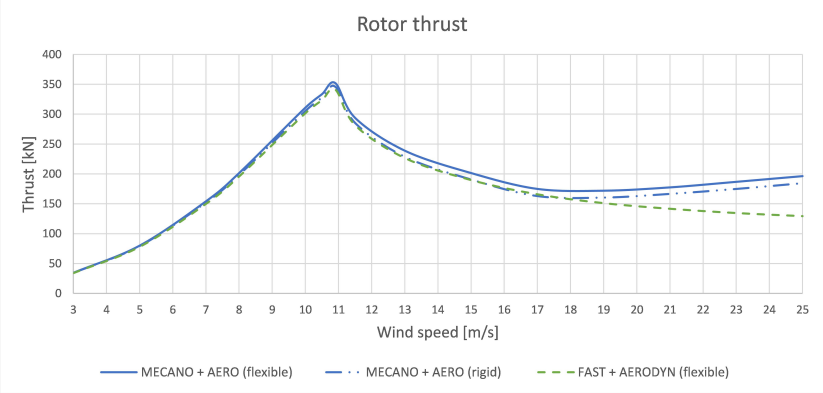

Figure 53: Steady-state response of the rotor thrust as a function of wind speed.

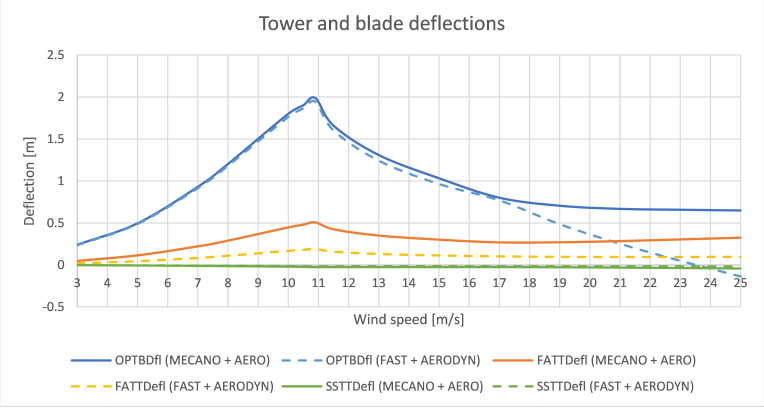

Figure 54: Steady-state response of the tower and blade deflections as a function of wind speed. (*OPTBDfl*: Out-of-plane tip blade deflection. *FATTDfl*: Fore-aft tower top deflection. *SSTTDfl*: Side-to-side tower top deflection.)

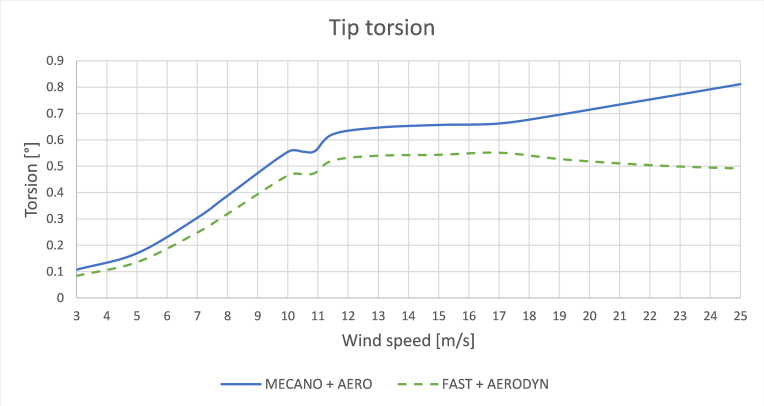

Figure 55: Steady-state response of the blade tip torsion as a function of wind speed.

5.2.3 Dynamic response

Once the point where the highest aerodynamic loads occur is known, $U_\infty = 10.9$ m/s, $\Omega = 16$ rpm and $\theta = 0°$, the dynamic response of the rotor is obtained at this operating point by introducing a uniform flow and an asymmetric one.

5.2.3.1 Uniform flow

Firstly, simulations haven been run with *MECANO + AERO* and *MECANO + Vortexje* with an axial, steady and uniform flow and without gravitational loads. The response obtained with both methods are compared for both rigid and flexible cases.

Figure 56 shows the pressure coefficient distribution obtained by *MECANO + Vortexje* with rigid and flexible elements. It can be seen that in this case the influence of the deformations is much less than in the case of the NREL 5-MW. And as previously mentioned, a pressure difference is observed at the trailing edge due to the implementation of the Morino's Kutta condition (Morino and Kuo [27]). Nevertheless this mismatch at the trailing edge could be solved following the method indicated in Section 7. Due to the absence of experimental or CFD data, the accuracy of the results could not be verified.

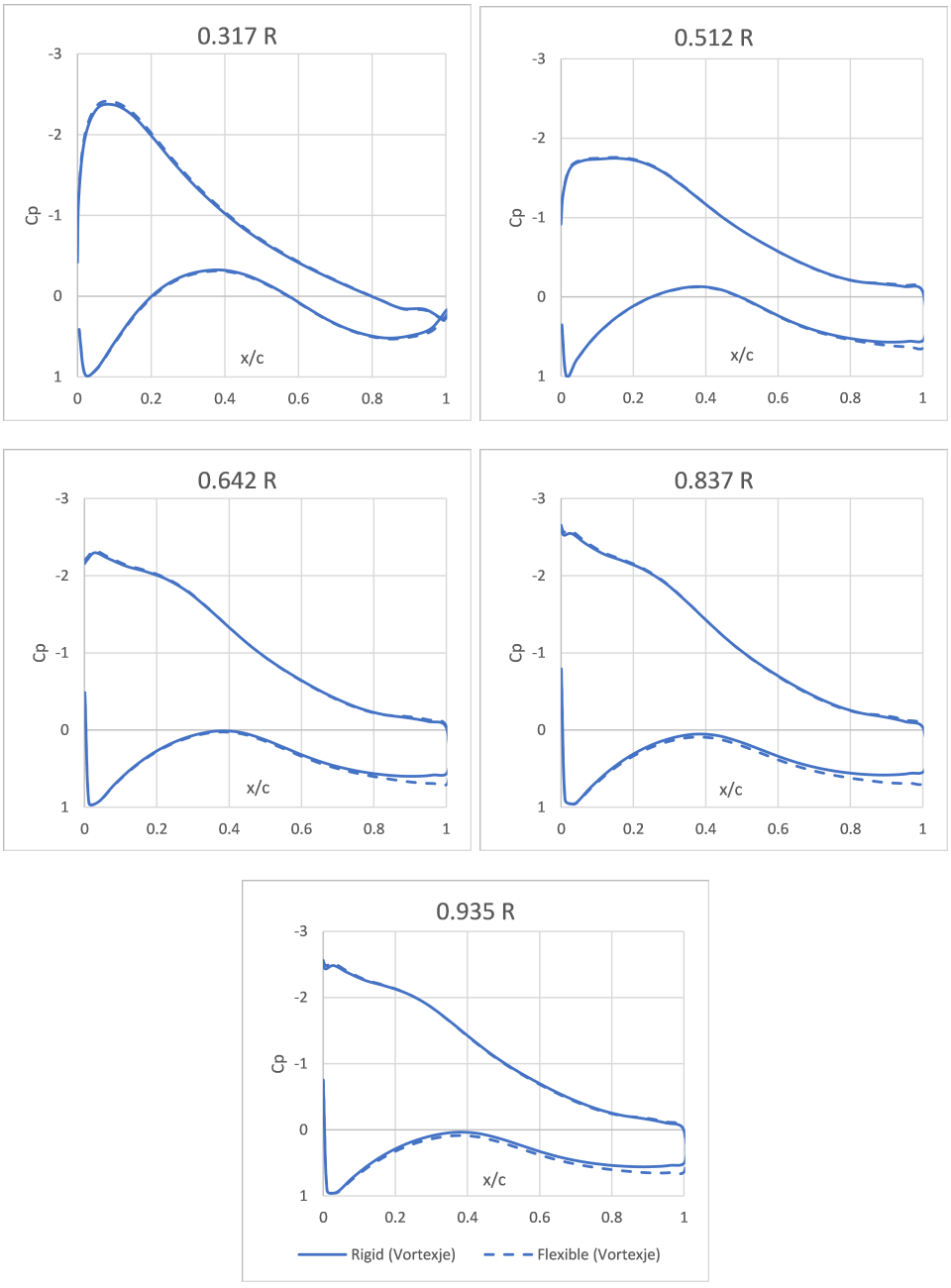

Figure 56: Pressure coefficient along the chord in different blade span sections.

Figures 57 and 58 show the aerodynamic rotor torque and thrust, respectively. And Figure 59 shows the out-of-plane and in-plane blade tip deflection and the blade tip torsion of the flexible cases. Due to the absence of periodical variations caused by effects of rotor tilt, gravitational forces or yaw angle, the responses converge to quasi-steady states. Table 17 shows the final

values reached after 16 rotor revolutions. Moreover the distribution of normal force, tangential force and out-of-plane blade deflection along the span are represented in Figures 60, 61 and 62. Comparing the results of *MECANO + AERO* and *MECANO + Vortexje*, the second one predicts higher aerodynamic loads, higher tip deflections and a lower tip torsion, in the same way as in the case of the NREL 5-MW. Due to the absence of experimental or CFD data of SWT 2.3-93 wind turbine it is not possible to know what results are more accurate. Although the results are slightly different, the values are representative. As discussed in Section 5.1.3.1, both methods have limitations, but the panel method implemented in *Vortexje* takes neither viscous effects nor rotational effects into account. According to Ramos et al.[33], taking these effects into account would produce lower tangential and normal forces along the blade, making the results obtained by *MECANO + AERO* and *MECANO + Vortexje* more similar.

Table 17: Final values of aerodynamic rotor thrust, aerodynamic rotor torque, out-of-plane tip deflection, in plane tip deflection and tip torsion.

	Rotor thrust (kN)	Rotor torque (kN·m)	Out-of-plane tip deflection (m)	In-plane tip deflection (m)	Tip torsion (°)
MECANO + AERO (rigid)	346.0	1347.5	-	-	-
MECANO + Vortexje (rigid)	417.5	1762.7	-	-	-
MECANO + AERO (flexible)	352.7	1350.5	1.99	0.027	0.56
MECANO + Vortexje (flexible)	427.4	1807.3	2.54	0.059	0.09

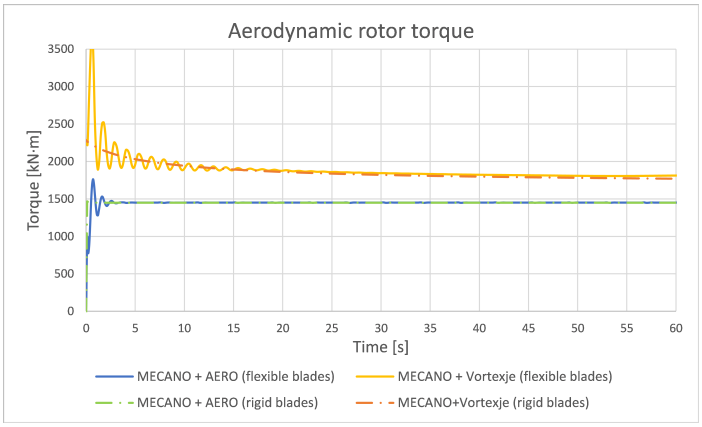

Figure 57: Dynamic response of the aerodynamic rotor torque.

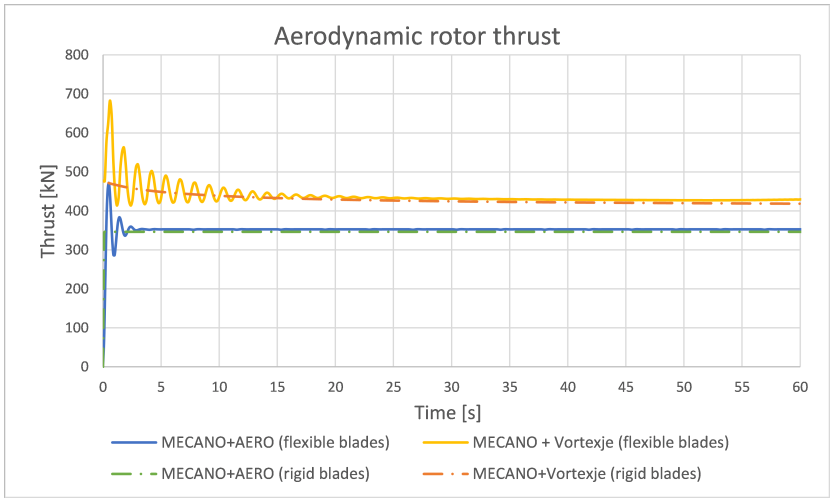

Figure 58: Dynamic response of the aerodynamic rotor thrust.

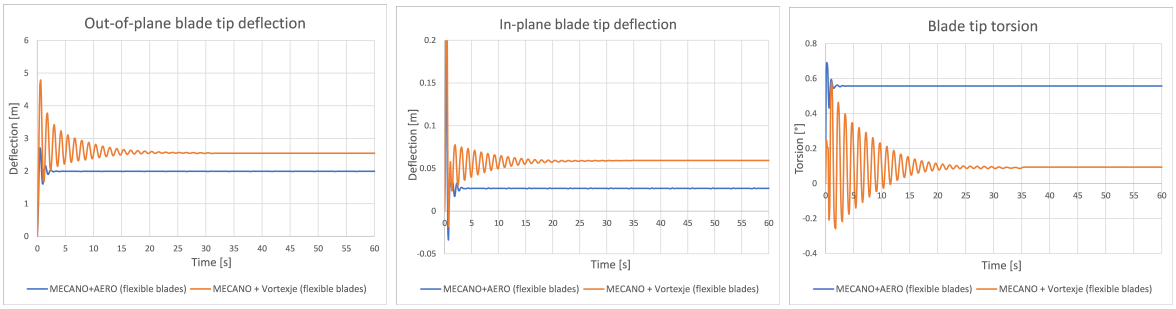

Figure 59: Dynamic response of the out-of-plane and in-plane blade tip deflection and blade tip torsion.

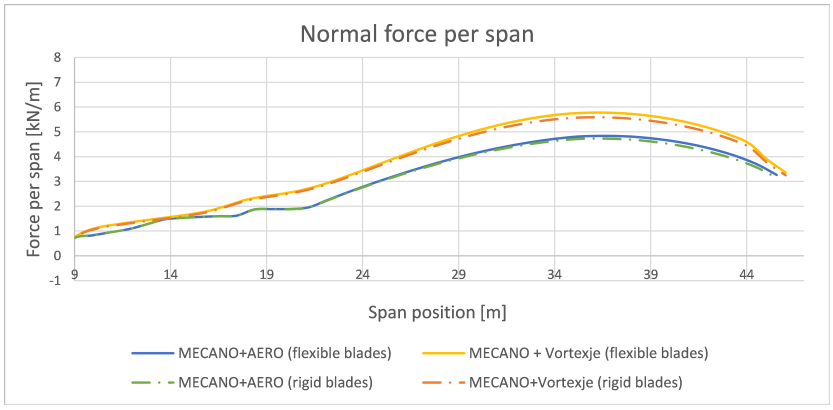

Figure 60: Distribution of normal force per span.

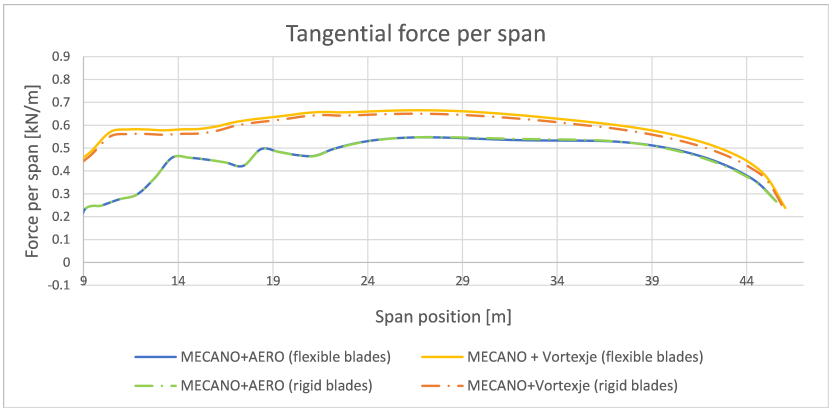

Figure 61: Distribution of tangential force per span.

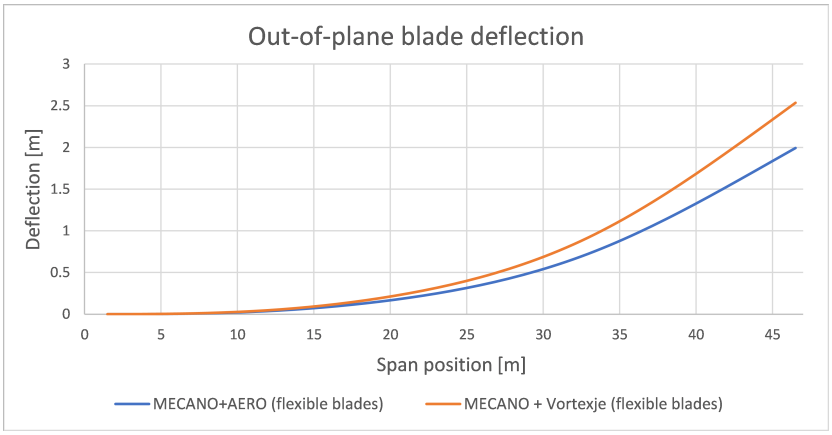

Figure 62: Out-of-plane blade deflection along the span.

5.2.3.2 Influence of gravity loads, tilt angle and yaw angle

Below it is studied the influence of asymmetries in the flow caused by the shaft tilt and yaw angle, and the effect of the gravitational loads on the SWT 2.3-93 wind turbine with *MECANO + Vortexje* and with flexible blades. As previously proceeded with the NREL 5-MW wind turbine, three different cases have been simulated: in the first case only the gravity loads have been taken into account, in the second one gravity loads and shaft tilt have been introduced, and in the third case the impact of the yaw angle under gravity loads is evaluated.

Table 18 shows that the mean values of rotor loads and deformations during the last rotation taking into account gravity and the shaft tilt, are very similar to those collected in Table 17. However an unsteady periodic response can be observed in Figure 63, which shows the azimuth variation of blade deformations during the last rotation. This periodic response is very similar to those obtained in the NREL 5-MW, but it can be noticed that, apart from the

variations having a lower peak-to-peak amplitude due to the size of the blades, in this case the tilt increase the amplitude of the variation in the out-of-plane tip deflection, contrary to what happened with NREL 5-MW.

Table 18: Mean values of aerodynamic rotor thrust, aerodynamic rotor torque, out-of-plane tip deflection, in plane tip deflection and tip torsion under gravity loads and a shaft tilt of 5° with *MECANO + Vortexje*.

	Rotor thrust (kN)	Rotor torque (kN·m)	Out-of-plane tip deflection (m)	In-plane tip deflection (m)	Tip torsion (°)
Gravity - no tilt - no yaw	422.9	1772.98	2.50	0.060	0.08
Gravity - tilt - no yaw	422.0	1765.8	2.50	0.060	0.08

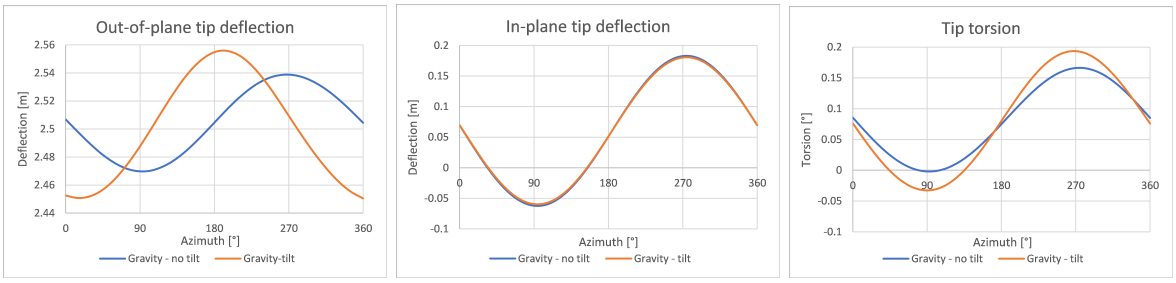

Figure 63: Out-of-plane and in-plane tip deflections and tip torsion under gravity loads and a shaft tilt of 5° with *MECANO + Vortexje*.

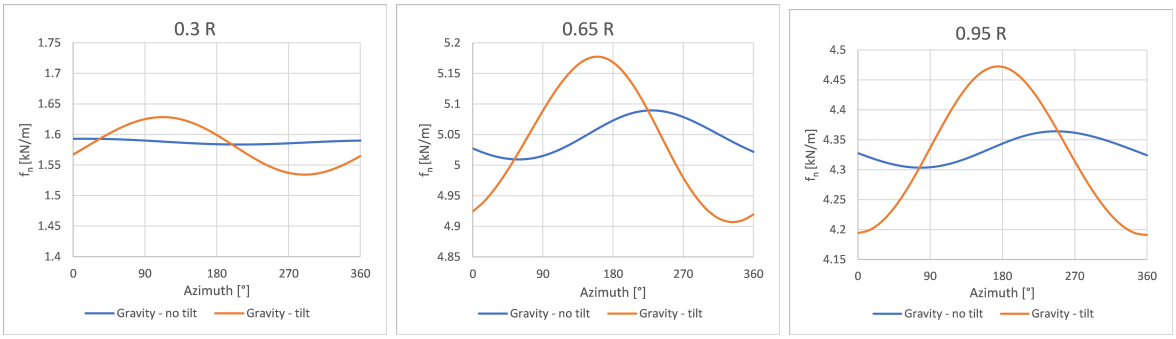

Figure 64: Normal force per span in different blade sections under gravity loads and a shaft tilt of 5° with *MECANO + Vortexje*.

Next, the effect of the wind turbine operating at a yaw angle of 30° and gravity loads is studied. Table 19 shows the mean values of aerodynamic rotor thrust and torque are lower than previous cases (Tables 17 and 18) due to the reduction of axial velocity produced by the yaw angle. The effect of the skewed wake produced by the yaw angle is shown in Figures 65 and 66, where the variations show the same behaviour as that explained in Section 5.1.3.2.

Table 19: Mean values of aerodynamic rotor thrust, aerodynamic rotor torque, out-of-plane tip deflection, in plane tip deflection and tip torsion under gravity loads and a yaw angle of 30° with *MECANO + Vortexje*.

	Rotor thrust (kN)	Rotor torque (kN·m)	Out-of-plane tip deflection (m)	In-plane tip deflection (m)	Tip torsion (°)
Gravity - no tilt - yaw	386.1	1434.7	2.32	0.067	0.02

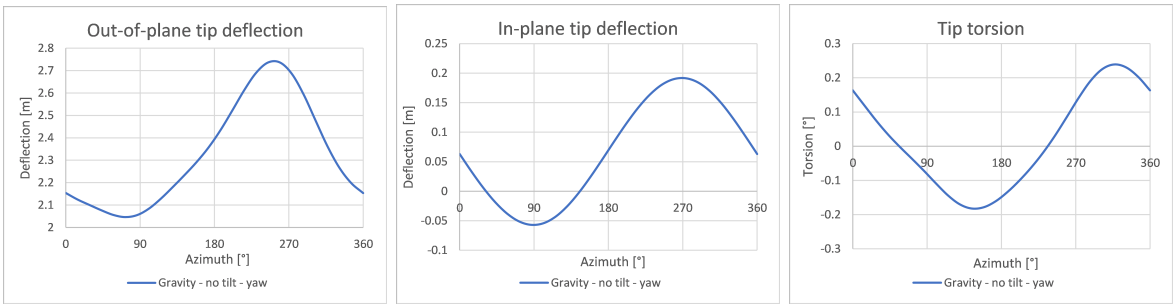

Figure 65: Out-of-plane and in-plane tip deflections and tip torsion under gravity loads and a yaw angle of 30° with *MECANO + Vortexje*.

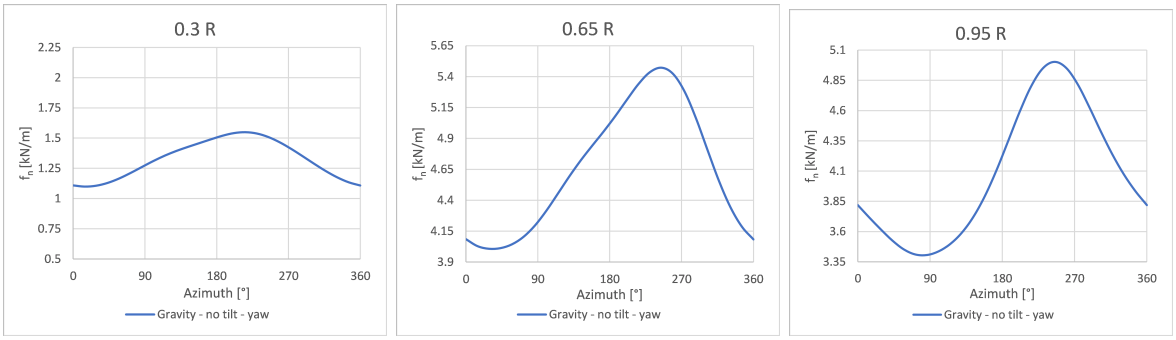

Figure 66: Normal force per span in different blade sections under gravity loads and a yaw angle of 30° with *MECANO + Vortexje*.

5.2.4 Efficiency

As the same number of elements have been used to model this wind turbine and a time step proportional to the rotation period, the simulation times are expected to be the same as in the case of the NREL 5-MW. The time step used in the simulations with *MECANO + AERO* is $\Delta t = 0.076\,s$, and the results converge after approximately one revolution, that is to say, after 50 iterations. Effectively, very similar CPU time is required until convergence $\sim 8\,s$, requiring an average value of CPU time of $0.16\,s$ per time step. For *MECANO + Vortexje* simulations, a time step of $\Delta t = 0.095\,s$ has been used and the results converge after approximately 16 revolutions (approximately 600 iterations). The CPU time required until convergence without last wake layer removal is 78514 s (21 hours and 48 minutes approximately). Figure 68 and Table 20 show CPU times that are practically the same as in the case of NREL 5-MW. So for more information about the comparison of the efficiency of the methods go to Section 5.1.4. Figure 67 shows the values of aerodynamic rotor thrust and torque when the last wake layer is removed after 4 and 7 revolutions and when the last wake layer is not deleted, for an axial wind of 10.9 m/s and a speed rotor of 16 rpm.

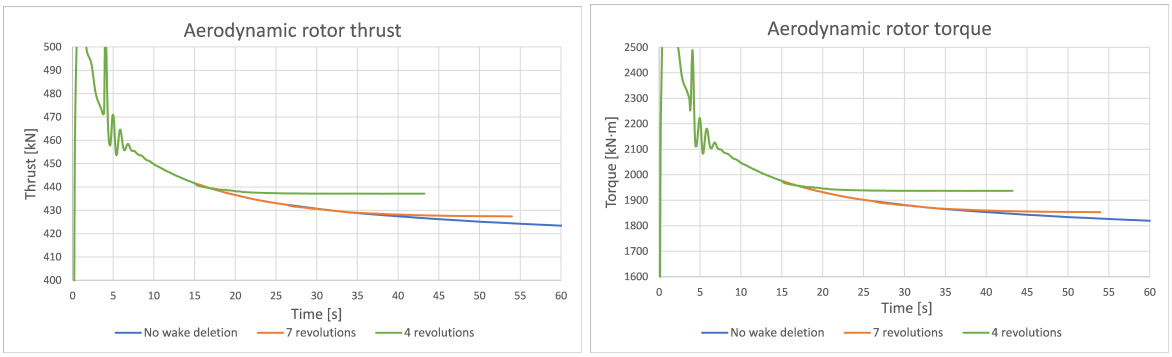

Figure 67: Aerodynamic rotor thrust and torque when the last wake layer is removed after 4 and 7 revolutions. SWT 2.3-93: $V_{wind} = 10.9\,m/s$, $\Omega = 16\,rpm$.

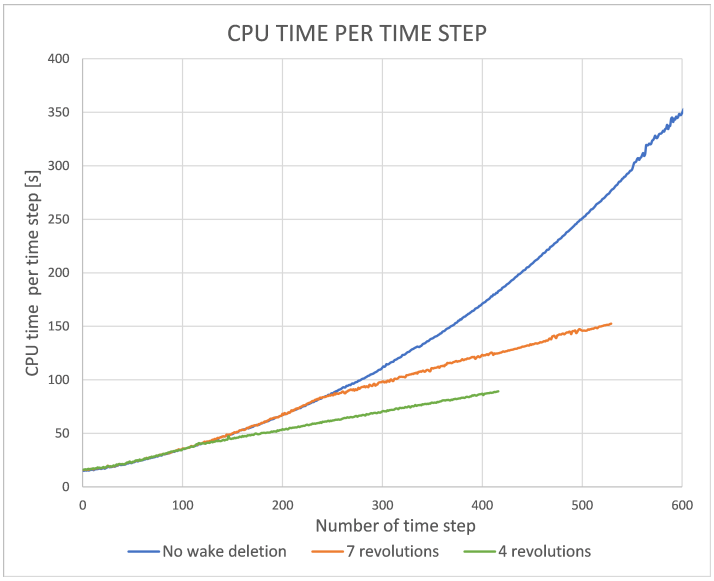

Figure 68: Required CPU time for each new time step when the last wake layer is removed after 4 and 7 revolutions (SWT 2.3-93).

Table 20: Simulation time needed to simulate the revolution number 6, 9, 12 and 15 of SWT 2.3-93 wind turbine.

Revolution number	*MECANO + AERO*	*MECANO + Vortexje* (removal after 7 revolutions)	*MECANO + Vortexje* (without removal)
6th	8 s	0 h 49 min 23 s	0 h 48 min 59 s
9th	8 s	1 h 10 min 59 s	1 h 26 min 53 s
12th	8 s	1 h 29 min 28 s	2 h 21 min 12 s
15th	8 s	-	3 h 35 min 19 s

6 Conclusions

In the present study, a comparison has been performed between the method most used by the industry, the Blade Element Momentum method, and the 3D panel method for the simulation of aerodynamic loads on wind turbines. Furthermore, in order to obtain the influence of deformations, a structural-aerodynamic coupling was carried out. *MECANO + AERO* has been the software used based on the BEM method and *MECANO + Vortexje* the one based on the panel method. The study was carried out for two wind turbines: NREL 5-MW and SWT 2.3-93.

Initially, a comparison of the steady-state response for different wind speeds was made between *MECANO + AERO* and other open software that is also based on the BEM method: *FAST + BeamDyn + Aerodyn*. The results obtained in terms of aerodynamic loads and deformations show great similarity, validating the *MECANO + AERO* method. Taking *MECANO + AERO* as reference, the dynamic response for a uniform wind and the rated operating point has been compared with *MECANO + Vortexje*, obtaining similar results. According to different works carried out using higher fidelity CFD approaches (Yu and Kwon [41], Dose et al.[10] and Imiela et al.[19]), the *MECANO + AERO* method seems to offer a more accurate result of the rotor torque while *MECANO + Vortexje* offers a better result in the rotor thrust. However, this comparison should not be taken as definitive, since two important effects are not taken into account in the panel method, such as the viscous effects or flow separation and the rotational effects produced from Coriolis and centrifugal forces that causes stall delay phenomena. It is expected (Ramos et al.[33]) that taking these effects into account, the results obtained will be closer to those obtained using the Blade Element Momentum theory, which takes into account the effects of flow separation and the rotational stall delay through the corrected experimental information on the aerodynamic coefficients of the profiles.

The main observed advantages of the *MECANO + AERO* method is its low computational cost compared to *MECANO + Vortexje*, in addition to the greater simplicity of its implementation. For this reason, a function has been implemented in *Vortexje* that removes the last wake layer when it has almost no effect on the rotor, trying to make it more competitive in terms of computational cost. However, the computing time is still much higher. On the contrary, the main advantage of the *MECANO + Vortexje* method is its ability to take into account unsteady effects produced by asymmetries in flow, modeling the dynamic wake effect and skewed wake aerodynamics. This has allowed a study of the effect of the shaft tilt and yaw angle on rotor deformations and loads. It is important to consider these effects because in real wind conditions it is inevitable that the wind direction will change. The results obtained show a great influence of the yaw angle on the amplitudes of the oscillations, causing them to increase considerably and, therefore, must be taken into account when predicting fatigue loads or in design aspects like tower-blade tip clearance. Another unsteady effect that has been studied is the effect produced by gravitational loads, which cause a fairly large unsteady periodic response that must also be taken into account.

Furthermore, the *MECANO + Vortexje* method does not require the use of experimental or empirical data, while *MECANO + AERO* does. This can be seen as an advantage or a disadvantage. The BEM method requires providing the lift, drag and moment coefficients. This can be a disadvantage if such data is not available or reliable, or if it is available it is normally limited to a number of attack angles having to extrapolate the information and make corrections for three-dimensional behavior. Furthermore, this process must be carried out for each wind turbine. On the contrary, it can be an advantage since it allows to introduce effects such as the stall of the airfoil produced by flow separation or the rotational stall delay.

Throughout the work, the results obtained with rigid and flexible elements have been compared, showing the non-negligible influence that deformations have on aerodynamic loads, especially due to the torsion produced in the blades. Comparing the results obtained in SWT 2.3-93 and NREL 5-MW wind turbines, it is observed that the use of larger blades produces greater aeroelastic deformations and, therefore, greater changes in the rotor loads. The trend in recent years is to build longer blades with the aim of obtaining more power. For this reason, the use of more precise and reliable methods with structural-aerodynamic coupling is increasingly necessary.

For an early-stage design work, it would be better to use the Blade Element Momentum due to computational costs are very low and the results quite reliable. However, for more advanced studies in which it is necessary to take into account unsteady effects, the use of higher fidelity methods is recommended. At a midpoint between high fidelity CFD methods, which are very computationally expensive, one would find the panel method by coupling it with a viscous boundary layer solution and introducing rotational effects.

7 Future work and *AERO* updating

In order to obtain more accurate results, some improvements can be included in both the BEM method implemented in the *AERO* module and in the panel method implemented in *Vortexje*. In fact, after the completion of this project a new version of *AERO* module is available with several improvements, leaving for future work the comparison between the new *AERO* module and the panel method.

Regarding to the new version of *AERO* module, the losses at the root are included in a similar way to the blade tip losses, simply defining a new loss factor $F = F_R F_T$ where F_T is the tip loss factor and that has been defined in Section 3.3.1.4, and F_R is the root loss factor that using the so-called Prandtl model (Glauert [11]) is defined by:

$$F_R = \frac{2}{\pi} \arccos\left(\exp\left(-\frac{b}{2}\frac{r - r_{hub}}{r_{hub}}\frac{1}{\sin\phi}\right)\right) \tag{88}$$

In order to predict the effects of asymmetric flow due to yaw or tilt angle, it has been introduced the skewed wake correction. The TUDk model from Snel and Schepers [38] is integrated in the SAMCEF solution. This correction has been implemented by other softwares based on the BEM method such as *Aerodyn*. For example, *Aerodyn* has implemented a method developed by Pitt and Peters [29].

To obtain more accurate results when the rotor is subjected to highly dynamic flow conditions, it has been introduced a dynamic stall model in the *AERO* module. There are different dynamic stall models, like those based on the Beddoes and Leishman method [5] such as the modified model developed in Dimitriadis et al. [6], or ONERA method (Mcalister et al.[25]). The model implemented in *AERO* is based on the Beddoes and Leishman method and is borrowed from Hansen et al.[15]. Finally, another improvement implemented is a model that takes into account the wake memory effect. The model for the introduction of this effect is developed in Snel and Schepers [38].

Regarding the panel method, some improvements can also be made, as indicated throughout the report. In order to better meet the Kutta pressure condition by reducing the pressure difference to zero at the trailing edge, it could be implemented the method developed in Wang et al.[40], where it is solved with the Newton-Raphson method with the initial values obtained with the Morino's Kutta condition.

In future works the panel method implemented in *Vortexje* could be improved by including the flow separation effect by a weak coupling of a viscous boundary layer solution as explained in Prasad and Dimitriadis [31]. Prasad and Dimitriadis [31] uses "the double wake model, where the separation is modeled by introducing a second wake from the separation point" (Prasad and Dimitriadis [31], p.1, 2017). More challenging seems the solution adopted in Ramos et al.[33], where the viscous effects are taken into account using a strong coupling between the

viscous and inviscid parts, solving the integral boundary layer equations and introducing the 'blowing' or 'transpiration' velocity as a boundary condition. Furthermore, it takes into account the rotational effects produced from Coriolis and centrifugal forces (Ramos et al.[32]).

It would also be interesting to study in future works the influence of the tower on the aerodynamic loads comparing the results obtained by *MECANO + AERO* and *MECANO + Vortexje*.

Appendix A Aerodynamic and structural data for SWT 2.3-93 wind turbine.

Table 21: Distributed Blade Structural Properties of SWT 2.3-93.

Radius (m)	BlFract (-)	AeroCent (-)	StrcTwst (°)	BMassDen (kg/m)	FlpStff (N·m^2)	EdgStff (N·m^2)	GJStff (N·m^2)	EAStff (N)	Alpha (-)	FlpIner (kg·m)	EdgIner (kg·m)
1.50	0	0.25	10	373.414	9.96E+09	9.96E+09	3.06E+09	5.35E+09	0	535.07	535.17
1.65	0.00325	0.25	10	373.414	9.96E+09	9.96E+09	3.06E+09	5.35E+09	0	535.07	535.17
2.38	0.01951	0.24951	10	425.350	1.07E+10	1.08E+10	2.99E+09	5.93E+09	0	600.34	586.51
3.11	0.03577	0.2451	10	407.303	9.60E+09	1.07E+10	2.75E+09	5.54E+09	0	531.35	576.05
3.84	0.05203	0.23284	10	407.023	8.41E+09	1.09E+10	2.57E+09	5.43E+09	0	480.60	604.86
4.57	0.06829	0.22059	10	325.873	5.93E+09	8.17E+09	1.91E+09	4.18E+09	0	356.70	480.16
5.30	0.08455	0.20833	10	247.651	3.98E+09	5.62E+09	1.28E+09	3.02E+09	0	251.22	352.82
6.04	0.10081	0.19608	10	233.230	3.47E+09	5.03E+09	1.05E+09	2.73E+09	0	220.29	326.55
6.77	0.11707	0.18382	10	220.351	3.04E+09	4.43E+09	8.64E+08	2.47E+09	0	193.39	300.95
7.50	0.13335	0.17156	10	210.134	2.74E+09	3.79E+09	6.37E+08	2.22E+09	0	173.87	269.96
8.23	0.14959	0.15931	10	219.810	2.72E+09	3.86E+09	5.51E+08	2.22E+09	0	166.98	277.12
8.96	0.16585	0.14706	10	234.477	2.58E+09	3.94E+09	4.71E+08	2.29E+09	0	159.08	299.59
9.69	0.18211	0.13481	10	229.251	2.17E+09	4.00E+09	3.70E+08	2.25E+09	0	135.61	313.45
10.43	0.19837	0.125	10	223.402	1.86E+09	3.89E+09	3.01E+08	2.25E+09	0	118.75	330.70
11.16	0.21465	0.125	10	209.781	1.61E+09	3.43E+09	2.47E+08	2.02E+09	0	102.91	300.61
11.89	0.23089	0.125	10	194.052	1.41E+09	2.78E+09	1.85E+08	1.73E+09	0	88.46	257.79
12.62	0.24715	0.125	10	192.212	1.31E+09	2.72E+09	1.71E+08	1.66E+09	0	81.71	249.57
13.35	0.26341	0.125	10	190.596	1.25E+09	2.64E+09	1.61E+08	1.59E+09	0	77.17	239.92
14.82	0.29595	0.125	10	186.633	1.13E+09	2.48E+09	1.44E+08	1.44E+09	0	68.54	219.00
16.28	0.32846	0.125	10	181.502	1.01E+09	2.33E+09	1.26E+08	1.30E+09	0	60.18	199.14
17.74	0.36098	0.125	10	177.095	8.74E+08	2.20E+09	1.10E+08	1.18E+09	0	51.90	184.26
19.21	0.3935	0.125	9.627	172.601	7.49E+08	2.06E+09	9.59E+07	1.07E+09	0	44.13	169.71
20.67	0.42602	0.125	8.117	162.104	6.06E+08	1.90E+09	7.95E+07	8.98E+08	0	34.47	145.13
22.13	0.45855	0.125	6.746	157.916	4.82E+08	1.73E+09	6.60E+07	7.88E+08	0	27.18	130.38
23.60	0.49106	0.125	5.508	144.839	3.75E+08	1.50E+09	4.47E+07	6.43E+08	0	20.54	108.03
25.06	0.52358	0.125	4.394	139.264	2.94E+08	1.41E+09	3.80E+07	5.76E+08	0	16.03	99.19
26.52	0.5561	0.125	3.398	132.916	2.25E+08	1.28E+09	3.16E+07	5.08E+08	0	12.19	89.34
27.99	0.58862	0.125	2.513	121.351	1.73E+08	1.01E+09	2.53E+07	4.18E+08	0	9.53	74.16
29.45	0.62115	0.125	1.733	110.161	1.31E+08	8.71E+08	1.98E+07	3.56E+08	0	7.32	63.97
30.91	0.65366	0.125	1.049	98.672	9.67E+07	7.28E+08	1.51E+07	2.97E+08	0	5.48	53.89
32.38	0.68618	0.125	0.456	90.802	6.93E+07	6.51E+08	1.15E+07	2.92E+08	0	4.02	54.41
33.84	0.7187	0.125	-0.053	84.926	5.90E+07	5.61E+08	1.02E+07	2.53E+08	0	3.42	47.18
35.30	0.75122	0.125	-0.487	76.414	5.00E+07	4.39E+08	8.95E+06	2.07E+08	0	2.85	38.48
36.77	0.78376	0.125	-0.851	71.255	4.20E+07	3.90E+08	7.99E+06	1.81E+08	0	2.40	33.78
38.23	0.81626	0.125	-1.152	58.995	3.36E+07	2.85E+08	4.99E+06	1.34E+08	0	1.85	24.99
39.70	0.84878	0.125	-1.397	54.327	2.72E+07	2.50E+08	4.43E+06	1.16E+08	0	1.51	21.76
41.16	0.8813	0.125	-1.594	49.636	2.16E+07	2.17E+08	3.89E+06	9.98E+07	0	1.22	18.75
41.89	0.89756	0.125	-1.677	45.651	1.91E+07	1.95E+08	3.35E+06	8.81E+07	0	1.06	16.57
42.62	0.91382	0.125	-1.750	40.098	1.67E+07	1.68E+08	3.16E+06	6.01E+07	0	0.93	11.08
43.35	0.93008	0.125	-1.814	37.825	1.46E+07	1.55E+08	2.93E+06	5.50E+07	0	0.82	10.19
43.72	0.93821	0.125	-1.843	36.445	1.31E+07	1.44E+08	2.72E+06	5.07E+07	0	0.74	9.41
44.09	0.94636	0.125	-1.870	32.637	1.08E+07	8.73E+07	2.33E+06	3.48E+07	0	0.61	6.35
44.45	0.95447	0.125	-1.896	30.753	8.80E+06	7.58E+07	2.01E+06	2.93E+07	0	0.49	5.37
44.82	0.9626	0.125	-1.920	28.866	7.06E+06	6.53E+07	1.72E+06	2.45E+07	0	0.39	4.50
45.18	0.97073	0.125	-1.942	27.013	5.54E+06	5.59E+07	1.45E+06	2.03E+07	0	0.31	3.75
45.55	0.97886	0.125	-1.963	25.200	4.15E+06	4.68E+07	1.19E+06	1.65E+07	0	0.23	3.06
45.91	0.98699	0.125	-1.983	22.918	2.53E+06	3.53E+07	8.69E+05	1.17E+07	0	0.14	2.21
46.28	0.99512	0.125	-2.001	6.299	1.38E+05	3.64E+06	1.38E+05	2.67E+06	0	0.02	0.52
46.50	1	0.125	-2.012	5.67545	9.35E+04	2.76E+06	1.05E+05	1.94E+06	0	0.01	0.37

Table 22: Distributed Blade Aerodynamic Properties of SWT2.3-93.

RNodes (m)	AeroTwst (°)	DRNodes (m)	Chord (m)	NFoil	PrnElm
2.5714	10	-	2.036	1	CYLD.txt
4.7143	10	-	2.065	2	CYLD.txt
6.8571	10	-	2.334	2	CYLD.txt
9	10	-	2.736	9	FFA_W3_301D.txt
11.1429	10	-	3.137	9	FFA_W3_301D.txt
13.2857	10	-	3.485	9	FFA_W3_301D.txt
15.4286	10	-	3.372	9	FFA_W3_301D.txt
17.5714	10	-	3.183	10	FFA_W3_211D.txt
19.7143	9.079	-	2.995	10	FFA_W3_211D.txt
21.8571	7.014	-	2.807	10	FFA_W3_211D.txt
24	5.231	-	2.618	10	FFA_W3_211D.txt
26.1429	3.589	-	2.43	10	FFA_W3_211D.txt
28.2857	2.303	-	2.242	10	FFA_W3_211D.txt
30.4286	1.281	-	2.054	10	FFA_W3_211D.txt
32.5714	0.406	-	1.865	10	FFA_W3_211D.txt
34.7143	-0.303	-	1.677	10	FFA_W3_211D.txt
36.8571	-0.84	-	1.489	10	FFA_W3_211D.txt
39	-1.274	-	1.3	10	FFA_W3_211D.txt
41.1429	-1.627	-	1.112	10	FFA_W3_211D.txt
43.2857	-1.842	-	0.924	10	FFA_W3_211D.txt
45.4286	-1.973	-	0.735	10	FFA_W3_211D.txt
46.5	-1.973	-	0.735	10	FFA_W3_211D.txt

Table 23: Distributed Tower Structural Properties of SWT 2.3-93.

Elevation (m)	HtFract (-)	TMassDen (kg/m)	TwFAStif (N•m^2)	TwSSStif (N•m^2)	TwGJStif (N•m^2)	TwEAStif (N)	TwFAIner (kg•m)	TwSSIner (kg•m)	TwFAcgOf (m)	TwSScgOf (m)
0.00	0.0	5590.87	614.34E+9	614.34E+9	472.75E+9	138.13E+9	24866.3	24866.3	0.0	0.0
8.76	0.1	5232.43	534.82E+9	534.82E+9	411.56E+9	129.27E+9	21647.5	21647.5	0.0	0.0
17.52	0.2	4885.76	463.27E+9	463.27E+9	356.50E+9	120.71E+9	18751.3	18751.3	0.0	0.0
26.28	0.3	4550.87	399.13E+9	399.13E+9	307.14E+9	112.43E+9	16155.3	16155.3	0.0	0.0
35.04	0.4	4227.75	341.88E+9	341.88E+9	263.09E+9	104.45E+9	13838.1	13838.1	0.0	0.0
43.80	0.5	3916.41	291.01E+9	291.01E+9	223.94E+9	96.76E+9	11779.0	11779.0	0.0	0.0
52.56	0.6	3616.83	246.03E+9	246.03E+9	189.32E+9	89.36E+9	9958.2	9958.2	0.0	0.0
61.32	0.7	3329.03	206.46E+9	206.46E+9	158.87E+9	82.25E+9	8356.6	8356.6	0.0	0.0
70.08	0.8	3053.01	171.85E+9	171.85E+9	132.24E+9	75.43E+9	6955.9	6955.9	0.0	0.0
78.84	0.9	2788.75	141.78E+9	141.78E+9	109.10E+9	68.90E+9	5738.6	5738.6	0.0	0.0
87.60	1.0	2536.27	115.82E+9	115.82E+9	89.13E+9	62.66E+9	4688.0	4688.0	0.0	0.0

Table 24: Distributed Tower Aerodynamic Properties of SWT 2.3-93.

Rnodes (m)	AeroTwst (°)	DRNodes (m)	Chord (m)	Nfoil	Pname
0	0	555	3.87	1	CYLD.txt
80	0	555	6	1	CYLD.txt
180	0	555	6	1	CYLD.txt

Table 25: Distributed Main shaft Properties of SWT 2.3-93.

ShFract	ExtRad (m)	IntRad (m)	YT (Pa)	NT	M
0	0.5	0.025	2E+11	0.3	7800
0.2	0.5	0.025	2E+11	0.3	7800
0.4	0.5	0.025	2E+11	0.3	7800
0.6	0.5	0.025	2E+11	0.3	7800
0.8	0.5	0.025	2E+11	0.3	7800
1	0.5	0.025	2E+11	0.3	7800

Table 26: Distributed Coupling shaft Properties of SWT 2.3-93.

ShFract	ExtRad (m)	IntRad (m)	YT (Pa)	NT	M
0	0.12	0.0025	2E+11	0.3	7800
0.5	0.12	0.0025	2E+11	0.3	7800
1	0.12	0.0025	2E+11	0.3	7800

Appendix B NREL PHASE VI: Comparison of MECANO-Vortexje with experimental data

In order to validate the *MECANO + Vortexje* method, it has been applied to the NREL Phase VI wind turbine by the coworker Xavier Dechamps and it has been compared against experimental data performed in the NASA AMES wind tunnel (Sicklinger [37]).

The studied case is the Sequence S0700000 described in Hand et al.[14], which corresponds to a simulation with 0° cone angle, a wind speed of 7 m/s, a rotor speed of 72 rpm, without yaw angle and a blade tip pitch angle of 3°. Figure 69 shows the pressure coefficient along the chord for different sections of the blade span obtained from *MECANO + Vortexje* after 12 rotor revolutions and experimental data. It is observed that the results obtained with the simulation represent the experimental data quite well. However, at the trailing edge of the profile the pressure difference is not 0 as stated by the pressure Kutta condition. This is because as stated previously, the *Vortexje* program implements the Morino's Kutta condition which always results in a nonphysical pressure mismatch at the trailing edge.

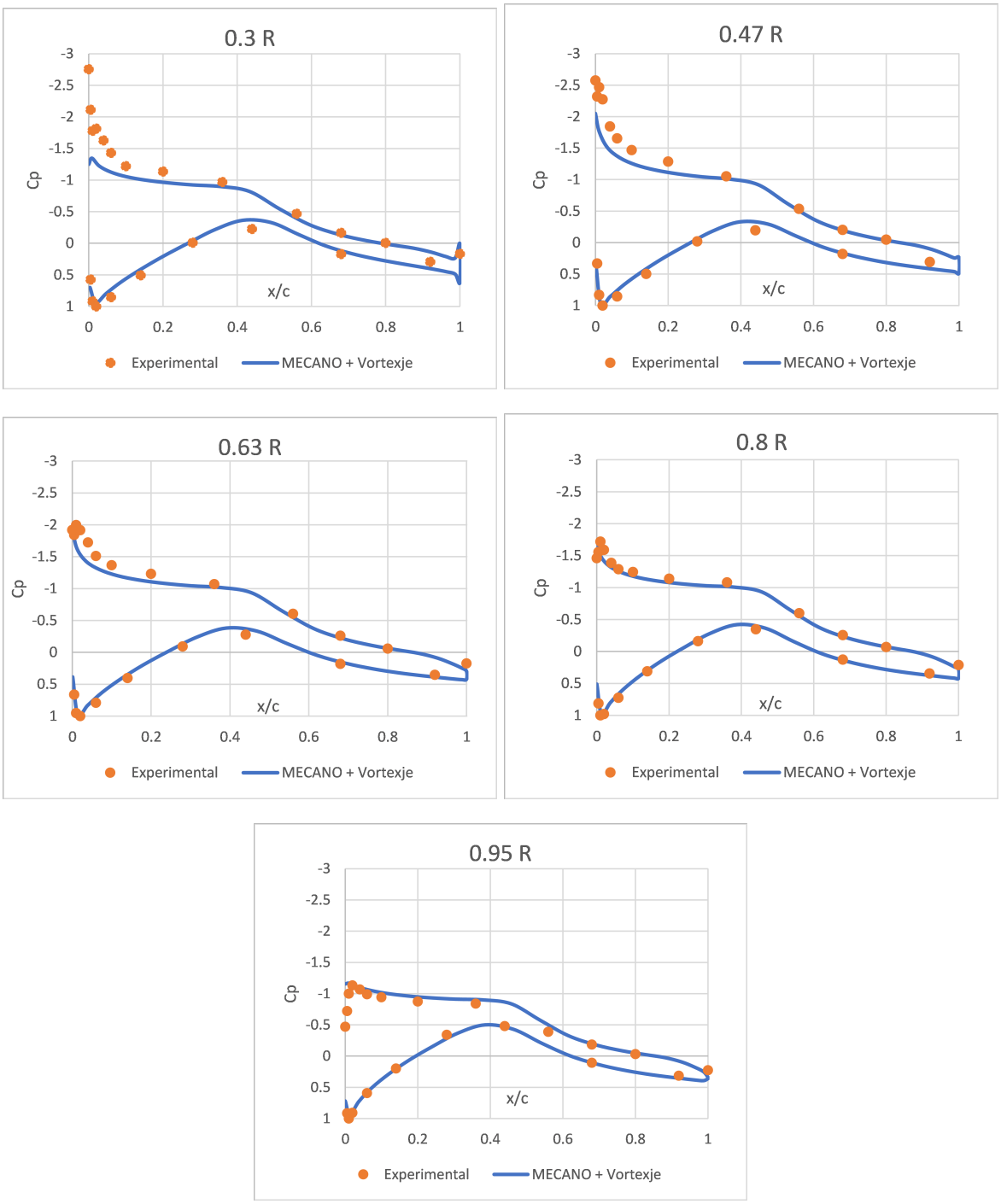

Figure 69: Pressure coefficient along the chord in different blade span sections.

References

[1] A. Ahlström. Influence of wind turbine flexibility on loads and power production. *Wind Energy*, 9:237 – 249, 05 2006.

[2] M. Arnold and O. Brüls. Convergence of the generalized-[alpha] scheme for constrained mechanical systems. 01 2007.

[3] J. Baayen. Vortexje. URL https://github.com/jbaayen/vortexje.

[4] J. H. Baayen. Vortexje - an open-source panel method for co-simulation. 03 2013.

[5] T. Beddoes and J. Leishman. A semi-empirical model for dynamic stall. *Journal of the American Helicopter Society*, 34(3):3–17, July 1989.

[6] J. Boutet, G. Dimitriadis, and X. Amandolese. A modified leishman–beddoes model for airfoil sections undergoing dynamic stall at low reynolds numbers. *Journal of Fluids and Structures*, 93:102852, 2020. ISSN 0889-9746. doi: https://doi.org/10.1016/j.jfluidstructs.2019.102852.

[7] M. L. Buhl. A new empirical relationship between thrust coefficient and induction factor for the turbulent windmill state. Technical Report NREL/TP-500-36834, National Renewable Energy Laboratory, 2004.

[8] T. Burton, D. Sharpe, N. Jenkins, and E. Bossanyi. *Wind Energy Handbook*. John Wiley & Sons, Ltd, Baffins Lane, Chichester, 2001.

[9] A. Cuerva Tejero, O. López García, and C. J. Gallego Castillo. Diseño conceptual de aerogeneradores. trabajo fin de grado, 2014.

[10] B. Dose, H. Rahimi, I. Herráez, B. Stoevesandt, and J. Peinke. Fluid-structure coupled computations of the nrel 5 mw wind turbine by means of cfd. *Renewable Energy*, 129:591 – 605, 2018. ISSN 0960-1481. doi: https://doi.org/10.1016/j.renene.2018.05.064. URL http://www.sciencedirect.com/science/article/pii/S0960148118305858.

[11] H. Glauert. Airplane propellers. In *Aerodynamic Theory*. Springer, Berlin,Heidelberg, 1935.

[12] H. Glauert and A. R. Committee. *A General Theory of the Autogyro*. Aeronautical Research Committee reports and memoranda. H.M. Stationery Office, 1926. URL https://books.google.es/books?id=8jIPnQEACAAJ.

[13] M. Géradin and A. Cardona. *Flexible Multibody Dynamics: A Finite Element Approach*, volume 4. 01 2001.

[14] M. M. Hand, D. Simms, L. J. Fingersh, D. W. Jager, J. R. Cotrell, S. Schreck, and L. S. M. Unsteady aerodynamics experiment phase vi: Wind tunnel test configurations and available data campaigns. Technical Report NREL/TP-500-29955, National Renewable Energy Laboratory, 2001.

[15] M. Hansen, M. Gaunaa, and H. Madsen. A beddoes–leishman type dynamic stall model in state-space and indicial formulations. 01 2004.

[16] J. L. Hess and A. M. O. Smith. *Calculation of Potential Flow About Arbitrary Bodies*. Elsevier Ltd., Douglas Aircraft Company, Aircraft Division, Long Beach, California, USA, 1967.

[17] T. J. Hughes, H. M. Hilber, and R. L. Taylor. A reduction scheme for problems of structural dynamics. *International Journal of Solids and Structures*, 12(11):749 – 767, 1976. ISSN 0020-7683. doi: https://doi.org/10.1016/0020-7683(76)90040-8.

[18] G. M. Hulbert and J. Chung. Explicit time integration algorithms for structural dynamics with optimal numerical dissipation. *Computer Methods in Applied Mechanics and Engineering*, 137(2):175 – 188, 1996. ISSN 0045-7825. doi: https://doi.org/10.1016/S0045-7825(96)01036-5.

[19] M. Imiela, F. Wienke, C. Rautmann, C. Willberg, P. Hilmer, and A. Krumme. Towards multidisciplinary wind turbine design using high-fidelity methods. *33rd Wind Energy Symposium*, 01 2015. doi: 10.2514/6.2015-1462.

[20] J. Jonkman, S. Butterfield, W. Musial, and G. Scott. Definition of a 5-mw reference wind turbine for offshore system development. Technical Report NREL/TP-500-38060, National Renewable Energy Laboratory, 2009.

[21] J. Katz and A. Plotkin. *Low-Speed Aerodynamics*. Cambridge University Press, Cambridge, 2001.

[22] H. Kooijman, C. Lindenburg, D. Winkelaar, and E. van der Hooft. Aero-elastic modelling of the dowec 6 mw pre-design in phatas. Technical Report DOWEC-F1W2-HJK-01-046/9, Dutch Offshore Wind Energy Converter, September 2003.

[23] Z. Li, B. Wen, X. Dong, Z. Peng, Y. Qu, and W. Zhang. Aerodynamic and aeroelastic characteristics of flexible wind turbine blades under periodic unsteady inflows. *Journal of Wind Engineering and Industrial Aerodynamics*, 197:104057, 2020. ISSN 0167-6105. doi: https://doi.org/10.1016/j.jweia.2019.104057.

[24] C. Lindenburg. Stall coefficients, release "dec-2000". Technical Report ECN-Wind Memo-00-031, Energy Research Centre of the Netherlands, January 2001.

[25] K. W. Mcalister, O. Lambert, and D. Petot. Application of the onera model of dynamic stall. Technical Report AVSCOM Technical Report 84-A-3, NASA, 1984.

[26] P. J. Moriarty and A. C. Hansen. Aerodyn theory manual. Technical Report NREL/TP-500-36881, National Renewable Energy Laboratory, 2005.

[27] L. Morino and C. C. Kuo. Subsonic potential aerodynamics for complex configurations: A general theory. *AIAA*, 12 (2):191 – 197, February 1974.

[28] N. M. Newmark. A method of computation for structural dynamics. *Journal of the engineering mechanics division*, 85(3):67–94, 1959.

[29] D. Pitt and D. Peters. Theoretical prediction of dynamic-in ow derivatives. *Vertica*, 5, 01 1981.

[30] C. Prasad, Q.-Z. Chen, O. Brüls, F. DAmbrosio, and G. Dimitriadis. Aeroservoelastic simulations for horizontal axis wind turbines. *Proceedings of the Institution of Mechanical Engineers, Part A: Journal of Power and Energy*, 231, 11 2016. doi: 10.1177/0957650916678725.

[31] C. S. Prasad and G. Dimitriadis. Application of a 3d unsteady surface panel method with flow separation model to horizontal axis wind turbines. *Journal of Wind Engineering and Industrial Aerodynamics*, 166:74 – 89, 2017. ISSN 0167-6105. doi: https://doi.org/10.1016/j.jweia.2017.04.005.

[32] N. Ramos-García, J. N. Sørensen, and W. Z. Shen. A strong viscous–inviscid interaction model for rotating airfoils. *Wind Energy*, 17(12):1957–1984, 2014. doi: 10.1002/we.1677.

[33] N. Ramos-García, J. Sørensen, and W. Z. Shen. Three-dimensional viscous-inviscid coupling method for wind turbine computations. *Wind Energy*, 19, 11 2014. doi: 10.1002/we.1821.

[34] A. Sabale and N. Gopal. Nonlinear aeroelastic response of wind turbines using simo-vu-quoc rods. *Applied Mathematical Modelling*, 65, 09 2018. doi: 10.1016/j.apm.2018.09.003.

[35] A. K. Sabale and N. K. V. Gopal. Nonlinear aeroelastic analysis of large wind turbines under turbulent wind conditions. *AIAA Journal*, 57(10):4416–4432, 2019. doi: 10.2514/1.J057404.

[36] K. Schweigler. *Aerodynamic Analysis of the NREL 5-MW Wind Turbine using Vortex Panel Method*. PhD thesis, 06 2012.

[37] S. Sicklinger. Simulation data & experimental data for nrel phase vi case s0700000, 08 2015.

[38] H. Snel and J. G. Schepers. Joint investigation of dynamic inflow effects and implementation of an engineering method. Technical Report ECN-C-94-107, Energy Research Centre of the Netherlands, April 1995.

[39] A. van Garrel. Multilevel panel method for wind turbine rotor flow simulations. Technical report, University of Twente, Enschede, 2016.

[40] Y. Wang, M. Abdel-Maksoud, and B. Song. A fast method to realize the pressure kutta condition in boundary element method for lifting bodies. *Ocean Engineering*, 130:398 – 406, December 2016.

[41] D. O. Yu and O. J. Kwon. Predicting wind turbine blade loads and aeroelastic response using a coupled cfd–csd method. *Department of Aerospace Engineering, Korea Advanced Institute of Science and Technology*, 04 2014.